

**AB INITIO COMPUTATION FOR RATIONAL DESIGN
OF CHEMICAL RECEPTOR IN SENSOR**

AHMAD NAZMI BIN ROSLI

**FACULTY OF SCIENCE
UNIVERSITY OF MALAYA
KUALA LUMPUR**

2014

**AB INITIO COMPUTATION FOR RATIONAL DESIGN
OF CHEMICAL RECEPTOR IN SENSOR**

AHMAD NAZMI BIN ROSLI

**DISSERTATION SUBMITTED IN FULFILLMENT OF
THE REQUIREMENTS FOR THE DEGREE OF
MASTER OF SCIENCE**

**DEPARTMENT OF CHEMISTRY
FACULTY OF SCIENCE
UNIVERSITY OF MALAYA
KUALA LUMPUR**

2014

UNIVERSITI MALAYA

ORIGINAL LITERARY WORK DECLARATION

Name of Candidate: **AHMAD NAZMI BIN ROSLI**

I/C/Passport No: **860627-30-5319**

Registration/Matric No.: **SGR120078**

Name of Degree: **MASTER OF SCIENCE**

Title of Project Paper/Research Report/Dissertation/Thesis ("this Work"):

"AB INITIO COMPUTATION FOR RATIONAL DESIGN OF CHEMICAL RECEPTOR IN SENSOR"

Field of Study: **INORGANIC CHEMISTRY**

I do solemnly and sincerely declare that:

- (1) I am the sole author/writer of this Work,
- (2) This Work is original,
- (3) Any use of any work in which copyright exists was done by way of fair dealing and for permitted purposes and any excerpt or extract from, or reference to or reproduction of any copyright work has been disclosed expressly and sufficiently and the title of the Work and its authorship have been acknowledged in this Work,
- (4) I do not have any actual knowledge nor do I ought reasonably to know that the making of this work constitutes an infringement of any copyright work,
- (5) I hereby assign all and every rights in the copyright to this Work to the University of Malaya ("UM"), who henceforth shall be owner of the copyright in this Work and that any reproduction or use in any form or by any means whatsoever is prohibited without the written consent of UM having been first had and obtained,
- (6) I am fully aware that if in the course of making this Work I have infringed any copyright whether intentionally or otherwise, I may be subject to legal action or any other action as may be determined by UM.

(Candidate Signature)

Date:26/08/2014

Subscribed and solemnly declared before,

Witness's Signature

Date:26/08/2014

Name **DR WOI PEI MENG**

Designation

Abstract

The advancement of computing power has greatly improved the application of computational chemistry for routine use in solving a wide variety of chemical problems. The once accurate but expensive methods such as Gn Theory and CCSD(T) calculation can now be completed within hours. The work presented here has utilized the power of computational chemistry to design the cation recognition molecules using carbonitrile functionality. The B3LYP with 6-31+g(d,p) and QZVP basis set had been verified and selected as the most appropriate methods to obtain optimized geometry and vibrational frequencies. The optimized geometries were later used to obtain Mulliken and CHELPG charges, GIAO nuclear magnetic shieldings, natural bonding orbitals (NBO) and overlap population (AOMix software). The accurate energies were obtained using composite Gn Theory methods (G3 and G4). The binding energies of unconjugated carbonitrile model (acetonitrile) with cations are showing a general trend of $H^+ > Be(II) > Mg(II) > Ca(II)$. Mg(II) is more strongly bound to acetonitrile by 33.3 kcal/mol compared to Ca(II). The carbonitrile-carboxaldehyde receptor models (2-cyano ethylene) had been employed to study the selectivity of Mg(II) against Ca(II) and examining the effects of keto-enol forms and negatively charged (enolate) sites. In both uncharged and anion forms, Mg(II) binds more strongly to the receptor model compared to Ca(II), by 55.1 and 30.3 kcal/mol, respectively. This study also includes three-dimensional design based on Ionomycin to elucidate interactions between the proposed receptor models with cations. The N and O terminals of 2-cyano ethanal enolate show comparable level of negative charge. The lack of charge disparity on the N and O terminals indicates efficient charge delocalization throughout the π -network that leads to stronger interactions. The unsaturated carbonitriles had also been studied using 2-cyano butadiene as Be(II) receptor. The terminal vinyl carbon in 2-CN BD rehybridizes from sp^2 to sp^3 with an increase of 7% of s character to allow interaction with Be(II) that

leads to the formation of six-membered cyclic complex. Fabricated potentiometric chemical sensors with carbonitrile-doped sensing membrane had shown distinct signal patterns that can be exploited in sensor applications.

Abstrak

Kemajuan kuasa pengkomputeran telah meningkatkan penggunaan pengkomputeran untuk kegunaan rutin dalam menyelesaikan pelbagai masalah dalam bidang kimia. Kaedah yang tepat tetapi perlahan seperti teori Gn dan CCSD(T) kini boleh disiapkan dalam masa beberapa jam. Kerja-kerja yang dibentangkan di sini telah menggunakan kuasa kimia pengkomputeran untuk mereka bentuk molekul pengecaman kation berdasarkan kumpulan berfungsi karbonitril. Kaedah B3LYP dengan 6-31+g(d,p) dan QZVP set asas telah dipilih sebagai kaedah yang paling sesuai untuk mendapatkan geometri optimum dan frekuensi getaran. Geometri optimum tersebut kemudiannya digunakan untuk mendapatkan cas Mulliken dan CHELPG, perisaian magnetik nukleus GIAO, *Natural Bond Orbital* (NBO) dan pertindihan populasi orbital (berdasarkan perisian AOMix). Tenaga jitu diperolehi dengan menggunakan kaedah komposit teori Gn (G3 dan G4). Tenaga pengikatan model karbonitril bukan konjugat (asetonitril) dengan kation menunjukkan trend $H^+ > Be(II) > Mg(II) > Ca(II)$. Mg(II) terikat lebih kuat kepada asetonitril sebanyak 33.3 kcal/mol berbanding dengan Ca(II). Model reseptor karbonitril-karboksaldehid (*2-cyano ethanal*) telah digunakan untuk mengkaji kesan pengikatan ke atas Mg(II) dan Ca(II), dan memeriksa kesan pembentukan keto-enol serta cas negatif (enolate). Dalam kedua-dua bentuk yang neutral dan anion, Mg(II) didapati terikat lebih kuat kepada model reseptor berbanding dengan Ca(II), dengan 55.1 berbanding 30.3 kcal/mol. Kajian ini juga menggunakan reka bentuk tiga dimensi yang berdasarkan *Ionomycin* untuk menerangkan interaksi di antara model reseptor dengan kation. Terminal N dan O bagi *2-cyano ethanal enolate* menunjukkan tahap cas negatif yang setara. Ini menunjukkan pentaksetempatan cas berlaku di sepanjang rangkaian- π yang membawa kepada interaksi yang lebih kuat. Karbonitril tak tepu juga telah dikaji dengan menggunakan *2-cyano butadiene* sebagai reseptor Be(II). Terminal vinil karbon dalam 2-CN BD mengalami penghybridan semula dari sp^2 kepada sp^3 dan

peningkatan sebanyak 7% ciri *s* untuk membolehkan ia berinteraksi dengan Be(II) yang mengakibatkan pembentukan kompleks siklik enam ahli. Pemfabrikatan sensor kimia potentiometrik dengan membran pengesanan berdasarkan karbonitril telah menunjukkan corak isyarat yang berbeza yang boleh dieksploitasi dalam aplikasi sensor.

Acknowledgements

I would like to thank my supervisor, Dr Woi Pei Meng, without who nothing would have been possible. I would also like to thank Dr Mohd Rais Ahmad for all his advice and for all the help he generously provided me into bringing me where I am now. I am also thankful to Prof Yatimah Alias, Dr Ninie Suhana and Prof Vannajan Lee for contributing to my research.

Many thanks to UMCIL lab and MIMOS chemical lab members such as Kak Mai, Mrs Marhaini, Ms Munirah, Mr Valentine, Mr Adam, Mr Aniq, Mrs Aiman and Mrs Norazah for being a great supporter.

I would like to thank my family who have always been of great advice and always there to support me during my study. Your prayer for me was what sustained me thus far. Not forgetting my beloved fiancée, Ms Noor Azuwa who always stood behind me during my study, always supporting me wholeheartedly.

Finally, I would like to thank Ministry of Education (MOE), Ministry of Science, Technology and Innovation (MOSTI) and University of Malaya, Malaysia for their financial supports.

***“Success is not final, failure is not fatal:
it is the courage to continue that counts.”***

Sir Winston Churchill

Table of Contents	Page
Abstract	III
Abstrak	V
Acknowledgements	VII
Table of Contents	IX
List of Tables	XIV
List of Figures	XVII
Lis of Abbreviations	XX
Chapter 1 :Introduction	1
1.1 Preface	1
1.2 Applications of Chemical Sensors	2
1.3 Aim of Study	3
1.4 Objectives	3
1.5 Thesis Outlines	3
Chapter 2 : Literature Review	5
2.1 Density Functional Theory	5
2.2 Basis Sets	8
2.2.1 Split Valence Basis Set	8
2.2.2 Polarized Basis Sets	9
2.2.3 Diffuse Function	9
2.3 The Gn Theory	10
2.3.1 The Gaussian-1 (G1) and Gaussian-2 (G2) Theories	10

2.4	Chemical Sensor	12
2.5	Ion-Selective Electrode	13
2.5.1	Acrylic Membrane Electrode	15
2.6	Potentiometry	16
2.7	Ionophores	17
2.8	Screen-Printed Electrode	18
2.9	Electrochemical Transducer	18
2.10	Chemical Field-Effect Transistor (ChemFET)	19
2.11	Reference Electrode	19
2.11.1	Silver/Silver Chloride Reference Electrode	22
Chapter 3 : Methodology		24
3.1	General Approach	24
3.2	Hybrid Functionals	26
3.3	Basis Sets	27
3.4	The Gaussian-3 (G3) Theory	29
3.5	The Gaussian-4 (G4) Theory	30
3.6	Special Tools	31
3.6.1	Natural Bond Orbital (NBO)	31
3.6.2	NMR Gauge-Independent Atomic Orbital (GIAO)	32
3.6.3	Integral Equation Formalism Polarizable Continuum Model (IEF-PCM)	32
3.6.4	AOMix	32
3.7	Hardware Details	33

3.8	Experimental Details	33
3.8.1	List of Chemicals	34
3.8.2	Sensor Fabrication	34
3.8.3	Sensor Evaluation	35
Chapter 4 : G3 Assisted Rational Design of Chemical Sensor Array Using Carbonitrile Neutral Receptors		37
4.1	Introduction	38
4.2	Results and Discussion	40
4.2.1.	Computational Benchmarks	40
4.2.2.	Acetonitrile – Carbonitrile Simple Receptor Model	44
4.2.3	Acetonitrile-Mg(II) Complex	49
4.2.4	Acetonitrile-Be(II) Complex	54
4.2.5	Protonated Acetonitrile	57
4.2.6	<i>n</i> -Pentane Carbonitrile-Mg(II) Complex	58
4.2.7	Magnesium(II) Bound to Two Acetonitrile Receptors	60
4.2.8	Malononitrile-Be(II) Complex	61
4.2.9.	Carbonitrile Reactivity and Binding Energies	65
4.2.10	Sensor cell signals	66
4.2.11	IR Measurement	67
4.3	Conclusions	68
Chapter 5 : Rational Design of Carbonitrile-Carboxaldehyde Cation Receptor Models - Probing The Nature of Heteroatom-Metal Interaction		70
5.1	Introduction	71

5.2	Results and Discussion	73
5.2.2	Optimized Structures of Receptor Models	73
5.2.3	Optimized Structures of Complexes	76
5.2.4	Deduction of Design Parameters for 2-Cyanoethanal	79
5.2.5	Deduction of Design Parameters for 1,2-Dicyanoethylene	83
5.2.6	3-Dimensional Rational Design with Carbonitrile-Carboxaldehyde Receptor Models and Ionomycin Fragment Models	85
5.2.7	Rationale for Magnesium <i>versus</i> Calcium Selectivity and Discrimination of Group I Cations	90
5.3	Conclusions	92
Chapter 6 : Computational Evaluation of Unsaturated Carbonitriles as Neutral Receptor Model for Beryllium(II) Recognition		94
6.1	Introduction	95
6.2	Results and Discussion	97
6.2.1	Optimized Geometries	97
6.2.2	NMR Shifts and Vibrational Frequencies	102
6.2.3	Electron Population Analysis	104
6.2.4	Frontier Molecular Orbital (FMO) Analysis	106
6.2.5	Energetics of Divalent Complexes	107
6.2.6	Overlap Population Analysis	110
6.2.7	Transition Structure	111
6.2.8	Rationale for Beryllium(II) Recognition using Unsaturated Carbonitriles	112
6.3	Conclusions	115

Chapter 7 : Conclusion	117
7.1 Major Achievements	117
7.2 Limitations	118
7.3 Future Works	118
References	120
Appendix A	133
Appendix B	149
Appendix C	161

List of Tables	Page
Table 2.1 Overview of steps and jobs for G1 and G2	11
Table 3.1 Overview of The G4 Theory	31
Table 4.1 Bond distances (r) and dissociation energies (De) of water dimer benchmark	41
Table 4.2 Bond distances (r) and dissociation energies (De) of ammonia-borane benchmark.	42
Table 4.3 G3 and G4 geometries and binding energies of Mg(II) complexes with HCN and H ₂ O [†]	43
Table 4.4 Bond distances of acetonitrile and its complexes with Be(II), Mg(II) and H ⁺	45
Table 4.5 ¹ H and ¹³ C NMR shifts (ppm) of acetonitrile and its complexes with Be(II), Mg(II) and H ⁺ .	46
Table 4.6 Mulliken charge[a] of acetonitrile and its complexes with Be(II), Mg(II) and H ⁺ .	47
Table 4.7 Vibrational stretching frequencies (cm ⁻¹) of acetonitrile and its Be(II), Mg(II) and H ⁺ complexes.	47
Table 4.8 Orbital occupancies [†] of acetonitrile and its complexes with Be(II), Mg(II) and H ⁺	51
Table 4.9 s versus p characters in C ₂ -N ₃ and C ₁ -C ₂ σ-bonds.	52
Table 4.10 G3, CBS-QB3 and G4 binding energies of acetonitrile complexes with Mg(II), Be(II) and H ⁺ in vacuum and water [†] .	55
Table 4.11 Vibrational frequencies and NMR shifts of Mg(II) and Be(II)	60

complexes with n-pentane carbonitrile, 2 equivalents of acetonitrile, malononitrile and the uncomplexed receptors.

Table 5.1. CHELPG charges for 1a, 1b, 1c, 2, 1c-Mg and 2-Mg .	77
Table 5.2 Overlap population, M-N spin, M-O spin, total spin and metal atomic valence for 2-cyanoethanal enolate (1c), 2-cyanoethanal keto form (1a) and 2-cyanoethanal enol form (1b).	82
Table 5.3 Design parameters for 1,2-dicyanoethylene.	84
Table 5.4 CHELPG charges of metal and heteroatoms in Mg(II) complexes with ethylene glycol methyl ether (3), butanal-3-one enol (4), 2-cyanoethanal enolate (1c) and 1,2-dicyanoethylene (2 or DCNE)	87
Table 5.5 Metal atomic valence and overlap population design parameters for Mg(II) and Ca(II) complexes with ethylene glycol methyl ether (3), butanal-3-one enol (4), 2-cyanoethanal enol (1b) and 1,2-dicyanoethylene (2 or DCNE)	89
Table 5.6 G4 Dissociation energies of HCO_2H and HCO_2^- .	90
Table 6.1 Mulliken atomic charges for 2-CN BD, 3-CN P and its complexes with beryllium(II).	100
Table 6.2 Dihedral angles of 2-CN BD, 3-CN P and its complexes with Be(II).	101
Table 6.3 Bond angle in 2-CN BD , 3-CN P and its complexes with Be(II).	101
Table 6.4.GIAO ^{13}C NMR shifts (ppm) with TMS reference of 2-CN BD, 3-CN P and its complexes with Be(II).	102
Table 6.5 Vibrational frequencies of Be-N and Be-C vinyl	103

Table 6.6 NBO populations of 2-CN BD and Be(II)- 2-CN BD	105
Table 6.7 Percentages of s versus p characters in C3-C4 and C5-N6 σ -bonds in 2-CN BD and Be(II)- 2-CN BD.	106
Table 6.8 Benchmark reactions involving beryllium compounds (G3 and NIST energies in kcal/mol)	107
Table 6.9 Beryllium(II) dissociation energies involving Be(II) complexes as measure of stabilization by receptor models; using one water molecule as reference.	109
Table 6.10 G4 dissociation energies of 2-cyanobutadiene complexes	109
Table 6.11. Metal valence and overlap population analysis	110

List of Figures	Page
Figure 2.1 Modern pH ISE glass membrane	14
Figure 2.2 Common setup for polymer membrane based ISE	15
Figure 2.3 Structures of a) Valinomycin, b) Ionomycin, c) Calcimycin and d) Nonactin	17
Figure 2.4 USB sensor with screen printed electrode	18
Figure 2.5 Typical setup for standard hydrogen electrode (SHE)	20
Figure 2.6 Saturated Calomel Electrode (SCE)	21
Figure 2.7 Two types of Ag/AgCl reference electrode (a) double junction and (b) single junction.	23
Figure 3.1 Generalized process flow which represents the adopted approach of this study.	25
Figure 3.2 Anatomy of a basis set: C atom, 6-31G**	28
Figure 3.3 Anatomy of a basis set: Mg atom, QZVP	29
Figure 3.4 Sensor cell layers	35
Figure 3.5 Typical test setup for sensor evaluation	36
Figure 4.1 α -p Conjugation stabilized acetonitrile-cation complex	38
Figure 4.2 G3 optimized geometries of acetonitrile and its complexes with Be(II), Mg(II) and H^+ .	45
Figure 4.3 Selected G3 molecular orbitals of acetonitrile and its complexes with Mg(II)	48
Figure 4.4 G4 Dissociation energy versus N-M vibrational frequency (in vacuum)	50
Figure 4.5 H6 1H NMR shift versus H6 charge (G3, vacuum)	54
Figure 4.6 N3-Cation bond distance versus acetonitrile binding energy (G4, vacuum)	57

Figure 4.7 Optimized geometries of n-pentane carbonitrile and its complex with Mg(II)	59
Figure 4.8 Optimized geometry of Mg(II) complex with two equivalents of acetonitrile	61
Figure 4.9 Optimized geometries of malononitrile and its complex with Be(II)	62
Figure 4.10 (a) Planar optimized structure of Be(II) complex with malononitrile; (b) conjugated π -network in malononitrile-Be(II).	63
Figure 4.11 Selected molecular orbitals of malononitrile (i) and (iii); malononitrile-Be(II) complex (ii) and (iv)	64
Figure 4.12 Lowering of acetonitrile MO energies due to interaction with cations	65
Figure 4.13 Response of fabricated chemical sensor with cyclopentane carbonitrile immobilized in acrylic copolymer membrane.	67
Figure 4.14 The IR spectra of acetonitrile and acetonitrile-Mg(II) complex	67
Figure 5.1. Ionomycin and extracted fragment models	72
Figure 5.2. Optimized geometries of 2-cyanoethanal keto form (1a) 2-cyanoethanal enol form (1b), 2-cyanoethanal enolate (1c) and 1,2-dicyanoethylene (2) calculated using B3LYP/6-31+G(d,p).	74
Figure 5.3. Optimized geometries of 1a-Mg, 1b-Mg, 1c-Mg and 2-Mg calculated using B3LYP with 6-31+G(d,p) basis sets for non-metals and QZVP for metals.	75
Figure 5.4. Electrostatic Potential contours of 2-cyanoethanal keto form (1a), 2-cyanoethanal enol form (1b), 2-cyanoethanal enolate (1c) and 1,2-dicyanoethylene (2). The red contour indicates the negative electrostatic potential.	77
Figure 5.5 CHELPG charges of (a) 2-cyanoethanal enolate (1c) (b) 1c-Mg	78
Figure 5.6 Population overlap and metal atomic valence plots obtained from AOMix calculations.a) M-N Spin vs M-O Spin(b) Metal Valence vs Total Spin.	79
Figure 5.7 G4 dissociation energy and total spin plots for complexes of cations with 2-cyanoethanal enolate (a) G4 Dissociation energy vs Total spin (b) The C-C-N bond angle vs Total Spin	81
Figure 5.8 Metal valence, G4 dissociation energy and total spin plots for complexes of cations with 2-cyanoethanal enolate (a) Metal valence vs Total Spin (b) G4 Dissociation energy vs Total Spin.	83
Figure 5.9 . Optimized geometries 3-dimensional rational design calculated using B3LYP with 6-31+G(d,p) basis sets for non-metals and QZVP for metals (a) complex of Mg(II) with ethylene glycol methyl ether (3), butanal-3-one enol (4) and formate (5b), (b) complex of Mg(II) with ethylene glycol methyl ether (3), butanal-3-one enol (4) and 1,2-dicyanoethylene (2), (c)	85

complex of Mg(II) with ethylene glycol methyl ether (3), butanal-3-one enol (4) and 2-cyanoethanal enolate (1c), (d) complex of Mg(II) with ethylene glycol methyl ether (3), butanal-3-one enol (4) and 2-cyanoethanal enol (1b) form, (e) complex of Mg(II) with ethylene glycol methyl ether (3), butanal-3-one enol (4) and (f) complex of Ca(II) with ethylene glycol methyl ether (3), butanal-3-one enol

Figure 5.10 Design parameter plots from complexes of	88
Figure 6.1 Computed B3LYP/6-31+G(d,p) geometries of	95
Figure 6.2. Optimized geometries of Be(II)-2-CN BD cyclic complex,	98
Figure 6.3 Optimized geometries of Be(II)-3-CN P cyclic complex and Be(II)-3-CN P acyclic complex.	99
Figure 6.4. Interaction between C4 and Be.	105
Figure 6.5 Frontier Molecular orbitals(FMO) of 1 and its cyclic complex with Be(II).	107
Figure 6.6. Plot of metal atomic valence versus overlap population in	111
Figure 6.7 Energy profile of 2-CN BD and its complexes with Be(II)(M) Uncomplex (C1) Reactant, (TS) Transition Structure and (C2) Product.	112
Figure 6.5 Frontier Molecular orbitals(FMO) of 1 and its cyclic complex with Be(II).	107
Figure 6.8 Optimized geometries of simple models	114

Lis of Abbreviations

CCSD(T)	Coupled-cluster theory with single, double and triple excitations
CHELPG	Charges from Electrostatic Potentials
ChemFET	Chemical Field-Effect Transistor
DFT	Density Functional Theory
GIAO	Gauge-Independent Atomic Orbital
Gn	Gaussian n, n=1,2,3,4
GTO	Gaussian Type Orbital
HF	Hatree-Fock
HLC	High level correlation
kcal/mol	Kilocalorie per mole
LDA	Local-density approximations
LSDA	Local spin-density approximation
MP2	Møller–Plesset perturbation theory 2 nd order
MP4	Møller–Plesset perturbation theory 4 th order
NBO	Natural Bonding Orbitals
NMR	Nuclear Magnetic Resonance
PPM	Parts-per-million
PVC	Polyvinyl Chloride
QCISD(T)	Quadratic configuration interaction with a pertubative treatment of triple substitution
STO	Slater Type Orital
ZPE	Zero Point Energy

Chapter 1 :Introduction

1.1 Preface

Computational chemistry allows chemists to simulate chemical structures and reactions numerically, exclusively or in part, based on fundamental laws of physics (Foresman *et al.*, 1996). The value of *ab initio* calculations for molecular geometries has been well established, particularly by the systematic work of Pople and co-workers (Yarkony, 1995). The improvements in theoretical methods and computing power have brought *ab initio* methods into the domain of accurate methods. These methods have been proven to reproduce experimental results and were unachievable in the previous decades (Tajti *et al.*, 2004). It is practical today to handle billions of configurations, and to achieve chemical accuracy in binding energies and geometries of reasonably complex molecules (Hoffmann, 1998). With the advantages provided by computational chemistry, it is justified to use computational methods to design the target receptor molecules based on systematic and logical approach, step-by-step and continuously guided, since the beginning, by sound rationale and chemical principles. In most cases interactions between heteroatom-containing functionalities and metal cations have been exploited as means for the receptor models to recognize monovalent and divalent cations from Group I and II of the periodic table.

1.2 Applications of Chemical Sensors

Charged organic and inorganic species have been the focus of intensive studies by numerous research groups over the past few decades. Two distinct categories of these workers seem apparent; those who resort in chemical technologies and novel materials and molecules to build selective sensing devices, and another who exploit the power of computing and information technology to build precision state-of-the-art instruments. Interesting, the same cationic and anionic analytes are of interest in a wide range of applications or industrial verticals. Plant macronutrients, essential to its growth and consumed in relatively large quantities, such as nitrate, phosphate, potassium, calcium and magnesium, must be routinely monitored at precision or parts-per-million (ppm) levels. While potassium, calcium and magnesium are also dietary requirement for the human body function, and thus relatively harmless, excessive uptake of nitrate by plants, and eventually stored in its roots, fruits and leaves, are toxic to human at sub-ppm levels (0.3 ppm according to some sources) (Greer *et al.*, 2005). On the other hand, excessive application of phosphate is not only a financial burden to farmers, its run-off also ends up in ground water and other sources of fresh and drinking water. Phosphate fertilizer run-off has been documented as the main cause of algae-blooming that kills aquatic lives in lakes due to suffocation (Arquitt *et al.*, 2004). Consequently, it is also crucial to continuously monitor the levels of these ionic analytes in the environment, and it could be significantly more challenging since it must be done autonomously and often at much lower levels, *i.e.* hundreds ppm of nitrate monitored as plant nutrient is now monitored at sub-ppm level as environmental pollutant. Using chemical sensor technology to address the above problems is often not straight forward and far from the preferred plug-and-play approach. In real field application, not only costly technologies are required to realize these systems, the accuracy of the measurement data is almost always hampered by the limitations of the sensing elements.

While selective determination can be achieved using sensor technology, signal error due to interference from competing ions can severely limit the use of this approach, if not aggressively mitigated (Umezawa *et al.*, 2000; Umezawa *et al.*, 1995).

1.3 Aim of Study

To evaluate the performance of nitrile and carbonyl based molecules as cation receptor

1.4 Objectives

The objectives of this study are as follows;

1. To study the electronic structure of the receptor molecules using computational method.
2. To calculate the dissociation energy of the receptors with target analytes.
3. To fabricate electrochemical sensor cells based on target receptors.
4. To characterise electrochemical sensor behaviour.

1.5 Thesis Outlines

The outline of this dissertation is as follows;

Chapter 1 briefly introduces computational chemistry and the application of chemical sensor. Chapter 2 provides literature background on computational chemistry and sensors. Chapter 3 describes the computational details and fabrication of chemical sensor.

Chapter 4 entitled “G3 Assisted Rational Design of Chemical Sensor Array Using Carbonitrile Neutral Receptors”, is the first of three chapters that exploit computational methods in systematically constructing recognition molecules for cations. This chapter revolves around the interaction of unsaturated carbonitriles such as acetonitrile and *n*-pentylcarbonitrile with cations utilizing G3 method. Details on the geometries,

frequencies, charge, population and energy are elaborated in this chapter. This work has been published by MDPI and can be accessed through the following; Sensors (Basel).2013 Oct 14;13(10):13835-60. doi: 10.3390/s131013835.

In Chapter 5, the nature of heteroatom-metal interaction based on carbonitrile-carboxaldehyde receptor models was probed. Three key heteroatom-containing functionalities in Ionomycin, ethylene glycol dimethyl ether, butanal-3-one and formic acid, have been used as cation receptor models. The three fragments, along with 2-cyanoethanal and 1,2-dicyanoethylene, have been individually examined, and three-dimensional structures involving these receptor models have been studied in order to provide rationale for magnesium *versus* calcium selectivity, and the ability of the chosen models to discriminate monovalent cations from Group I of the periodic table. This work has been accepted by the Journal of Molecular Modeling, Springer for publication.

Chapter 6 deals with a rarely reported divalent cation – the beryllium cation. In this chapter, the possibility of employing conjugated carbonitriles as recognition molecules for Be(II) was studied. 2-Cyanobutadiene (2-CN BD) and 3-Cyanopropene (3-CN P), stabilized by π -network have been extensively examined in its ability to form covalent interaction with Be(II) at the vinyl terminal carbon. The differences between the cyclic and acyclic form of Be(II)-2 CN BD in terms of geometries, charge, NMR shift and energy were investigated. This work has been submitted to the New Journal of Chemistry, Royal Society of Chemistry for publication.

Chapter 2 : Literature Review

The following chapter describes the background of computational details which are applied in this work. This chapter also includes the literature review on sensor development with a particular focus on metal ion detection.

2.1 Density Functional Theory

The Density Functional Theory (DFT) methods derived from quantum mechanics especially the Thomas-Fermi-Dirac model (Dirac, 1928; Fermi, 1928; Thomas, 1927). DFT approach uses modeling of electron *via* general functional of the electron density. An early approximation of the exchange function (E_X) can be described using the Slater's exchange;

$$E_X[\rho(\mathbf{r})] = -\frac{9\alpha}{8} \left(\frac{3}{\pi}\right)^{1/3} \int \rho^{4/3}(\mathbf{r}) d\mathbf{r}$$

ρ =ground-state density of the system

$\alpha=2/3$ for true electron gas

(Equation 2.1)

The successful applications of DFT in computing molecular structures and ground state energies were initially demonstrated by the Hohenberg-Kohn theorem (Hohenberg *et al.*, 1964). Most of the current DFT methods follow the approach of Kohn and Sham (Kohn *et al.*, 1965). In their breakthrough work in 1965, Kohn and Sham suggested that

a Hamiltonian can be expressed as a sum of one-electron operator having eigenvalues that are sum of the one-electron eigenvalues;

$$h_i^{KS} X_i = \varepsilon_i X_i$$

Where;

$$h_i^{KS} = -\frac{1}{2}\nabla_i^2 - \sum_K^{nuclei} \frac{Z_K}{|r_i - r_K|} + \int \frac{\rho(r')}{|r_i - r'|} dr' + V_{xc}$$

Where;

$$V_{xc} = \frac{\delta E_{xc}}{\delta \rho}$$

X=Exchange

C=Correlation

ε_i = the orbital energy

(Equation 2.2)

The electronic energy in the above approximate function has been partitioned into several terms and can simplified in the following equation;

$$\mathbf{E} = \mathbf{E}^T + \mathbf{E}^V + \mathbf{E}^J + \mathbf{E}^{xc} \quad \textbf{(Equation 2.3)}$$

\mathbf{E}^T = kinetic energy term

\mathbf{E}^V = nuclear-electron attraction and nucleic pair repulsion

\mathbf{E}^J = electron-electron repulsion term

\mathbf{E}^{xc} = exchange-correlation term

All terms, except the nuclear-nuclear repulsion, are functions of electron density (ρ), the heart of the density functional approach.

The exchange-correlation term is determined exclusively by electron density and is therefore a functional of ρ . It includes the dynamic correlation for the motion of individual electrons under investigation.

In hybrid functional such as the widely used B3LYP (Becke, 1993a), the exchange-correlation term (E^{XC}) is commonly further partitioned to separate the exchange (E^X) and correlation (E^C) parts of the electron density functional;

$$E^{XC} = E^X + E^C \quad \text{(Equation 2.4)}$$

Furthermore, the E^X and E^C components can be further categorized as having two types; when it depends only on electron density (ρ), and the gradient at ($\nabla\rho$) must be considered, it is called gradient-corrected.

The early density functional approximations focusing only on local density (LDA or LSDA) have been ruled to be quite inaccurate due to poor description of the used spatial terms.

Significant improvements in molecular calculations have been obtained when non-local or gradient of density terms are added to the density function. This correction to the insufficient local approximation is known as the ‘generalized gradient approximation’ or GGA. In most applications, the gradient corrected functionals are built by adding the gradient correction term to the local term *i.e* LDA or LSDA;

$$\varepsilon_{X/C}^{GGA}[\rho(r)] = \varepsilon_{X/C}^{LSDA}[\rho(r)] + \nabla\varepsilon_{X/C} \left[\frac{|\nabla\rho(r)|}{\rho^{4/3}(r)} \right] \quad \text{(Equation 2.5)}$$

2.2 Basis Sets

A basis set in theoretical and computational chemistry refers to the set of functions which are combined in linear combinations (generally as part of a quantum chemical calculation) to build molecular orbitals. John C. Slater first introduced the basis set known as Slater-Type Orbital (STO) (Slater, 1930) that was improved later by S. Francis Boys and known as Gaussian-Type Orbitals (GTO) (Boys, 1950). Slater-type orbitals proved to be too computationally demanding for routine calculations and the improvement done by S.F Boys, who used linear combinations of Gaussian orbitals to approximate the Slater-type orbitals, was found to be more practical, and thus was employed and further improved until recently. The GTO is four to five times faster than STO but with reduced accuracy that can be compensated by combining more Gaussian equations. The “minimal” basis set given by the form of STO-NG (N represents the number of GTO’s combined), where the shape of the STO function can be approximated by summing up a number of GTOs with different exponents and coefficients.

2.2.1 Split Valence Basis Set

The minimal basis set describes only the most basic aspects of the orbitals. The problem with the minimal basis set is its lack of flexibility. When bonds are formed, orbitals usually contract, and the minimal basis set cannot adequately describe such changes in orbitals. The solution is to represent each orbital with two and more functions denoted as “extended” basis set and that’s the idea behind n-tuple- ζ basis sets (double-zeta, triple-zeta, quadruple-zeta, *etc.*) (Davidson *et al.*, 1986). Due to the enormous amount of calculation required to calculate a double-zeta for every orbital, the group of John Pople introduced the “split-valence” basis set that only treat the valence orbital as

double-zeta and the inner-shell orbital as single Slater orbital (Frisch *et al.*, 1984). Their basis sets come in the form of;

$$\mathbf{X-Yzg}$$

(Equation 2.6)

where X represents the number of primitive Gaussian orbital for core atomic orbital; Y and Z indicate that the valence orbitals are composed of two basis functions each. Commonly used basis-sets are 3-21G and 6-31G. The presence of two numbers (Y and Z) implies that this basis set is a split-valence double-zeta basis set. The triple and quadruple zeta basis sets are represented by X-YZWg and X-YZWWg respectively.

Dunning and co-workers adopt double-zeta, triple-zeta, quadruple-zeta with “correlation-consistent polarized” and valence-only basis-set. The basis sets are known as cc-pVNZ where N=D,T,Q,5,6 (Dunning, 1989).

2.2.2 Polarized Basis Sets

Polarized basis sets allow the orbital (*s*, *p*, *d* and *f*) to distort due to polarization effects. Pople and co-workers introduced a simple nomenclature scheme to indicate the presence of these functions, the ‘*’. Thus, 6-31G* implies a set of *d* functions added to polarize the *p* functions in 6-31G. A second star (**) implies *p* function is added to describe H and He, (6-311G**) (Frisch *et al.*, 1980).

2.2.3 Diffuse Function

Standard basis sets are often ‘augmented’ with diffuse basis functions when the calculation involves molecules with lone pair, anions, system with large electron

separation from nucleus and excited states system. Diffuse basis sets are represented by the '+' signs. One '+' means that we are accounting for the 'p' orbitals, while '++' signals that we are looking at both 'p' and 's' orbitals (Foresman *et al.*, 1996).

2.3 The Gn Theory

The Gaussian-n (Gn) theories had been developed by Pople and Curtiss (Curtiss *et al.*, 2002; Curtiss *et al.*, 1998; Curtiss *et al.*, 1991; Curtiss *et al.*, 2007; Pople *et al.*, 1989) aimed at getting accurate energies without requiring extensive computer resources. The composite technique used by Gn theory involved multi-step jobs of *ab-initio* calculation in order to obtain accurate energies with mean absolute deviation of less than 1 kcal/mol for Gaussian-4 (G4) (Curtiss *et al.*, 2011).

2.3.1 The Gaussian-1 (G1) and Gaussian-2 (G2) Theories

The Gaussian-1 (G1) theory was the first composite method developed by Pople's group (Pople *et al.*, 1989) that covers both the first and second row of elements in the periodic table. The Gaussian-1 (G1) theory was replaced within two years by the Gaussian-2 (G2) theory (Curtiss *et al.*, 1991) to fix some known issues. Table 2.1 shows the overview of steps and jobs involved for the G1 and G2 theory.

Gaussian-2 (G2) theory is a composite procedure, using HF, MP2, MP4 and QCISD(T) to obtain accurate energy determination. The total energy for G2 is as follows;

$$\begin{aligned}
 E_0[\text{G2}] = & E(\text{QCISD(T)/6-311G(d,p)}) + E(\text{plus}) \\
 & + E(2\text{df,p}) + E(\Delta) + E(\text{HLC}) \\
 & + E(\text{ZPE})
 \end{aligned}
 \tag{Equation 2.7}$$

Table 2.1 Overview of steps and jobs for G1 and G2

Step	Job	Result	Notes
1	HF/6-31G(d) Opt Freq	ZPE	Scale by 0.8929
2	MP2(Full)/6-31G(d) Opt	Geometry	Start from HF result: use this geometry for all later job
3	MP4/6-311G(d,p)	E^{base}	Base level energy
4	MP4/6-311+G(d,p)	ΔE^+	$=\text{Energy}-E^{\text{base}}$
5	MP4/6-311G(2df,p)	$\Delta E^{2\text{dpf}}$	$=\text{Energy}-E^{\text{base}}$ (set to 0 if >0)
6	QCISD(T)/6-311G(d,p)	ΔE^{QCI}	$=\text{Energy}-E^{\text{base}}$
7	Any Job	ΔE^{HLC}	$=-0.00019n_{\sigma} + -0.00595n_{\beta}$
8	MP2/6-311+G(3df,2p)	Δ^{G2}	$=\text{Energy} - E^{\text{step5(MP2)}} - E^{\text{step4(MP2)}} + E^{\text{step3(MP2)}}$
9	Any Job	Δ^{HLC}	$=+0.00114n_{\beta}$

A frequency calculation with the HF/6-31G(d) basis set is used to obtain the zero-point vibrational energy, $E(\text{ZPE})$. The geometry generated from the result was further optimized using MP2/6-31G(d) basis set. This optimized geometry is used for all subsequent calculations. The correlated energy, $E(\text{QCISD(T)}/6\text{-}311\text{G(d,p)})$ calculated from quadratic configuration interaction calculation with single and double excitations and a triple excitation contribution (QCISD(T)) with the 6-311G(d) basis set. The difference between MP4/6-311G(d,p) and MP4/6-311+G(d,p) calculations was labelled as E^+ , to assess the effect of diffuse functions. The effect of higher polarization functions, $E(2\text{df,p})$, is obtained as the difference between MP4/6-311G(d,p) and MP4/6-311G(2df,p) calculations.

The $E(\Delta)$ value obtained from this equation;

$$E(\Delta) = E(\text{MP2/6-311+G(3df,2p)}) - E(\text{MP2/6-311G(2df,p)}) - \\ E(\text{MP2/6-311+G(d,p)}) + E(\text{MP2/6-311G(d,p)}) \quad \textbf{(Equation 2.8)}$$

Finally, the $E(\text{HLC})$ is a ‘higher level correction’ equal to $-An_{\beta}-Bn_{\alpha}$, wherein n_{β} and n_{α} are the number of β and α valence electrons, respectively, with $n_{\alpha} \geq n_{\beta}$. The G2 theory had been validated by using G2/97 test set with a mean absolute deviation from experiment of 1.57 kcal/mol for the enthalpy of formation. Even though the G2 theory performed well on the test set, the errors became significantly higher for larger molecules thus leading to the rise of G2 variant, and subsequently, the formation of the Gaussian-3 Theory.

2.4 Chemical Sensor

Chemical sensor can be defined as “A device that transforms chemical information, ranging from the concentration of a specific sample component to total composition analysis, into an analytically useful signal, mostly an electrical signal that can be translated by an analyzer” (Adam *et al.*, 1991). The input signal for chemical sensor is the chemical composition of a sample solution in contact with the sensor while the output signal in the form of electrical signal be it voltage, current or capacitance (Mikhelson, 2013). This work focused only on potentiometric-based chemical sensor namely the ion-selective electrode (ISE) that will be explained in the next section.

2.5 Ion-Selective Electrode

Koryta defined an ion-selective electrode (ISE) as an electroanalytical sensor with a membrane whose potential indicates the activity of the ion to be determined in a solution (Koryta, 1986). The ISE had gain the interest of many researchers for many decades owing to its ability to measure without the burden of turbidity or color of analytes (Arnold *et al.*, 1984; Buck, 1978). Many industrial players already realized the potential of ISEs in view of its low operating costs, ease of handling and the possibilities for continuous monitoring (Koryta, 1986).

The ISEs can be classified by its membrane, whether it is glass or polymer based membrane. The glass membrane ISEs (Figure 2.1) had been used in the early 20th century particularly for pH sensing. Cremer was the first to observe potential changes between two solutions with different acidity that was separated by a thin glass membrane (Cremer, 1906). Haber and Klemensiewicz were the first to report the utilization of glass membrane as a tool to measure hydrogen ion (pH) (Haber *et al.*, 1909). The glass membrane electrode for pH had been the most frequently used among other ISEs. Nowadays, pH sensitive glasses membrane are manufactured primarily from silicon dioxide (SiO₂) which is connected *via* a tetrahedral network. SiO₂ based glass membrane had been known to be resistant towards aggressive chemicals thus can be used on harsh condition (Mikhelson, 2013).

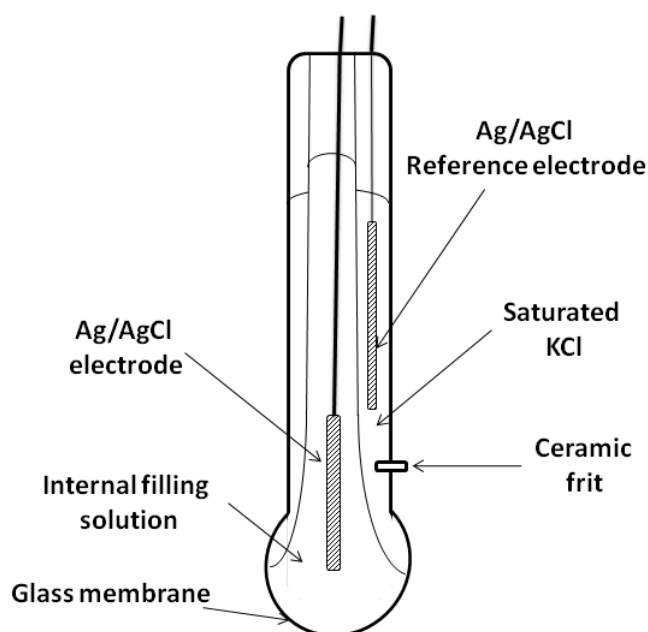


Figure 2.1 Modern pH ISE glass membrane

Polymer based membrane (Figure 2.2) had been devised in view to obtain sensitivity towards other cation and anion with the use of ionophores. With large variety of ionophores available, the ability to fabricate many types of ISEs is possible. The details for ionophores will be covered later in section 2.6. The most widely used polymeric membrane is poly(vinyl chloride) (PVC) although other types of membrane are also gaining interest such as silicone rubbers, polyurethanes, acrylates and perfluoropolymers (Armstrong *et al.*, 1990; Bakker *et al.*, 1997; Craggs *et al.*, 1974). The desired characteristics of the polymer membrane material includes the ability to repel water (hydrophobic), mechanically robust, stable within the operational temperature range and chemically inert (Mikhelson, 2013). PVC-based membranes required a plasticizer to increase its durability and flexibility to become functional (Cadogan *et al.*, 1996). Because of the high amount of plasticizer used in the membrane, the leaching of the membrane components into sample solution had become an issue. The solution of this issue will be discussed later.

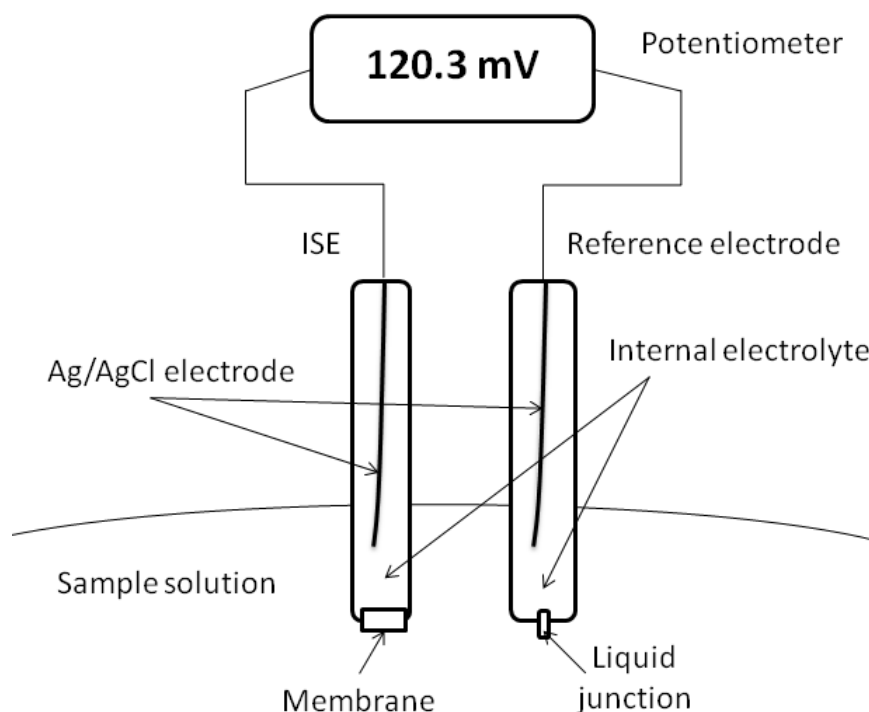


Figure 2.2 Common setup for polymer membrane based ISE

2.5.1 Acrylic Membrane Electrode

Acrylic-based membrane electrode had been utilized to overcome the limitation of widely used PVC-based membrane (Dror *et al.*, 1987). Acrylic-based membrane has superior strength, durability and adhesion on the surface compared to PVC-based membranes. (Levichev *et al.*, 1994; Stibor *et al.*, 2005). Even though the acrylic-based membrane had been studied since the 1970s, only during this decade had it been gaining popularity due to the success on fabricating sensor (Heng *et al.*, 1996).

The usage of plasticizer was required to soften the PVC-based membrane to make it functional. Due to the high portion of plasticizer used (up to 60% w/w), it leads to the leaching of the plasticizer from membrane, that could limit the lifetime of sensors (Zahran *et al.*, 2014). In order to eliminate the needs for plasticizer, self-plasticizing membrane had been explored successfully with the application of photocuring method

on methacrylic–acrylic co-polymers (Ambrose *et al.*, 1996; Heng *et al.*, 2001). Methyl methacrylate (MMA) and *n*-butyl acrylate (nBA) co-polymer had the photocuring ability to be utilized as photocurable membrane with the help of 2,2-dimethoxy-2-phenylacetophenone (DMPP) photoinitiator and hexanediol diacrylate (HDDA) crosslinker.

2.6 Potentiometry

According to Nernst equation (Equation 2.9), potential difference (voltage signal) in the potentiometry sensor at constant temperature is directly related to the difference in activity between the analyte and the internal reference (represented by K_{eq}) which is directly above the electrochemical transducer layer. The natural logarithmic form can be converted to logarithmic of base 10, and the product of gas constant, Faraday constant at 273.15 K gives a constant of 59 mV. Equation 2.9 predicts that a change in a decade (ten fold) in activity would give a potential difference of 59 mV for singly charged ions, and the change is halved to about 29 mV for doubly charged ions (Daniel, 1987).

$$E_{cell} = E_0 - \frac{RT}{nF} \ln(K_{eq}) \quad \text{(Equation 2.9)}$$

E = total potential (mVolt)

E_0 = standard potential by 297.15K (mVolt)

R = universal gas constant (8.314 J/mol K)

T = temperature (K)

n = charge of ion

F = Faraday constant (96485.3 C/mol)

2.7 Ionophores

An ionophore is a lipid-soluble molecule that facilitates transmission of an ion across a lipophilic membrane by combining with the ion or by increasing the permeability of the barrier to it. These molecules make complexes with such cations and provide ion binding specificity due to the size of the cavity created when the cyclic molecule is formed. Some notable ionophores are Valinomycin (Lofrumento *et al.*, 2011; Watanabe *et al.*, 2005; Zhao *et al.*, 2010), Ionomycin (Erdahl *et al.*, 1995; Kauffman *et al.*, 1980), Calcimycin (Erdahl *et al.*, 1994; Raatschen *et al.*, 2012) and Nonactin (Kosaki *et al.*, 2012; Patko, 2009; Tan *et al.*, 2011). The strcture are as shown in Figure 2.3

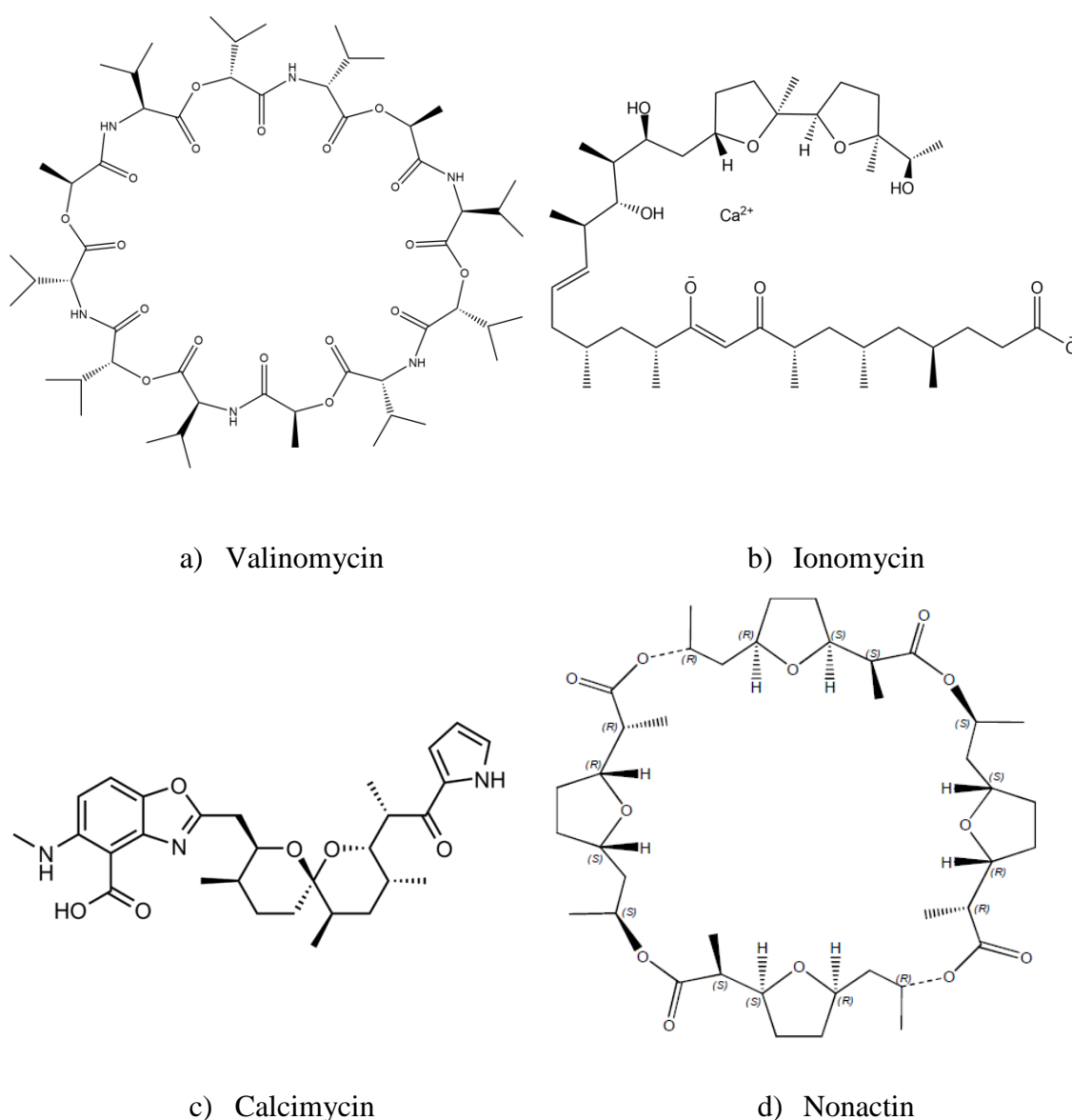


Figure 2.3 Structures of a) Valinomycin, b) Ionomycin, c) Calcimycin and d) Nonactin

2.8 Screen-Printed Electrode

Screen-printed electrode (SPE), commonly utilized for miniaturized devices are manufactured by printing multiple layers of different ink materials on a Printed Circuit Board (PCB). The ink used is usually based on carbon, gold, platinum or silver. Semi-automatic screen-printer can be used to prepare disposable SPE with a well-designed pattern (Figure 2.4). The printed electrochemical cells consist of working electrode, counter-electrode and a reference electrode. The low production cost, the ease of mass production, the flexibility in design, and the possibility of using small volumes make these devices very attractive for practical use (Cristea *et al.*, 2009; Wang *et al.*, 2012).

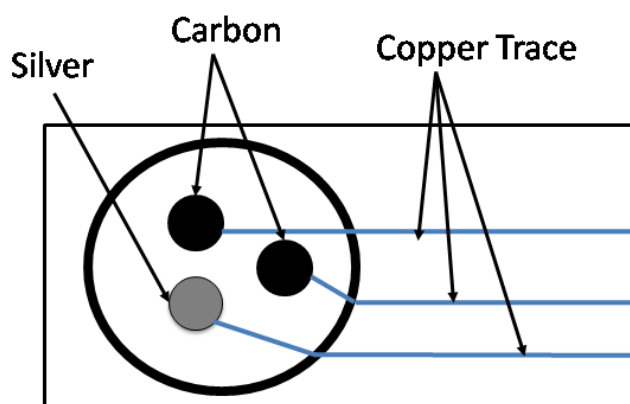


Figure 2.4 USB sensor with screen printed electrode

2.9 Electrochemical Transducer

The transducer functions in converting one form of energy to another (Agarwal *et al.*, 2005). The electrochemical transducer uses a chemical change to measure the input parameter; the output is a varying electrical signal proportional to the chemical change.

A Chemical transducer is commonly made of a conducting or semiconducting material that is coated with a selected monomolecular, multimolecular, ionic, or polymeric membrane of a chemical modifier and that, by means of faradaic (charge-transfer)

reactions or interfacial potential differences (no net charge transfer), exhibits chemical, electrochemical, and/or optical properties of the film. The transducer as such does not show selectivity towards multiple ions (Durst *et al.*, 1997).

2.10 Chemical Field-Effect Transistor (ChemFET)

Potentiometric sensors can be miniaturized into a FET-based architecture, called a ChemFET, among the smallest chemical sensors available, particularly suitable for miniaturization because the integrity of the transduced signal that carries chemical information does not depend on the sensing area. The schematic of a ChemFET is similar to that of a metal–oxide–semiconductor field-effect transistor (MOSFET), except that the gate structure is slightly modified. Based on the gate structure, the family of chemFETs can be divided into three main types, which are the ion-sensitive field-effect transistors (ISFETs), enzymatically selective field-effect transistors (ENFETs), and basic ChemFETs (Polk, 2002; Wilson *et al.*, 2001). All of these ChemFET structures work on the basic principle that the surface charge changes at the interface between the insulator and the overlying layer (Yotter *et al.*, 2004). Extensive research had been conducted on ChemFETs for monitoring ammonium (Brzózka *et al.*, 1997; Senillou *et al.*, 1998), cadmium and lead (Reinhoudt, 1995), Cu^{2+} (Taillades *et al.*, 1999), hydrogen (Domanský *et al.*, 1998), and pH (Bausells *et al.* 1999; (Bausells *et al.*, 1999; Chiang *et al.*, 2001).

2.11 Reference Electrode

IUPAC's Gold Book defined reference electrode as “An electrode that maintains a virtually invariant potential under the conditions prevailing in an electrochemical measurement, and that serves to permit the observation, measurement, of the indicator

working electrode” (McNaught *et al.*, 1997). A reference electrode is needed to provide stable potential signal as reference (Scott *et al.*, 2007).

The standard hydrogen electrode (SHE) had been used as a universal reference electrode for many years. The reference electrode consists of platinized platinum electrode immersed in an acidic solution, with constant supply of hydrogen (H₂) gas (refers to Figure 2.5). Redox reaction occurs on the surface of the inert platinum electrode (Boyes, 2002; Zoski, 2007). The redox reaction is as follows;



The constant flow of hydrogen gas over platinised platinum caused the reaction to reach equilibrium. The standard electrode potential (E⁰) generated from this reaction assigned as 0.00 V and becomes the standard reference point for other electrodes (Skoog, 2004; Trasatti, 1986).

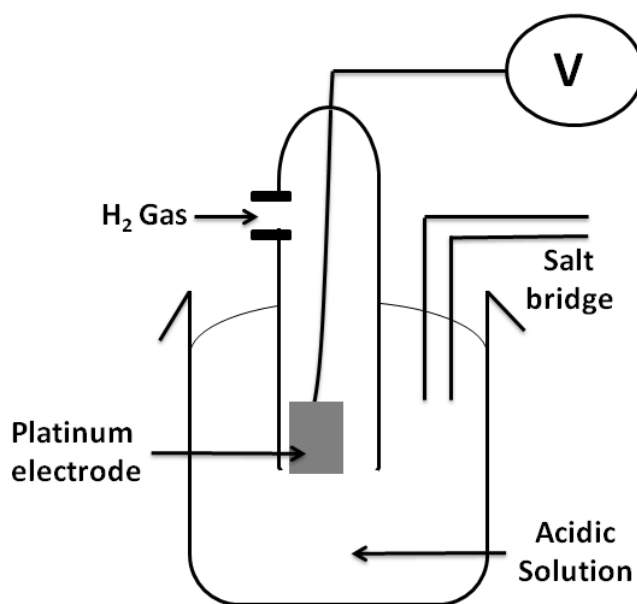
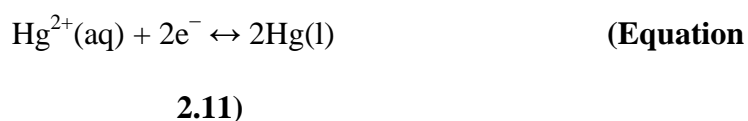


Figure 2.5 Typical setup for standard hydrogen electrode (SHE)

This type of electrode can be constructed using readily available lab apparatus. Due to the size and the needs for constant H₂ gas supply, SHE was almost impossible to be used on field for *in situ* measurement. Hence, the inception of other types of reference electrode namely saturated calomel electrode (SCE) and silver-silver chloride electrode (Ag/AgCl).

Saturated calomel electrode (SCE) was the most utilized reference electrode during the 60s-70s (Gagne *et al.*, 1980; Glasoe *et al.*, 1960). This electrode was based on Hg/Hg₂Cl₂ in saturated KCl solution (Bhasin, 2012).



The mercury/mercury chloride paste is filled in a tube with tiny opening that allows contact with saturated KCl (Figure 2.6). The saturated KCl keeps the potential of the electrodes stable; $E^0 = +0.2444 \text{ V vs SHE}$ at 25 °C (Skoog, 2004).

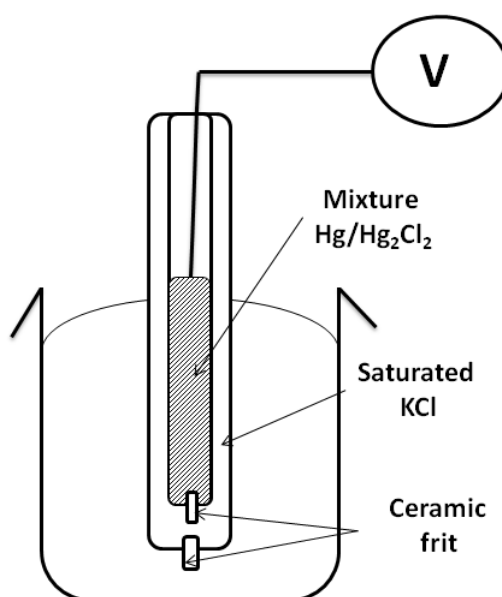
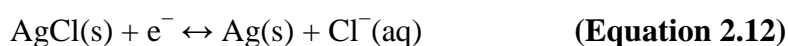


Figure 2.6 Saturated Calomel Electrode (SCE)

As stated above, SCE contains liquid mercury that can pose danger to both the human and environment (Gustafsson, 1995; Hylander, 2001). As of today, The United Nations Environment Programme (UNEP) has signed off on the Minamata Convention, a new global agreement that will ban mercury from most uses by the year 2020 (Selin, 2014). Considering the effects of mercury, another type of reference electrode, the silver/silver chloride electrode had become the current standard for reference electrode.

2.11.1 Silver/Silver Chloride Reference Electrode

In the interest of having a reference electrode which is reliable, cost effective, simple to construct and low toxicity, the silver/silver chloride electrode fulfils all the desired requirements for reference electrode. Typically, this reference electrode comprises of a single silver (Ag) wire coated with silver chloride (AgCl) which both immersed in aqueous saturated potassium chloride (KCl) and silver chloride (AgCl) solution. The potential of Ag/AgCl was determined by the redox reaction of silver and its chloride salt ion generating standard potential (E^0) of 0.230 V vs SHE (Ewing, 1997; Janz *et al.*, 1968; Skoog, 2004).



The stability and reversibility of this electrode are achieved by the usage of partially soluble AgCl and saturated KCl that provide fixed amount of chloride ions. As with SCE, Ag/AgCl electrode system also requires liquid junction in order to maintain a steady flow of electrolyte to complete its circuit. The existence of liquid junction in the form of ceramic frit allows the leakage of electrolyte (saturated KCl and AgCl) to the sample solution. Likewise, reverse-contamination can also happen when the sample solution leaked into the electrolyte thus rendering the reference electrode

unusable (Zoski, 2007). Double junction reference electrode had been introduced to overcome this problem (Figure 2.7).

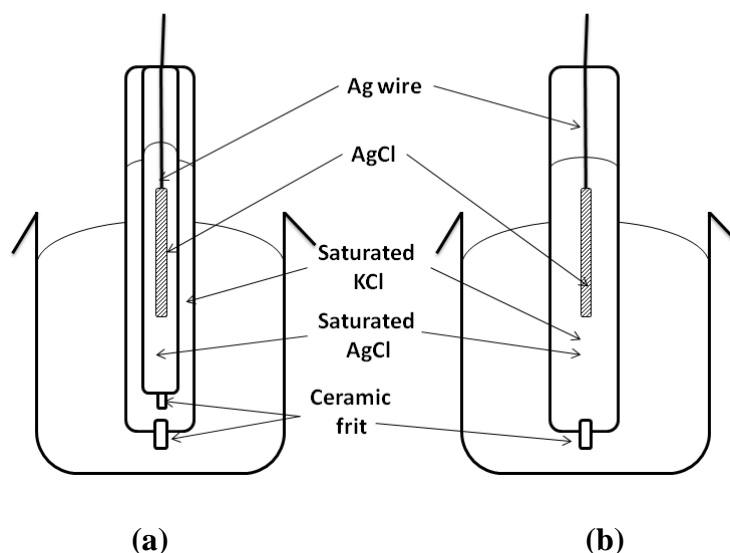


Figure 2.7 Two types of Ag/AgCl reference electrode
(a) double junction and (b) single junction.

The design of double junction reference electrode required physical separation between the saturated AgCl against saturated KCl. Typical approach to achieve this is to provide an inner tube that contains both Ag wire and saturated AgCl, which is in contact with the outer tube containing saturated KCl through a ceramic frit. The outer tube with the electrolyte (KCl) formed a 'salt bridge' between the inner tube and the sample solution. The outer tube works as a buffer, slowing down the changes in the composition of the reference electrode electrolyte (Cazes, 2004; Comeau *et al.*, 2008).

Chapter 3 : Methodology

3.1 General Approach

This research focuses on designing molecules to recognize specific examples of Group I and II cations. While most efforts are dedicated to computational works, some of the rationally designed molecules are fabricated and the sensor was tested for response in the desired range.

Most of Group I and II cations have been looked out throughout this work but the following have received most attention; magnesium(II) and calcium(II) have been dealt with significant depth in order to understand the nature of heteroatom interaction with these divalent cations, and in providing logical explanation to the effects of charge (at higher pH) to selectivity. Disparity in overlap population, in electron-sharing mechanism, between different heteroatoms and their forms (keto, enol and enolate) in interacting with these two divalent cations have also been emphasized. Beryllium(II) is another divalent cation that has received special attention. This work focuses on the ability of Be(II) to form a covalent interaction with terminal vinyl group, after first forming a strong bond with cyano nitrogen atoms. Group I cations, especially H^+ , Li^+ , Na^+ and K^+ , are discussed mainly in the sensor array application wherein consistent signal ratio is the main concern.

In rational design of divalent cation ionophores, Group I cations are discussed again, in providing explanation on how the alkali metal monovalent cations can be discriminated based on charge-to-radius ratio (or surface charge density argument). Size exclusion argument, presumably is an important design strategy, is not explored in this work. Figure 3.1 showed the generalized workflow of this study.

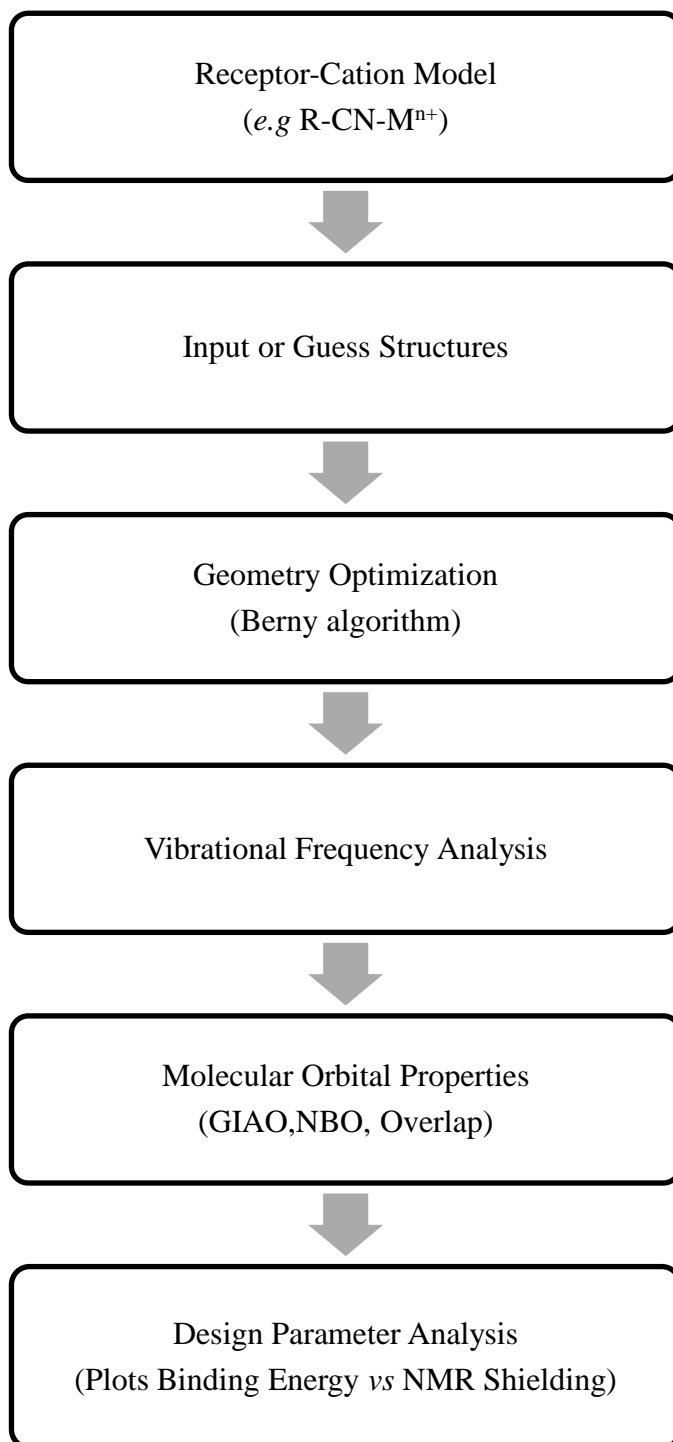


Figure 3.1 Generalized process flow which represents the adopted approach of this study.

Three specific cases have been investigated in significant depths as described in chapter four, five and six;

Case 1: The use of DFT and G3 theory in providing rational design of cation sensor array using saturated carbonitrile receptor models.

Case 2: Exploitation overlap population from AOMix in heteroatom-metal interaction to design selective divalent cation ionophores having Ionomycin fragment models and carbonitrile-carboxaldehyde receptor models.

Case 3: Exploitation of π -network in conjugated carbonitrile in forming favourable vinyl-beryllium interaction.

In the following sections, descriptions of the adopted methods and tools for the following simulation jobs are dealt with in details; geometry optimization, molecular orbital analysis, population analysis, nuclear magnetic shielding analysis, overlap population and charge analysis.

3.2 Hybrid Functionals

In this section specific and widely used exchange and correlation functional are provided but without elaborate comments. Becke88 has been widely used in DFT method (Becke, 1988). This is an example of the so-called gradient-corrected exchange functional, having the following description;

$$E_{Becke88}^X = E_{LDA}^X - \delta \int \frac{\rho^{4/3} X^2}{1 + 6 \delta \sin^{-1} X} d^3 \vec{r} \quad (\text{Equation 3.1})$$

The Becke Three Parameter Hybrid Functionals is a well known hybrid functional which is popular amongst quantum chemists. These functionals have the form devised by Becke in 1993 (Becke, 1993b; Vosko *et al.*, 1980).

$$A * E_X^{\text{Slater}} + (1-A) * E_X^{\text{HF}} + B * \Delta E_X^{\text{Becke}} + E_C^{\text{VWN}} + C * \Delta E_C^{\text{non-local}} \quad (\text{Equation 3.2})$$

where A , B , and C are 0.20, 0.72, 0.81, respectively, (constants determined *via* fitting to the G1 test set). There are several variations of this hybrid function. **B3LYP** uses the non-local correlation provided by the LYP expression, and VWN functional III for local correlation (not functional V). Note that since LYP includes both local and non-local terms, the correlation functional used is actually

$$C * E_C^{\text{LYP}} + (1-C) * E_C^{\text{VWN}} \quad (\text{Equation 3.3})$$

wherein VWN is used to provide the excess local correlation required, since LYP contains a local term essentially equivalent to VWN.

3.3 Basis Sets

Pople's split-valence double-zeta basis set was used in this calculation with the keyword syntax as follows: 6-31+G(d,p) designates the 6-31G; the core orbital is a Contracted Gaussian-type Orbital (CGTO) made of 6 Gaussians, and the valence is described by two orbitals — one CGTO made of 3 Gaussians, and one single Gaussian, the basis set supplemented by diffuse s and p functions for non-hydrogen atoms, one set of d functions and supplemented by one set of p functions on hydrogens. This basis set 6-31+G(d,p) was used for all non-metal atoms (Figure 3.2).


```

****
C      0
S      6      1.00
      3047.5249000      0.0018347
      457.3695100      0.0140373
      103.9486900      0.0688426
      29.2101550      0.2321844
      9.2866630      0.4679413
      3.1639270      0.3623120
SP     3      1.00
      7.8682724      -0.1193324      0.0689991
      1.8812885      -0.1608542      0.3164240
      0.5442493      1.1434564      0.7443083
SP     1      1.00
      0.1687144      1.0000000      1.0000000
D      1      1.00
      0.8000000      1.0000000
****

```

Figure 3.2 Anatomy of a basis set: C atom, 6-31G**

The Ahlrichs basis set, quadruple zeta valence quality (QZVP), made popular by H.F. Schaefer had been utilized in our calculation for metal atoms. It is believed, QZVP is the most accurate polarized Gaussian basis set that is available for our metal of interest (Figure 3.3) (Weigend *et al.*, 2005; Weigend *et al.*, 2003b).

```

****
Mg      0
S      10      1.00
      605967.7875300      0.14430176617E-04
      90569.0946920      0.11249871807E-03
      20574.2528440      0.59264972450E-03
      5818.6284865      0.24988770424E-02
      1895.6296075      0.90230775141E-02
      683.45941021      0.28579919806E-01
      266.18219762      0.79064453923E-01
      110.11220010      0.18269337814
      47.777041234      0.32157193967
      21.542166149      0.35028259389
S      3      1.00
      174.12136378      0.22931111278E-01
      53.484972498      0.19151777552
      20.500213307      0.61155711055
S      1      1.00
      9.8056826922      1.0000000
S      1      1.00
      3.5402989348      1.0000000
S      1      1.00
      1.5450850046      1.0000000
S      1      1.00
      0.66540195432      1.0000000
S      1      1.00
      0.14355439071      1.0000000
S      1      1.00
      0.66624673468E-01      1.0000000

```

S	1	1.00		
		0.29772648266E-01		1.0000000
P	8	1.00		
		893.20460829	0.34958267428E-03	
		211.78258286	0.29811890111E-02	
		68.443200537	0.15517845758E-01	
		25.727265349	0.57578659557E-01	
		10.606634281	0.15610307853	
		4.5934126484	0.29230912580	
		2.0100469807	0.37219024072	
		0.87384841536	0.27578088891	
P	1	1.00		
		0.35615076666	1.0000000	
P	1	1.00		
		0.18995954356	1.0000000	
P	1	1.00		
		0.74580135669E-01	1.0000000	
P	1	1.00		
		0.29221641309E-01	1.0000000	
D	1	1.00		
		3.8100000	1.0000000	
D	1	1.00		
		0.6500000	1.0000000	
D	1	1.00		
		0.2000000	1.0000000	
D	1	1.00		
		0.0520000	1.0000000	
F	1	1.00		
		0.1600000	1.0000000	

Figure 3.3 Anatomy of a basis set: Mg atom, QZVP

3.4 The Gaussian-3 (G3) Theory

G3 geometry optimization (Curtiss *et al.*, 1998; Pickard *et al.*, 2006) is done at MP2 level using smaller 6-31G basis set instead of the 6-311G basis set employed in G2 Theory (Curtiss *et al.*, 1991), and the structure is used to calculate harmonic frequencies and for all subsequent calculations. The final MP2 calculations use a larger basis set (G3large) and both the core and valence electrons are correlated. Correction for correlation effects beyond a fourth-order perturbation theory is done with quadratic configuration interaction calculation with single and double excitations and a triples excitation contribution (QCISD(T)) (Curtiss & Raghavachari, 2002). Additional core correlation corrections are included through a spin-orbit and valence electron empirical

correction. Different empirical parameters are also introduced in the higher level correction (HLC) (Namazian *et al.*, 2008).

3.5 The Gaussian-4 (G4) Theory

The Gaussian-4 Theory is the improvement over G3 theory with mean absolute deviation of 0.83 kcal/mol from experiment for the comprehensive collection of 454 energies (for main group molecules) in the G3/05 test set (Curtiss *et al.*, 2011). G4 Theory uses B3LYP/6-31G(2df,p) instead of MP2(full)/6-31G* (in G3), for structure optimization, harmonic frequency and all subsequent calculations (Curtiss *et al.*, 2007). Hartree-Fock energy limit E (HF/limit) is determined using two-point extrapolation scheme and Dunning's aug-cc-pVnZ basis sets. For correlation correction beyond the fourth-order perturbation theory, CCSD(T)/6-31G* is used instead of QCISD(T)/6-31G* (in G3). The HLC has the same form as in G3 but with two additional parameters. MQZVP basis sets are parts of Truhlar's M06 and M06-2X functionals (Zhao *et al.*, 2008a, 2008b). These are modified version of Ahlrich's higher polarization QZVP basis set recommended for correlated treatments (Jensen, 2013; Weigend *et al.*, 2003a). The Ga to Kr QZVP bases include a diffuse d function to polarize $4p$ AO and add $2f1g$ sets from Dunning (Zhong *et al.*, 2008). Table 3.1 shows the overview of the G4 method.

Table 3.1 Overview of The G4 Theory

Step	Job	Result	Notes
1	B3LYP/6-31G (2df,p) Opt Freq	Optimized structure	
2	B3LYP/6-31G (2df , p)	E (ZPE)	Scaled by 0.9854
3	HF/aug-cc-pVnZ	$E_{\text{HF/aug-cc-pVnZ}}$	$= E_{\text{HF/limit}} + B \exp(-\sigma n)$
4	MP4/6-31G (d)	$\Delta E(\text{G3LargeXP})$	$E[\text{MP2}(\text{full})/\text{G3LargeXP}]$ $- E[\text{MP2}/6-31\text{G}(2\text{df},\text{p})]$ $- E[\text{MP2}/6-31 + \text{G}(\text{d})]$ $+ E[\text{MP2}/6-31\text{G}(\text{d})]$
5	NA	$E(\text{combined})$	$E[\text{MP4}/6-31\text{G}(\text{d})] + \Delta E(+)$ $+ \Delta E(2\text{df},\text{p}) + \Delta E(\text{CC})$ $+ \Delta E(\text{G3LargeXP}) +$ $\Delta E(\text{HF}) + \Delta E(\text{SO})$
6	NA	$E_e(\text{G4})$	$= E(\text{combined}) + E(\text{HLC})$
7	NA	$E_0(\text{G4})$	$= E_e \text{ G4} + E \text{ ZPE}$

3.6 Special Tools

These special tools are integrated inside Gaussian09 software package and can be accessed by using specific keywords except for AOMix. The AOMix software package can be downloaded for free from their website.

3.6.1 Natural Bond Orbital (NBO)

Gaussian NBO version 3.1 has been utilized to calculate atomic orbital occupancies and its contribution to bonding interaction and delocalization of electron density within the receptor models and its complexes (Reed *et al.*, 1988).

3.6.2 NMR Gauge-Independent Atomic Orbital (GIAO)

The ^{13}C NMR isotropic shielding tensors was calculated with the GIAO method using the optimized structures obtained from DFT calculation (Cheeseman *et al.*, 1996). All of the NMR spectroscopy results were referred to tetramethylsilane, $(\text{CH}_3)_4\text{Si}$ as reference. The shielding and deshielding effects can be seen on the chemical shift parameter.

3.6.3 Integral Equation Formalism Polarizable Continuum Model (IEF-PCM)

The IEF version of the PCM solvation method was employed to estimate the effect of water solvation on binding energies (Tomasi *et al.*, 1999). IEF is one of the family members of Polarizable Continuum Model (PCM) (Miertuš *et al.*, 1981) along with DPCM (Barone *et al.*, 1998) and CPCM (Klamt *et al.*, 1993). The IEF-PCM had been adopted due to its general flexibility and faster than the other two methods (Tomasi *et al.*, 2005).

3.6.4 AOMix

The AOMix package helps to analyze the nature of the chemical bonding in molecular systems. The $2\mathbf{c}_{ai} \mathbf{c}_{bi} \mathbf{S}_{ab}$ terms, where $a \in \text{atom } A$ and $b \in \text{atom } B$, are the overlap populations between the two atoms with atomic orbitals χ_a and χ_b respectively of the i^{th} MO. The total overlap population (TOP) between atoms A and B in a molecule is calculated by adding together overlap populations for orbitals centered on these two atoms:

$$\text{TOP}_{AB} = \sum_i n_i \sum_{a \in A} \sum_{b \in B} 2\mathbf{c}_{ai} \mathbf{c}_{bi} \mathbf{S}_{ab} \quad (\text{Equation 3.4})$$

where \mathbf{c}_{ai} is the LCAO-MO coefficient of χ_a on atom A , \mathbf{c}_{bi} is the coefficient of χ_b on atom B , both in the i^{th} MO, and \mathbf{S}_{ab} is the overlap integral for these two AOs.

The overlap populations (OP) concept can be extended to the analysis of the bonding between the central atom and the ligands in transition metal complexes or other large molecules. In AOMix, Equation 3.5 is applied to user-defined fragments (which can be individual atoms, groups of atoms, or an atomic orbital or groups of orbitals):

$$OP_{AB,i} = \sum_{a \in A} \sum_{b \in B} 2c_{ai} c_{bi} S_{ab} \quad \text{(Equation 3.5)}$$

The TOP_{AB} and $OP_{AB,i}$ values are printed in the *AOMix* output files. Positive OP_{AB} values represent a bonding interaction and $OP_{AB} \approx 0$ indicates no bonding between the fragments.

3.7 Hardware Details

Calculations were performed with a Gaussian 09 Revision C.01 program package (Frisch *et al.*, 2010) on Intel Core i5-2467M CPU @ 1.60GHz with 4.00 GB of ram. Higher level of calculations require utilization of UM workstation with Intel Xeon CPU E31245 @ 3.30GHz with 8.00 GB of RAM.

3.8 Experimental Details

In the following sections, options of specific chemical sensor fabrication device platform such as screen printed electrode, electrochemical transducer and polymeric membrane of choice are explained.

3.8.1 List of Chemicals

Methyl methacrylate (MMA), *n*-butyl acrylate (n-BA), 2-hydroxyethyl methacrylate (HEMA) hexanediol diacrylate (HDDA) crosslinker, 2,2-dimethoxy-2-phenylacetophenone (DMPP) photoinitiator and sodium tetraphenyl borate lipophilic agent were purchased from Sigma-Aldrich (Milwaukee, WI, USA). Cyclopentane carbonitrile cation recognition molecule was procured from Fluka (Buchs, Switzerland). Magnesium chloride and potassium chloride were obtained from Merck KGaA (Darmstadt, Germany). All chemicals were used as received without further purification.

3.8.2 Sensor Fabrication

The sensor was fabricated as depicted in Figure 3.4. The sensing membrane is a self-plasticized acrylic co-polymer having 2 parts of MMA and 8 parts of n-BA, by volume, called MB28. Acrylic co-polymer had been chosen due to its superiority against commonly used PVC as described in Section 2.5.1. Initially, 100 μ L of MMA, 400 μ L of n-BA, 6.2 mg of DMPP and 0.5 μ L HDDA were prepared as MB28 monomer mixture. DMPP act as photoinitiator to promote the polymerization of acrylic co-polymer upon exposure to intense UV light. Adequate amount of HDDA is required to link the co-polymer together. Later, 100 μ L of the MB28 mixture was mixed with 1 mg of sodium tetraphenylborate and 5 μ L of cyclopentylcarbonitrile to afford the cation sensing cocktail. The sodium tetraphenylborate replacing the generally-used potassium tetrakis(4-chlorophenyl)borate as ion-exchange sites due to its better price-to-performance ratio.

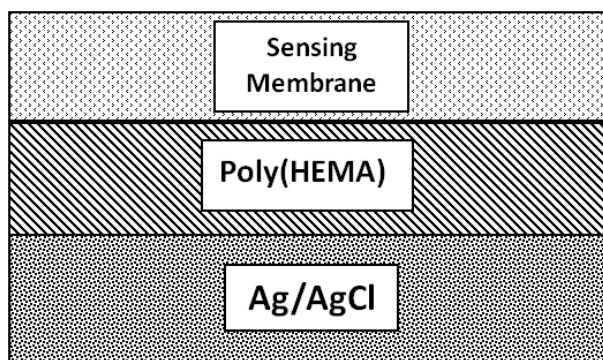


Figure 3.4 Sensor cell layers

Poly(HEMA) was used as the internal layer that provides a constant concentration of cation. The HEMA cocktail was prepared by mixing 500 μL of HEMA, 6.2 mg of DMPP and 0.5 μL HDDA. The electrochemical transducer electrode was prepared by screen printing of silver-silver chloride paste onto FR4 printed board and oven dried at 120 $^{\circ}\text{C}$ to give a dry thickness of approximately 100 μm . The HEMA cocktail (2 μL) was dispensed on the silver-silver chloride electrode and photocured under UV for 3 min. The photocured poly(HEMA) hydrogel was hydrated by conditioning in 0.1 M KCl for 10 min. The MB28 cocktail (3 μL) was dispensed on top of the hydrated poly(HEMA) hydrogel and photocured under UV for 3 min.

3.8.3 Sensor Evaluation

Three concentrations (1×10^{-4} , 1×10^{-3} and 1×10^{-2} M) of Mg(II) and K^{+} solutions were prepared by dissolving the chloride salts respectively in deionized water. Calibration curve was obtained from the standard solution prepared before. Mg(II) and K^{+} mixtures in 1:1 and 1:10 were also prepared in order to investigate the sensor response in mixtures.

The sensing electrode and a double-junction reference electrode (Thermo Fisher Scientific, Waltham, MA, USA) are connected to Thermo Orion ion meter, immersed in the calibration solutions and the potential signals recorded (as shown in Figure 3.5).

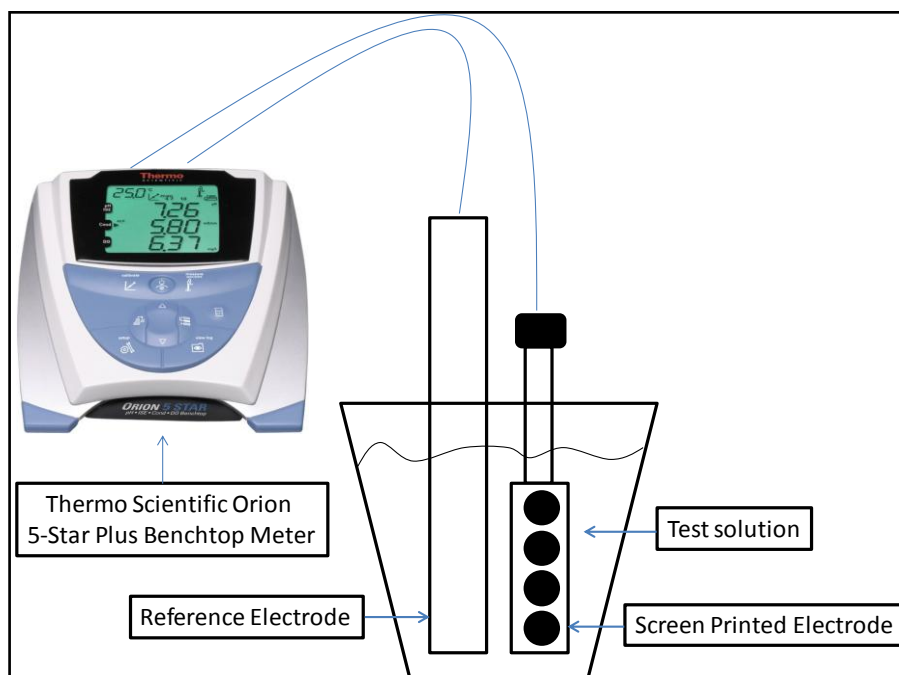


Figure 3.5 Typical test setup for sensor evaluation

Chapter 4 : G3 Assisted Rational Design of Chemical Sensor Array Using Carbonitrile Neutral Receptors

Combined computational and experimental strategies on systematic design of chemical sensor array using carbonitrile neutral receptors are presented. Binding energies of acetonitrile, *n*-pentane carbonitrile and malonitrile with Ca(II), Mg(II), Be(II) and H⁺ have been investigated with B3LYP, G3, CBS-QB3, G4 and MQZVP methods, showing a general trend of H⁺ > Be(II) > Mg(II) > Ca(II). Hydrogen bonding, donor-acceptor and cation-lone pair electron simple models were employed in evaluating the performance of the computational methods. Mg(II) is bound to acetonitrile in water by 12.5 kcal/mol, and in the gas phase the receptor is more strongly bound by 33.3 kcal/mol to Mg(II) compared to Ca(II). Interaction of bound cations to carbonitrile reduces the energies of the MO's involved in the proposed σ -p conjugated network. Planar malonitrile-Be(II) complex possibly involves π -network with cationic methylene carbon. Fabricated potentiometric chemical sensors show distinct signal patterns that can be exploited in sensor array applications.

4.1 Introduction

Carbonitriles can be synthesized by a variety of preparative procedures and the functionality can be transformed further to numerous functional groups (March, 1992). The cyano functional group appears as synthetic equivalents in useful carbon-carbon formation steps (Fleming, Gudipati, *et al.*, 2002; Fleming & Shook, 2002; Fleming *et al.*, 2000; Fleming, Zhang, *et al.*, 2002). However this synthetically feasible functionality has rarely been considered for detection of ionic species. In this work we described combined computational and experimental strategies in exploiting unconjugated carbonitrile moieties for chemical sensor array applications (Duarte *et al.*, 2009; Duarte *et al.*, 2010). Acetonitrile is a simple model for unconjugated carbonitrile receptor and extensively analyzed in this work. The carbon-carbon bond in acetonitrile is much shorter compared to that in ethane (Afeefy *et al.*, 2005), and this has been attributed to σ -conjugation that could facilitate binding to metal cations (Fleming, 2011) (Figure 4.1).

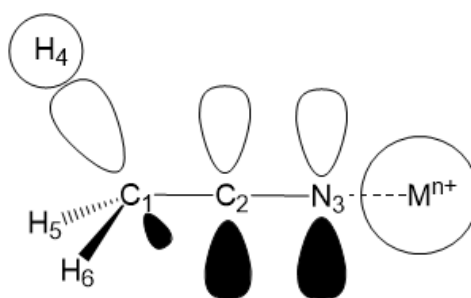


Figure 4.1 α -p Conjugation stabilized acetonitrile-cation complex

Electrochemical sensors such as ion selective electrode (ISE) (Heng & Hall, 2001) and chemically modified field effect transistor (ChemFET) (Moschou *et al.*, 2001; Reinhoudt, 1995; Wroblewski *et al.*, 2001) are the most commonly employed devices for detecting ionic analytes. In these sensors, chemical activity is converted to voltage signal using reversible reduction-oxidation electrode such as silver-silver

chloride or doped conducting polymer (Zhu *et al.*, 2003). The sensor signal is baselined to a reference electrode, typically a double-junction silver-silver chloride electrode having constant chloride concentration and suitable external electrolytes. A common sensor error arises from false signals due to interfering ions. Only when the sensor selectivity is very high and in the presence of low concentrations of interfering ions, this type of noise can be neglected (Umezawa *et al.*, 1995). In cases where the analyte is surrounded by high concentration of interfering ions, a high selectivity sensor will no longer give reliable measurement. The situation is even worse when the required linear range is narrow or the limit of detection is at sub-ppm level.

Selectivity requirement for chemical sensors depends on the intended target application. Our electrochemical sensors primarily target ionic analytes in agriculture, aquaculture, environmental monitoring and medical applications. Linear range and accuracy requirement for the same analyte differ tremendously across verticals. For example nitrate sensor in precision agriculture normally monitors the nutrient in the range of 100 to 300 ppm, whereas, for nitrate-poisoned carrot detection capability at less than 10 ppm is more appropriate. A more striking difference in requirement can be seen in dissolved ammonia sensors. The requirement for monitoring dissolved ammonia in industrial discharge before treatment is at tens of ppm, whereas, in aquaculture application, unionized ammonia is considered lethal at sub-ppm levels (*National Recommended Water Quality Criteria*, 2002).

Here in this chapter, we employed computational method in designing neutral receptor molecules for charged analytes. Our target applications require detection of sodium, potassium, magnesium, calcium, ammonium, nitrate, phosphate, chloride and sulfate. In sensor array approach the burden on achieving very high selectivity towards

target analyte is relieved because the accuracy is no longer determined by sensor selectivity alone. In fact, the main challenge in sensor array approach is the ability in recognizing signal patterns produced by different analyte concentrations in the presence of interfering ions.

Neutral receptor molecules (ionophores) typically exploit organic functional groups to achieve binding with target analyte (Duncan *et al.*, 2001; Malinowska *et al.*, 2000). In cation recognition, electron lone-pairs on heteroatoms, carbonyl group and heterocycles are often used, whereas for binding to anions, different types of hydrogen bonds are utilized (Antonisse *et al.*, 1997). In cation recognition, the combination of heteroatom lone pairs and ring cavity size could discriminate metal cations based on ionic radius size. This strategy does not work for anions, where the Hofmeister effect dominates selectivity trend (Zhang *et al.*, 2006). Selective detection of neutral molecules is much more challenging and enzymes give the most reliable results. Synthetic receptors for small neutral molecules need to use combinations of the already mentioned strategies including complex cavity shape or molecular imprint (Boyd *et al.*, 2004; Pernites *et al.*, 2011).

4.2 Results and Discussion

4.2.1. Computational Benchmarks

Accuracy of the adopted computational methods has been benchmarked with receptor-analyte binding models. The benchmarks compare the performance the computational methods with each other and whenever available, with experimental values. The benchmark models illustrate simple cases relevant to interactions between chemical sensor and target molecules.

Table 4.1 Bond distances (r) and dissociation energies (De) of water dimer benchmark

2(H ₂ O)	G3	CBS-QB3 ^[b]	MQZVP	Exptl ^[a]
H-O ($r_{\text{H-O}}$, Å)	1.954	1.925	1.956	NA
O-O ($r_{\text{O-O}}$, Å)	2.913	2.886	2.918	2.978
H-O Freq (cm ⁻¹)	181.3	204.0	184.6	186.83
D _e (kcal/mol)	3.5	3.4	3.1	3.16

[a] Experimental values from refs (Keutsch *et al.*, 2003; Xu *et al.*, 2004)
[b] Complete Basis Set (CBS) methods of Petersson and coworkers for computing very accurate energies involving several pre-defined calculations on the specified system.

The geometry, vibrational frequencies and binding energy of water dimer represent a simple and useful benchmark for receptor-analyte weak interaction involving hydrogen bonding. The experimental distance between the two water molecules measured as the distance between two oxygen atoms ($r_{\text{o-o}}$) is 2.978 Å (Table 4.1) (Keutsch *et al.*, 2003; Xu & Goddard III, 2004). The G3 and MQZVP methods give comparable $r_{\text{o-o}}$ (2.913 Å and 2.918 Å, respectively) and close to the experimental value, whereas, the separation in CBS-QB3 is considerably shorter (3%). Similarly, the G3 and MQZVP vibrational frequencies for hydrogen bonding are closer to each other while CBS-QB3 predicts the interaction to be stronger by 20 cm⁻¹. All three computational methods are able to reproduce experimental dissociation energy of water dimer within 1 kcal/mol.

Donor-acceptor type interaction is another well-known computational benchmark that is applicable to chemical sensor design. Optimized structures of ammonia-borane complex, nitrogen-boron bond distances, vibrational frequencies and dissociation energies of the complex were calculated using G3, CBS-QB3 and MQZVP methods (Table 4.2). Available experimental data are provided for comparison purposes (Cramer *et al.*, 1997; Richardson *et al.*, 1995).

Table 4.2 Bond distances (r) and dissociation energies (De) of ammonia-borane benchmark.

NH ₃ -BH ₃	Vacuum			H ₂ O ^[b]			Exptl ^[a]
	G3	CBS-QB3	MQZVP	G3	CBS-QB3	MQZVP	
B-N ($r_{\text{B-N}}$, Å)	1.661	1.664	1.658	1.626	1.627	1.630	1.580
B-H ($r_{\text{B-H}}$, Å)	1.209	1.208	1.206	1.214	1.213	1.190	1.150
N-H ($r_{\text{N-H}}$, Å)	1.020	1.017	1.014	1.020	1.018	1.010	0.960
B-N Freq(cm ⁻¹)	605.0	636.5	642.4	NA	722.4	NA	NA
D _e (kcal/mol)	28.0	27.8	24.8	35.1	34.9	31.8	NA

[a] Experimental values from ref (Cramer & Gladfelter, 1997; Richardson *et al.*, 1995).
[b] Water solvation effect was modeled using iefpcm method as in (Tomasi *et al.*, 1999)

Due to the stability of the ammonia-borane adduct in water, the respective results in water media are also provided. The three methods afford practically the same gas-phase boron-nitrogen bonds that reproduces the experimental bond length determined by neutron diffraction method on NH₃-BH₃ crystals (Klooster *et al.*, 1999). In water, the $r_{\text{B-N}}$ values are consistently shorter and practically identical. The G3 and CBS-QB3 gas-phase dissociation energies are quite comparable, that is about 3 kcal/mol higher than predicted by MQZVP method. The dissociation in water follows similar trend, with MQZVP gives 3 kcal/mol lower. The shorter $r_{\text{B-N}}$ bond lengths and higher D_e in water strongly suggest greater stability of the ammonia-borane pair in water, presumably due to stabilization of the ionic complex in polar solvents. The three methods predict the same value (1.21 Å) for nitrogen-hydrogen bond distances, and there is no solvent effect on $r_{\text{B-H}}$ values. However, the neutron diffraction measurement reported a shorter bond length (1.15 Å). Likewise, all the predicted nitrogen-hydrogen bond lengths are almost identical (1.02 Å), and again there is no solvent effect. The experimental $r_{\text{N-H}}$ measured by neutron diffraction method is slightly less than 1 Å. MQZVP and CBS-QB3 predicts boron-nitrogen stretching frequencies of approximately 640 cm⁻¹, 40 cm⁻¹ higher than G3 prediction. The computed N-B stretching in water is about 80 cm⁻¹ higher –

consistent with a stronger interaction and shorter bond distance. Furthermore, the ammonia-borane binding energies are in keeping with the predicted geometries. The three methods show that the ammonia-borane complex is strongly bound, and the interaction is more than 5 kcal/mol stronger in water. The energy predicted by MQZVP is 3 kcal/mol lower compared to the G3 and CBS-QB3 energies. If this benchmark can be generalized to other donor-acceptor systems, MQZVP method is expected to predict lower binding energies.

Another important benchmark useful in neutral receptor design is the interaction of electron lone pairs on heteroatom to metal cations. Interactions of Mg(II) ion with water and hydrogen cyanide in the gas phase are compared by employing the G3 and G4 methods on the lone-pair-cation system (Table 4.3).

Table 4.3 G3 and G4 geometries and binding energies of Mg(II) complexes with HCN and H₂O[†]

Mg(II)-NCH	G3	G4	Mg(II)-OH ₂	G3	G4
Mg-N ($r_{\text{Mg-N}}$, Å)	2.016	1.965	Mg-O ($r_{\text{Mg-O}}$, Å)	1.948	1.917
N-C ($r_{\text{N-C}}$, Å)	1.168	1.149	O-H ($r_{\text{O-H}}$, Å)	0.989	0.979
Mg-N Freq (cm ⁻¹)	498.7	510.2	Mg-O Freq (cm ⁻¹)	563.1	571.5
D _e (kcal/mol)	92.0	92.6	D _e (kcal/mol)	80.6	81.5
[†] Experimental data are unavailable					

The binding energies differences between the G3 and G4 methods, for both cases (H₂O and HCN), are less than 1 kcal/mol. The G4 Mg-N and Mg-O bonds are shorter and consequently the stretching frequencies are larger with the G4 method. The C-N and O-H bonds produced by the two Gn methods differ by about 0.01 Å.

4.2.2. Acetonitrile – Carbonitrile Simple Receptor Model

Acetonitrile lacks a π -conjugation system and serves as a simple model for unconjugated carbonitrile. Geometry optimizations in vacuum and solvated media were initially explored using B3LYP method and 6-31+G(d,p) basis set. Subsequently G3, G4, CBS-QB3 and MQZVP methods were performed to obtain structures and energies at these levels of theory. The C1-C2 bond distance, predicted by all computational methods are apparently shorter (1.460 Å, G3; Figure 4.2 and Table 4.1) compared to the carbon-carbon single-bond in ethane (1.532 Å, B3LYP)(Data provided in Appendix A). These results are in good accord with experimental bond distances that report shorter carbon-carbon bond distances in acetonitrile (1.458 Å) and butadiene (1.476 Å), compared to that in ethane (1.536 Å) (Afeefy *et al.*, 2005).

Shortening of the carbon-carbon bond in butadiene by 4% has been attributed to *p-p* conjugation, widely known as hyperconjugation (Carey *et al.*, 2007). Practically this refers to interaction of two $2p_z$ orbitals at C2 and C3 in butadiene that improves the entire π -network. This is supported by preference for adoption of planar conformation that maximizes the overlapping of adjacent $2p_z$ orbitals (Fleming, 2011; Rauk, 1994; Yu, 2012). Likewise, as depicted in Figure 4.1, the shrinking of the C1-C2 bond in acetonitrile by close to 5% compared to ethane (B3LYP) can be attributed to σ -*p* interaction similar to the hyperconjugation reasoning, described earlier (Pauling, 1960a).

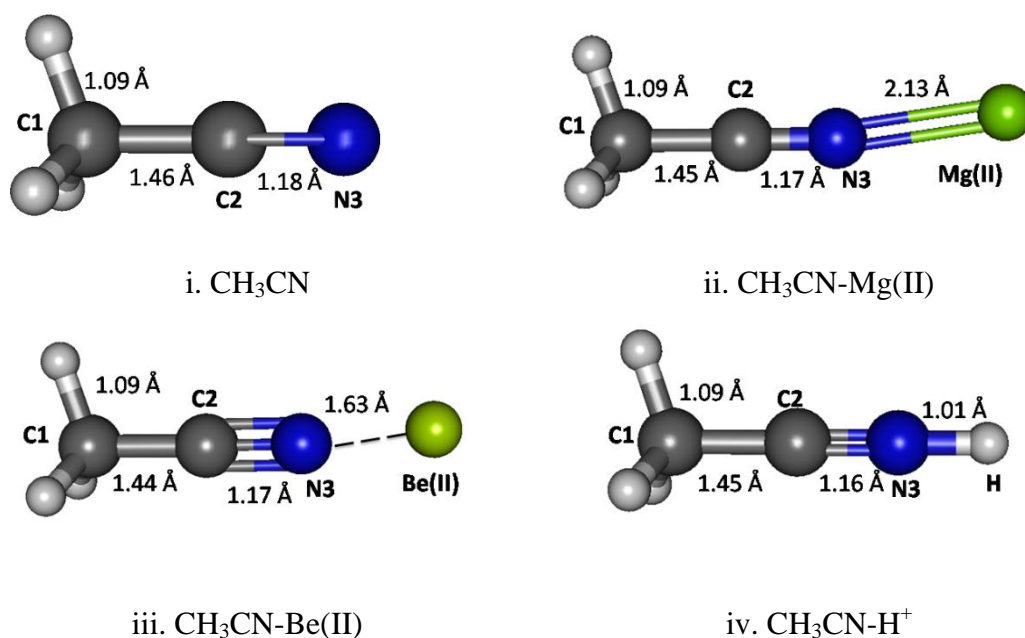


Figure 4.2 G3 optimized geometries of acetonitrile and its complexes with Be(II), Mg(II) and H⁺.

The G3 C2-N3 bond distance in acetonitrile is 1.178 Å, about 2% longer than the experimentally determined value (1.157 Å) (Afeefy *et al.*, 2005). However, experimental C-N bond in hydrogen cyanide (1.156 Å) (Afeefy *et al.*, 2005) is practically identical to that in acetonitrile. This indicates that the cyano functional group retains the essential carbonitrile triple bond and lone-pair character regardless of the neighbors. Consequently, in weak interactions of interest to chemical sensor design and function, the C-N multiple bond in carbonitrile most probably is inaccessible, and thus the interaction is primarily determined by the cyano lone-pair electron and the nature of the positively charged analytes (this work focused on Ca(II), Mg(II), Be(II) and H⁺).

Table 4.4 Bond distances of acetonitrile and its complexes with Be(II), Mg(II) and H⁺

Molecule ^[a]	Bond Distance (Å) ^[b]				Bond Angle ^[b]		
	C1-C2	C2-N3	N3-M	C1-H	C2-N3-M	H6-C1-C2	H5-C1-H4
CH ₃ CN-Be(II)	1.444	1.165	1.625	1.092	175.5	108.6	110.1
CH ₃ CN-Mg(II)	1.453	1.170	2.131	1.091	172.5	109.6	109.6
CH ₃ CN-H ⁺	1.445	1.155	1.014	1.091	180.0	108.7	110.2
CH ₃ CN	1.460	1.178	NA	1.091	NA	109.9	109.0

[a] Numbering of atoms according to Figure 4.1. [b] Bond distances and bond angles obtained from G3 calculations

According to the σ - p conjugation model, the shrinking of the C1-C2 bond in acetonitrile could possibly increase the bond order, and discriminate the hydrogen atoms attached to C1. The C1-H bond distances should no longer be identical. Analyzing the three C-H bond distances at four decimal places revealed the following bond lengths; C1-H6 (1.0910 Å) and C1-H5 and C1-H4 (1.0911 Å both). However, when rounded to three decimal places, the optimized geometries at all levels of theory, give the same C1-H bond distance for the three C-H bonds (1.091 Å, G3 water) and practically identical H-C1-H bond angles (109.9°, G3 water). Moreover, GIAO ^1H NMR simulation (versus TMS B3LYP/6-311+G(2d,p) reference) on uncomplexed acetonitrile receptor using the B3LYP optimized structure affords a single peak at 2.28 ppm (Table 4.5) for the three protons. The GIAO ^{13}C NMR (*versus* TMS B3LYP/6-311+G(2d,p) reference) gives -8.72 and 103.77 ppm for C1 and C2, respectively, consistent with a normal sp^3 and sp hybridized carbon nuclei (Lampman *et al.*, 2009).

Table 4.5 ^1H and ^{13}C NMR shifts (ppm) of acetonitrile and its complexes with Be(II), Mg(II) and H^+ .

Molecule ^[a]	C1	C2	N3	H6	H4,H5
CH ₃ CN-Be(II)	-8.37	115.36	155.96	3.16	3.13
CH ₃ CN-Mg(II)	-8.18	111.03	187.74	2.64	2.67
CH ₃ CN- H^+	-9.93	86.50	186.39	2.94	2.94
CH ₃ CN	-8.72	103.77	232.75	2.28	2.28

[a] Numbering of atoms according to Scheme 1 [b] Bond distances and bond angles obtained from B3LYP/6-31+G(d,p) calculations.

The Mulliken charges on uncomplexed acetonitrile (Table 4.6) is consistent with the expected electronegativity of the atoms. Nitrogen atom being the most electronegative carries the most negative charge of -0.516. C2 which is directly attached to nitrogen loses significantly its electron density to N3, resulting in a net of 0.295 Mulliken charge. Holding three hydrogen with 0.106 Mulliken charge, C1 has a normal small negative charge of -0.097.

The C1-C2 stretching frequency in acetonitrile, computed by B3LYP method is 924.8 cm⁻¹, while the C-C stretch in ethane gives 999.36 cm⁻¹ (Table 4.7). The results indicated that C-C single bonds in both cases were essentially the same. A higher frequency was expected for acetonitrile if the proposed σ - p conjugation results in substantial barrier to C-C rotation and strong orbital ($2p_z$) overlap. In keeping with the hyperconjugation reasoning, the computed cyano C2-N3 stretch in acetonitrile is 2586.1 cm⁻¹ (RHF/6-31+G(d,p)), 148 cm⁻¹ higher than that in hydrogen cyanide (2438.2 cm⁻¹).

Table 4.6 Mulliken charge[a] of acetonitrile and its complexes with Be(II), Mg(II) and H⁺.

Molecule ^[b]	C1	C2	N3	M	H6	H4,H5
CH ₃ CN-Be(II)	-0.239	0.364	0.212	1.252	0.136	0.137
CH ₃ CN-Mg(II)	-0.362	0.379	-0.141	1.754	0.124	0.123
CH ₃ CN-H ⁺	-0.082	0.392	-0.095	0.368	0.139	0.139
CH ₃ CN	-0.097	0.295	-0.516	NA	0.106	0.106

[a] Mulliken charge obtained from G3 calculations.

[b] Numbering of atoms according to Figure 4. 1

Table 4.7 Vibrational stretching frequencies (cm⁻¹) of acetonitrile and its Be(II), Mg(II) and H⁺ complexes.

Molecule ^[a]	C1-C2	C2-N3	N3-M
CH ₃ CN-Be(II)	1056.8	2623.0	728.2
CH ₃ CN-Mg(II)	966.7	2620.8	311.4
CH ₃ CN-H ⁺	920.6	2609.0	3938.0
CH ₃ CN ^[b,c]	954.8	2586.1	NA

[a] Numbering of atoms according to Figure 4.1 [b] Vibrational frequencies of acetonitrile was obtained using RHF calculations and the rest using G3 method. [c] The vibrational frequencies of ethane calculated at B3LYP/6-31+G(d,p) for comparison purposes.

Natural Bond Orbital (NBO) can help elucidate the effect of orbital occupancy on the structure and reactivity of the carbonitrile receptor, as well as the relative stability of the receptor-analyte complexes (Reed *et al.*, 1988; Weinhold, 2012). The change in *s* versus *p* character in chemical bond of interest usually gives rise to significant difference in structure and reactivity. In chemical sensor design, orbital occupancy can be used to explain delocalization of valence electron clouds through some sorts of resonance networks, either exclusively π -bonds or mixture of σ - and π -bonds.

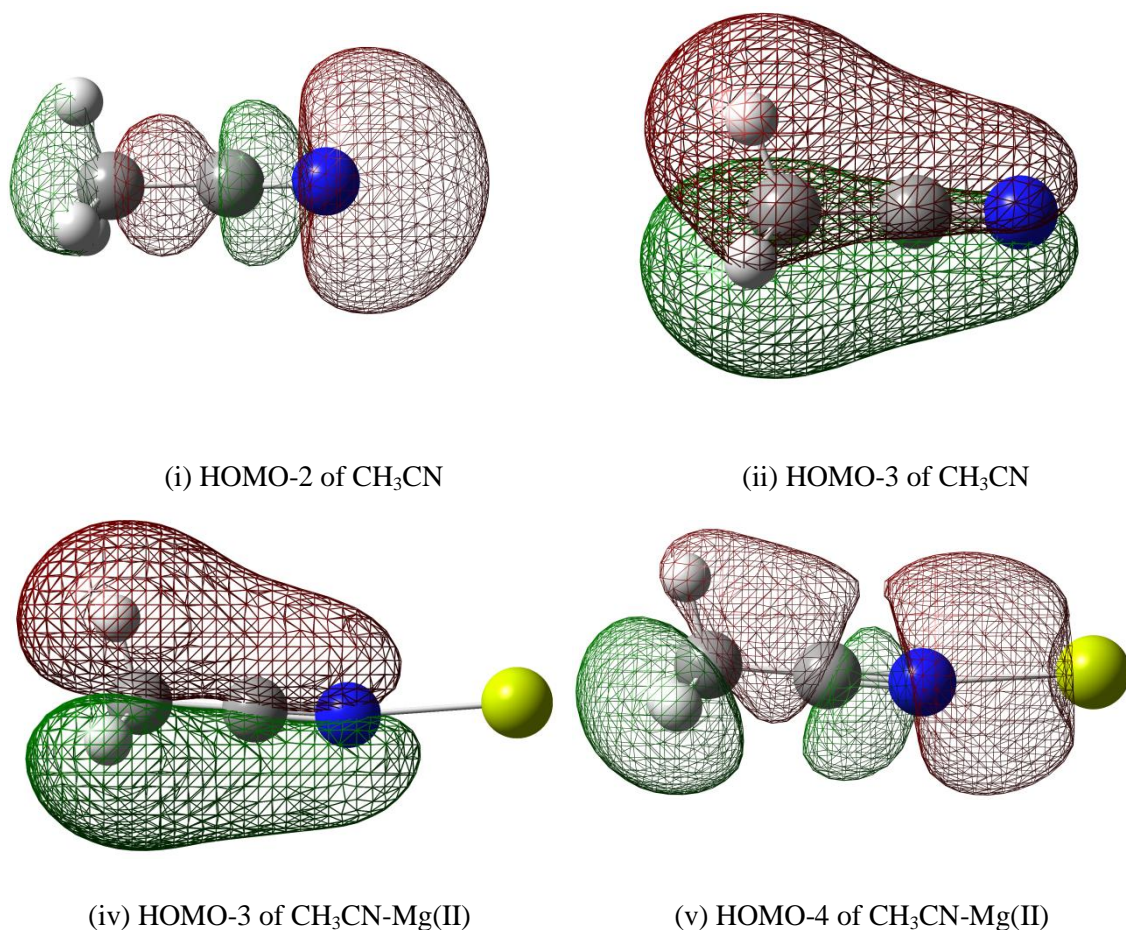


Figure 4.3 Selected G3 molecular orbitals of acetonitrile and its complexes with Mg(II)

The orbital occupancy data are also intuitively connected to molecular orbitals and their energy levels in order to assign frontier orbitals involved in receptor-analyte binding (Figure 4.3). For example, in assigning the orbital for lone-pair electron, orbital degeneracy suggests that it is safe to assign these equal energy MO's to two π -bonds – thus the lower energy sp hybrid MO is more suitable for a lone pair (the HOMO-2 in acetonitrile).

In acetonitrile the C1 carbon has a lower $2p_x$ (1.08) occupancy compared to the $2p_y$ and $2p_z$ orbitals (both 1.30), while the $2s$ occupancy is 1.14 (Table 4.8). All the C1 orbitals have occupancies in excess of 1 because of the contribution of the three hydrogen atoms attached to C1. Likewise the occupancy of the H orbitals are all less

than 1 (0.699), after donating to the more electronegative C1. On the contrary, all C2 orbitals have occupancy less than 1 ($2p_x$ (0.99); $2p_y$ and $2p_z$ (both 0.88); $2s$ (0.89)), giving up to the more electronegative nitrogen neighbour. The $2p_y$ and $2p_z$ occupancies in C2 are consistently remain the same, suggesting that these $2p$ orbitals are used to form two π -bonds in the carbonitrile triple-bonded functionality. Consequently, the $2s$ and $2p_x$ orbitals are used by C1, C2 and N3 to form σ -bonds, and one is also available to accommodate a lone-pair electron on N3. The s and p characters of the σ -bonds of interest are consistent with these occupancy data, while essentially all π -bonds are constructed with pure $2p$ orbitals (Table 4.8). The C1-C2 σ -bond in acetonitrile uses typical sp^3 orbitals for bonding having close to ideal 24% s and 76% p characters on C1, and employs close to ideal sp hybrid orbital from C2 (54% s and 46% p characters, Table 4.9). Likewise, the C2-N3 σ -bond shows close to ideal sp hybridized orbitals (46% s and 54% p on C2, and 45% s and 55% p on N3 – the sp orbital having more p character in uncomplexed acetonitrile).

4.2.3 Acetonitrile-Mg(II) Complex

Acetonitrile approaches and interacts with positively charged analytes through its lone-pair electrons. Unlike olefins, where protonation involves direct interaction between hydrogen and the $2p$ orbitals in the π -bond, resulting in a new C-H σ -bond and carbocation. The breaking of the cyano C-N π -bond of acetonitrile is not feasible due to the formation of unstable vinyl cation (Apeloig *et al.*, 1982; Kobayashi *et al.*, 1993; Müller *et al.*, 2004; Winter *et al.*, 2009; Yates *et al.*, 1973). In protonated olefin, the resulting cation occupies a $2p_z$ orbital, having three substituents in the x-y plane that can interact and stabilize the positively charged carbon center. On the contrary, the empty orbital in vinyl cation is on the same plane with the double bond and not stabilized by the neighbours (Fleming, 2011; March, 1992).

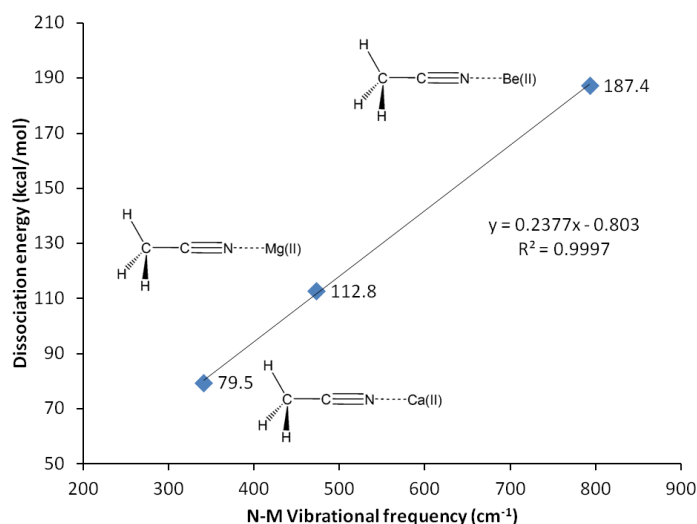


Figure 4.4 G4 Dissociation energy versus N-M vibrational frequency (in vacuum)

G3 calculations indicated that divalent magnesium cation is bound to acetonitrile in water with a binding energy of 12.5 kcal/mol (Table 4.10). Using the same method, the ammonia-borane benchmark shows three-fold stronger binding in water (35.1 kcal/mol, Table 4.2). The binding energy calculations have been repeated using G4 method in order to include calcium(II) and allow plotting of Figure 4.4. The C2-N3 σ bond in acetonitrile-Mg(II) complex shows significant increase (18%) of the s character at the sp orbital used to accommodate nitrogen lone-pair electrons, now forming bonding with magnesium(II), compared to the uncomplexed receptor model (increased from 45.1 to 57.9% s character, Table 4.9). On the contrary, as the N3 increases its s character in order to optimize overlapping with Mg(II), C2 increases its p character by 3% (Table 4.9). The $2s$ and $2p_x$ orbitals in C2 and N3 are involved in the C2-N3 σ bond. Interaction with Mg(II) presumably is limited to these orbitals, as the binding process would avoid forming vinyl cation (Apeloig & Stanger, 1982; Kobayashi *et al.*, 1993; Müller *et al.*, 2004; Winter & Falvey, 2009; Yates *et al.*, 1973).

The interaction with Mg(II) causes reduction of 10% of the occupancy in the C2 orbitals involved in π -bondings, but negligible difference in the $2p_x$ orbital used for σ -bonding. On the contrary, the interaction with magnesium cation causes N3 to receive 8% additional occupancy in the $2p$ orbitals for π -bonding, and 5% increase in the occupancy for σ -bond. This balance would possibly leave the C2-N3 π -bonding characteristics unchanged. Moreover, the combined C2 and N3 $2s$ occupancies in the uncomplexed and the complex after binding with Mg(II) remains essentially the same (Table 4.8). As a whole, the interaction with Mg(II) affords no noticeable change in π -bonds characteristics, whereas, the observed shortening of the C2-N3 triple bond could be attributed to a more effective σ -bond that accompanies significant increase in N3 s character (28%, Table 4.9).

Table 4.8 Orbital occupancies[†] of acetonitrile and its complexes with Be(II), Mg(II) and H⁺

	2s	2P_x	2P_y	2P_z	Total
CH ₃ CN-Mg(II)					
C2	0.875	0.974	0.793	0.793	3.435
N3	1.542	1.583	1.244	1.244	5.614
C1	1.149	1.056	1.310	1.310	4.824
CH ₃ CN-Be(II)					
C2	0.876	0.962	0.726	0.727	3.291
N3	1.497	1.607	1.324	1.323	5.751
C1	1.155	1.043	1.316	1.317	4.830
CH ₃ CN-H ⁺					
C2	0.866	0.957	0.734	0.734	3.291
N3	1.298	1.467	1.323	1.323	5.411
C1	1.156	1.035	1.320	1.320	4.830
CH ₃ CN					
C2	0.887	0.987	0.879	0.879	3.631
N3	1.598	1.511	1.147	1.147	5.403
C1	1.138	1.076	1.297	1.297	4.808

[†] Calculated using B3LYP/6-31+G(d,p)

As acetonitrile interacts with magnesium cation, the C1-C2 bond becomes shorter – G3 calculations show 0.5% shortening of the bond (shrinking from 1.460 Å to 1.453 Å, Table 4.4). The shortening of C2-N3 due to the interaction is less than 1% (from 1.170 Å to 1.178 Å, Table 4.4). Effectively, interaction with magnesium shortens both bonds.

When rounded to three decimal places, all the three C1-H bonds remain essentially unchanged (1.091 Å).

^1H NMR of the three H atoms attached to C1 provides valuable probe to monitor changes in C1-H bond due to σ -p conjugation in acetonitrile-analyte complex. Likewise, NMR shifts of the C1, C2 and N3 nuclei could elucidate changes in electron clouds shielding these nuclei. Despite insignificant change in the C1-H bond distance (1.091 Å), the H atoms attached to C1 experience significant deshielding effect due to interaction with Mg(II). The interaction with magnesium cation helps discriminate the H nuclei giving two types of H - one H in the x-z plane and two H's at x-y plane. The two types of H are deshielded by close to 15% due to the interaction with Mg(II) (Table 4.5, Figure 4.5). Similarly, direct interaction with Mg(II) significantly causes shielding on the N3 nuclei – the N3 NMR shift reduces by about 20%, in keeping with a buildup of electron density surrounding the N3 nuclei. Logically, a shift of electron density from C2 to N3 could in turn deshield C2, and as expected a 6% increase in C2 NMR shift is observed. The deshielding effect on both carbon nuclei occurs at the same extent as C1 also records an increase of 7% in NMR shift.

Table 4.9 *s* versus *p* characters in C2-N3 and C1-C2 σ -bonds in acetonitrile and its Mg(II), Be(II) and H complexes[†]

C2-N3 σ-bond <i>s</i> and <i>p</i> characters by percentage				
	C2 % <i>s</i>	C2 % <i>p</i>	N3 % <i>s</i>	N3 % <i>p</i>
CH ₃ CN-Be(II)	44.8	55.2	53.2	46.5
CH ₃ CN-Mg(II)	43.4	56.5	57.9	42.0
CH ₃ CN-H ⁺	43.6	56.3	51.9	48.1
CH ₃ CN	46.5	53.5	45.1	54.5
C1-C2 σ-bond <i>s</i> and <i>p</i> characters by percentage				
	C1 % <i>s</i>	C1 % <i>p</i>	C2 % <i>s</i>	C2 % <i>p</i>
CH ₃ CN-Be(II)	23.6	76.4	55.4	44.6
CH ₃ CN-Mg(II)	22.9	77.0	56.6	43.4
CH ₃ CN-H ⁺	56.6	43.4	22.7	77.2
CH ₃ CN	24.2	75.7	53.8	46.2
[†] Calculated using B3LYP/6-31+G(d,p)				

In binding with acetonitrile receptor, magnesium cation transfers 0.246 of its charge to the receptor. The changes in Mulliken charges due to this interaction are the most noticeable – the key questions here are; i) How does acetonitrile distribute the 0.246 of plus charge it receives from Mg(II)? and ii) Which atom(s) receive most of this charge? The charge on nitrogen has become less negative by 73% due to direct contact with magnesium cation, and each of the H atom are more positively charged by 17% - apparently these account for almost all of the imparted charge from magnesium. The structural changes in the complex (compared to the uncomplexed acetonitrile) can be explained in terms of redistribution of the imparted charge from Mg(II) in order to sustain interaction with the analyte. For example, C1 undergoes a huge decrease in Mulliken charge by 273% to balance the highly positive hydrogen atoms. This is in good agreement with the observed deshielding of these nuclei. Sandwiched by and in direct contact with highly negative C1 and strongly positive N3, C2 undergoes a net increase in positive charge by 27%. This effectively leaves the cyano group as a positively charged functional entity.

The errors in theoretical vibrational frequencies, computed using different methods, could be in tens of cm^{-1} . Therefore, it is not considered reliable to use small differences in observed stretching frequencies to probe structural changes (Scott *et al.*, 1996)- thus information from experimental FTIR measurement is more appropriate for chemical sensor design. Nevertheless, computational methods correctly confirm earlier structural observations that interaction with Mg(II) increases overlap in bonding orbitals between C1 and C2 and between C2 and N3, leading to the prediction of higher stretching frequencies and shorter bond distances. Table 4.7 shows increase of C1-C2 stretching frequency from 954.8 cm^{-1} to 966.7 cm^{-1} and C2-N3 triple bond vibration from 2586.1 cm^{-1} to 2620.8 cm^{-1} .

In actual chemical sensor applications, it is more important to compare magnesium cation binding to that of calcium, another divalent cation analyte of significant importance in metabolite detection. However, our attempts using all computational methods lead us to conclude that acetonitrile is bound to calcium only in vacuum. The characteristics of solvated receptor-analyte interaction especially in water medium is much more important, whereas Ca(II) is presumably not bound to unconjugated carbonitriles in water medium. In a separate report (Woi *et al.*, 2014) demonstrated that conjugated carbonitrile was strongly bound to magnesium cation in aqueous medium.

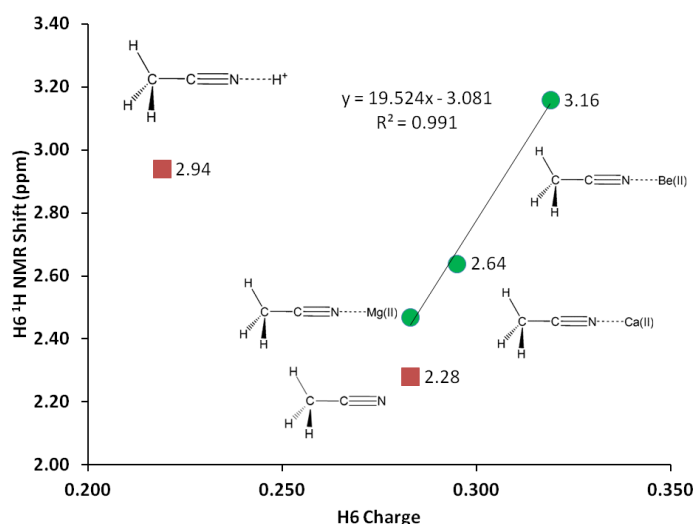


Figure 4.5 H6 ¹H NMR shift versus H6 charge (G3, vacuum)

4.2.4 Acetonitrile-Be(II) Complex

Beryllium(II) is much more strongly bound to acetonitrile compared to its Group II neighbors; magnesium(II) and calcium(II). The three methods employed, G3, CBS-QB3 and MQZVP are in good agreement in showing that the binding energy of Be(II) to acetonitrile is three fold strong as compared to Mg(II) (12.5 kcal/mol with Mg(II)

compared to 42.3 kcal/mol with Be(II), Table 4.10). In general, beryllium(II) and magnesium(II) showed consistent trends in all the structural and reactivity parameters analyzed in this work.

NBO analysis reveals that Be(II) affects the orbital occupancy in all the atoms and bonds in acetonitrile to greater extents compared to the effects by Mg(II) described earlier. After binding with beryllium(II) cation, the cyano N3 becomes more electronegative, as can be seen in the decrease of the occupancies of $2p_y$ and $2p_z$ orbitals in C2, directly attached to N3 (17% decrease from uncomplexed acetonitrile), and a reduction of 3% in the $2p_x$ occupancy (Table 4.8). On the contrary, the change in $2s$ orbital occupancy in C2 is negligible.

Table 4.10 G3, CBS-QB3 and G4 binding energies of acetonitrile complexes with Mg(II), Be(II) and H^+ in vacuum and water[†].

Complex	G3 ΔH_{rxn} (kcal/mol)		CBS-QB3 ΔH_{rxn} (kcal/mol)		G4 ΔH_{rxn} (kcal/mol)
	Vac	H ₂ O	Vac	H ₂ O	Vac
CH ₃ CN-Be(II) \rightarrow Be(II) + CH ₃ CN	187.2	42.3	185.1	40.7	187.4
CH ₃ CN-Mg(II) \rightarrow Mg(II) + CH ₃ CN	112.4	12.5	109.1	10.4	112.8
CH ₃ CN- H^+ \rightarrow H^+ + CH ₃ CN	NA	186.7	NA	138.2	186.8
CH ₃ CN-Ca(II) \rightarrow Ca(II) + CH ₃ CN	NA	NA	NA	NA	79.5

[†]Binding energies were calculated using G3 and CBS-QB3 methods. Water solvation effect was accounted for using iefpcm model.

The electron density is transferred to N3 that experiences a 15% increase of its $2p_y$ and $2p_z$ orbitals. Unlike C2 that retains its $2s$ electron, N3 $2s$ orbital loses 6% of its electron population while forming bond with Be(II). In similar trend with Mg(II) but in greater extents, binding with Be(II) causes significant changes in the s versus p character of the cyano functionality. While in uncomplexed acetonitrile the C2-N3 sigma bond is essentially constructed using close to 50/50 of s/p character making it an ideal sp hybrid orbital, the occupancy is now changed to 40/60 in C2 and 60/40 in N3 (both s/p in % characteristics, Table 4.9). Likewise, the $2p_y$ and $2p_z$ orbitals in C1

receive higher (1%) occupancy compared to uncomplexed acetonitrile. The $2p_x$ orbital in C1 undergoes a 4% reduction of its occupancy while the $2s$ orbital occupancy increase by 2%, compared to uncomplexed acetonitrile. The net result after the give-and-take between C2 and N3 in the C2-N3 π -bond, and between the s versus p in the C2-N3 σ -bond could possibly leave the cyano triple bond unchanged. The optimized acetonitrile-Be(II) structure shows that both C1-C2 and C2-N3 bonds are shorter compared to those in acetonitrile (Table 4.4). The shortening of the C1-C2 bond could be attributed to σ - p conjugation. The shrinkage of the cyano bond distance presumably due to a stronger C-N bond - either more efficiently rehybridized sp orbitals in the σ -bond alone or with additional contribution from more efficient π -bonds.

Beryllium cation transfers 0.75 of its positive charge to acetonitrile and the impact of beryllium cation on N3 is so significant that in the complex its Mulliken charge has become positive (from -0.516 in acetonitrile to 0.212 in the Be(II) complex). Interestingly, the Mulliken charge analysis provides the only example where the beryllium effect on C1 is less significant compared to that of Mg(II) – C1 becomes less electronegative in the former. Moreover, Be(II) effect on C2 is also less compared to that of Mg(II). However, the Mulliken charges of the H atoms increase by close to 30% compared to uncomplexed acetonitrile, and the 2 H nuclei separated even further.

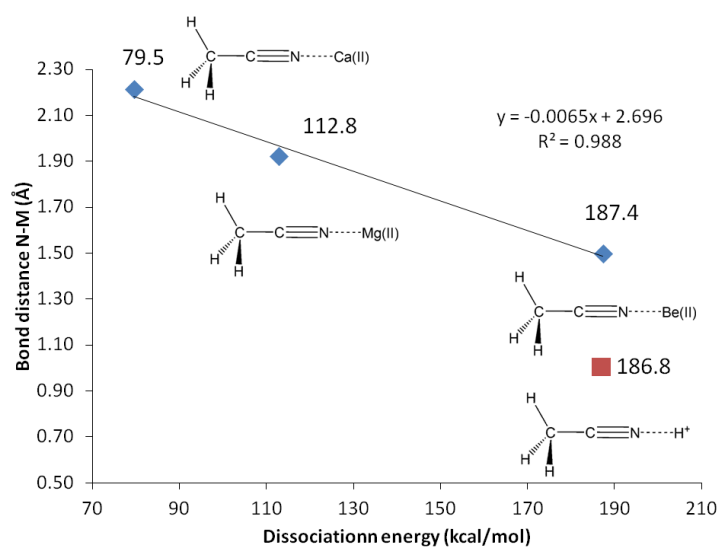


Figure 4.6 N3-Cation bond distance *versus* acetonitrile binding energy (G4, vacuum)

In similar trend with Mg(II) but to a greater extent, the Be(II) binding affords noticeable changes on the vibrational frequencies. G3 C1-C2 stretching frequency is increased by 102 cm^{-1} in the Be(II) complex, whereas the increase in the C2-N3 triple bond stretch is only 37 cm^{-1} . The Be-N stretch is at 728 cm^{-1} , about two-fold compared to Mg-N stretching frequency (Table 4.7). Be(II) effects on C1 and C2 nuclei are similar to the effects of Mg(II), with only slightly higher deshielding effects (Table 4.5, Figure 4.5). However, the change on the three H nuclei due to Be(II) is much more significant – 30% increase in ^1H NMR shifts and the two types of H are even more separated (by 0.04 ppm).

4.2.5 Protonated Acetonitrile

Protonated acetonitrile does not follow the general trends of either the Group I or the Group II cation analytes. With dissociation energy of 138.2 kcal/mol, proton is bound to acetonitrile more than ten times as strong, in comparison to the binding energy in $\text{CH}_3\text{CN-Mg(II)}$ (Table 4.10, G3). In protonated acetonitrile, the C2-N3 bond is shortened even further (1.155 Å) compared to those in the magnesium and beryllium

complexes – reduction of 2% compared to the cyano bond in acetonitrile. Likewise, the C1-C2 bond in the protonated complex is shortened by 1% (Table 4.4). The protonation of acetonitrile does not lead to significant change to the C1-H bond length (Table 4.4). However, there are noticeable changes in the H-C1-H bond angles (109.0° and 110.2°, Table 4.4). The protonation of acetonitrile does not affect the Mulliken charge on C1. On the contrary, the changes on C2 and N3 Mulliken charges are large where C2 experiences an increase in the Mulliken charge by 0.097 and N3 becomes less negative by 0.421. By forming the protonated complex, proton imparts 0.632 of its charge, and almost all of it is received by N3 (Table 4.6). NBO analysis shows the C2-N3 σ -bond having more *s* character in N3 while the *s* and *p* characters at C2 are essentially the same as in the uncomplexed receptor. The C1-C2 σ -bond orbitals show no noticeable change in the uncomplexed and protonated receptor – the C2 orbital is almost ideal *sp* hybrid orbital constructed with 50/50 *s* and *p* and the C1 is a typical *sp*³ hybrid orbital (Table 4.9). The ¹H nuclei in the protonated acetonitrile are significantly deshielded (by 0.66 ppm or an increase of 22%) but there is only one type of H nuclei, whereas, in striking contrast to Mg(II) and Be(II) complexes, both the C1 and C2 nuclei are shielded (Table 4.5). Consistent with the observed shortening of the cyano C-N bond distance, protonation affords a slightly higher stretching frequency (2609.0 cm⁻¹). The N3-H stretching frequency (3938 cm⁻¹) indicates a very strong bond, in keeping with the observed short bond distance (1.014 Å, Table 4.4).

4.2.6 *n*-Pentane Carbonitrile-Mg(II) Complex

Lipophilicity is an essential physical characteristic of membrane-based sensing layer. Long hydrocarbon chains are typically employed to make a recognition molecule more compatible with the membrane – small molecules tend to leach out from the solid phase during long exposure to aqueous environment. *n*-Pentane is considerably a better model

for a lipophilic carbonitrile in terms of structure and reactivity, compared to acetonitrile, and is still computationally feasible. Our results confirm that in all key parameters investigated, *n*-pentane, carbonitrile and acetonitrile essentially show identical characteristics. In keeping with the observed C1-C2 bond in acetonitrile, B3LYP calculation gives a bond distance of 1.460 Å, apparently shorter (Figure 4.7) compared to the carbon-carbon single-bond in ethane (1.532 Å, B3LYP). Likewise, B3LYP shows that C2-N3 bond distance in water solvated *n*-pentane carbonitrile is 1.163 Å - longer than the experimental value for the CN bond in acetonitrile (1.157 Å) and hydrogen cyanide (1.156 Å). The B3LYP stretching frequencies for the C-N triple bond and C1-C2 single bonds are 2338 and 945.9 cm⁻¹, respectively, noticeably lower than those in acetonitrile (Table 4.11).

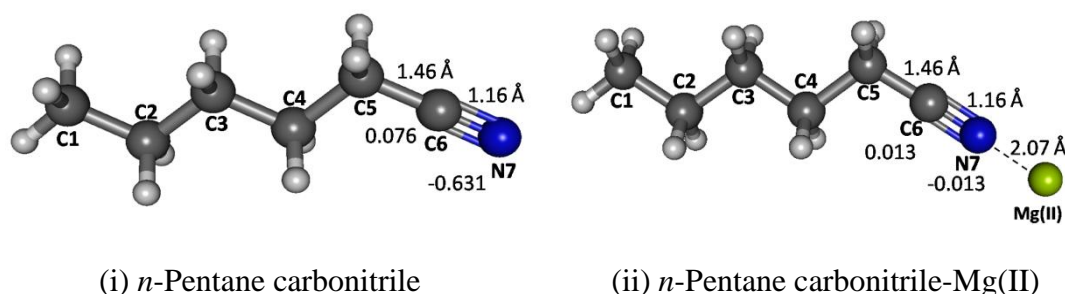


Figure 4.7 Optimized geometries of *n*-pentane carbonitrile and its complex with Mg(II)

The NBO and Mulliken charge analysis further confirm that *n*-pentane carbonitrile and acetonitrile show similar trends; cyano nitrogen with the most negative charge (-0.631) and the cyano carbon is the most positive carbon (0.076) but much less positive compared to the cyano carbon in acetonitrile (0.295). Similar to the acetonitrile model, GIAO ¹H NMR simulation (versus TMS B3LYP/6-311+G(2d,p) reference) of *n*-pentane carbonitrile receptor using the B3LYP optimized structure affords a single peak at 2.54 ppm, slightly more deshielded (2.28 ppm in acetonitrile) for the two protons attached to C1 (Table 4.11). The cyano carbon (C6) and C1 show similar ¹³C NMR shifts compared

to those in acetonitrile; 107.46 and 9.41 ppm respectively, and slightly more deshielded (103.77 and -8.72 ppm in acetonitrile, respectively).

Table 4.11 Vibrational frequencies and NMR shifts of Mg(II) and Be(II) complexes with *n*-pentane carbonitrile, 2 equivalents of acetonitrile, malononitrile and the uncomplexed receptors.

Molecules	Vibrational frequency (cm ⁻¹)				NMR shift (ppm)		
	C-N	C-C ^[a]	N-Mg	N-Be	C1	C _{cyano}	H _(on C1)
<i>n</i> -Pentane carbonitrile ^[c]	2338.4	945.9	NA	NA	9.41	107.46	2.54
Malononitrile ^[d]	2631.8	1044.3	NA	NA	-0.05	96.36	3.91
<i>n</i> -Pentane carbonitrile ^[c] -Mg(II)	2381.5	965.2	413.3	NA	8.46	111.51	2.92
(Acetonitrile) ₂ ^[d] -Mg(II)	2623.5	969.0	386.6	NA	-8.32	110.25	2.62
Malononitrile ^[d] -Be(II)	2540.0	977.7	NA	NA ^[b]	15.21	152.57	5.30

[a] C-C refers to methylene carbon atoms. [b] No value for the corresponding stretch. [c] The geometry was optimized at B3LYP/6-31+G(d,p) with iefpcm solvation model. [d] The geometry was optimized using G3 with iefpcm solvation model.

4.2.7 Magnesium(II) Bound to Two Acetonitrile Receptors

Interaction between magnesium(II) cation and two acetonitrile receptor molecules in water solvent has been studied using B3LYP and G3 methods (Figure 4.8). The G3 optimized geometry show that when bound to two acetonitrile molecules, Mg(II) imparts 0.401 of its charge to the receptors, more effectively than it does to one receptor molecule resulting only 80% remains at magnesium (88% in case of one acetonitrile molecule). The nitrogen atom retains more negative charge (-0.176) and the cyano carbon less positive charge (0.356), compared to the binding with only one receptor. The charge on H atoms for both cases is the same (0.124). The imparted positive charge from magnesium in this case is shared equally between two acetonitrile molecules and thus the polarization in the cyano functionality becomes less dramatic.

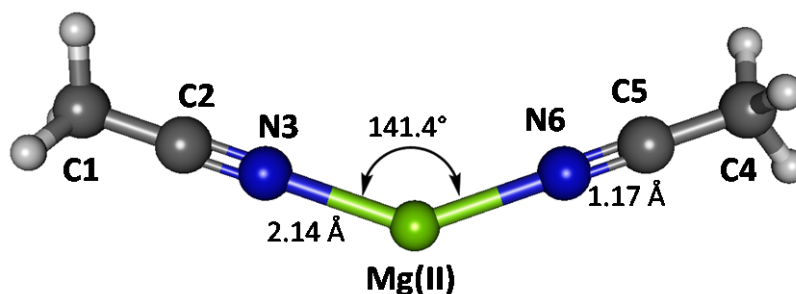


Figure 4.8 Optimized geometry of Mg(II) complex with two equivalents of acetonitrile.

The two receptors bound to Mg(II) form a N-Mg-N angle of 141.4° , in striking contrast to the perfectly linear disubstituted magnesium such as MgCl_2 . The H-C1-H bond angles are close to the ideal tetrahedral angle (109.6°). The differences in the acetonitrile bond lengths in the two cases (1 and 2 equivalents) are essentially negligible – all the C2-N3, C1-C2 and C1-H have essentially the same bond distances. Only the N-Mg bond is longer; 2.142 \AA with two equivalents of acetonitrile *versus* 2.131 \AA with one equivalent. The C-N and C-C stretching frequencies in the doubly bonded complex are noticeably higher; 2623 and 969 cm^{-1} , respectively, suggesting higher energies required to stretch these bonds. The doubly bound complex affords new bands of interest at 168.2 and 386.8 cm^{-1} , attributed to symmetric N-Mg-N bend and asymmetric N-Mg-N stretch, respectively (Table 4.11).

4.2.8 Malononitrile-Be(II) Complex

We have examined malononitrile complexes with magnesium and beryllium cations in the gas phase and in water medium. In the aqueous medium of interest only Be(II) complex with one molecule of malonitrile is found to be bound (Figure 4.9). Magnesium(II) can form a bound complex with only one molecule of malonitrile and the complex remains intact only in the gas phase. On the contrary, beryllium(II) forms

complexes with one and two equivalents of malononitrile in vacuum, but only the one equivalent adduct survive in water.

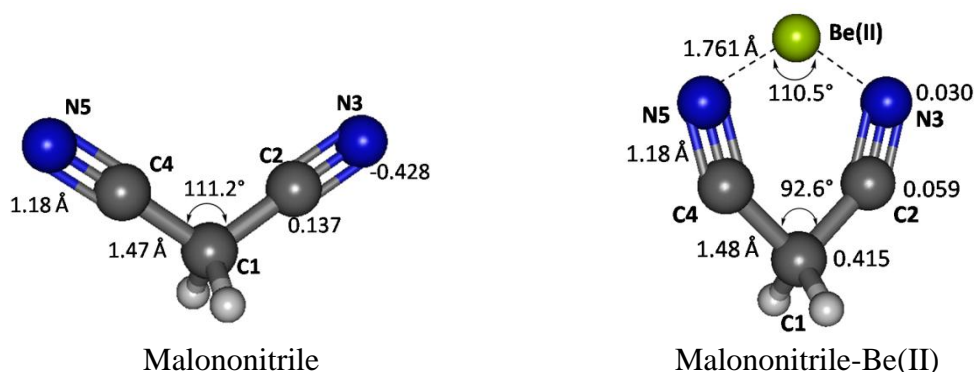


Figure 4.9 Optimized geometries of malononitrile and its complex with Be(II)

Malononitrile receptor model provides interesting insights on the cage-like complex structure where two carbonitrile functionalities are tied together, separated by only one methylene unit. The two electron lone-pairs can be imagined as pointing at the opposite directions from each other and the two need to come together and bind at the side of the cyano groups with an angle N-Be-N much less than 180°, rather than forming a linear adduct as in the acetonitrile-Be(II) described earlier.

When binding to malononitrile at both of the cyano groups, Be(II) transfers 0.938 of its charge to the receptor (Data provided in Appendix A). As a result, nitrogen becomes more positive by 0.354 and the methylene carbon (C1) has a positive charge built up by 0.144. The methylene hydrogens also experience increase in positive charge. In striking contrast to acetonitrile and its complex with Be(II) the cyano carbon in malononitrile and its beryllium complex carry only small positive Mulliken charge. The σ - p conjugation in malononitrile is presumably very different from the one in acetonitrile described earlier. The methylene carbon does not accumulate negative charge as malononitrile binds to Be(II). The six-membered malononitrile-Be(II)

complex is a perfectly planar structure having bond angles of 110.5° for N-Be-N, 106.3° for Be-N-C, 92.6° for C-C-C and 111.3° for H-C-H. The σ - p conjugated network presumably covers the entire six-membered ring, stabilized by resonance and thus relieves the burden of extreme negative charge on the methylene carbon. In striking contrast to the methyl carbon in acetonitrile, the malononitrile methylene carbon can be considered as having positively charged characteristic wherein the $2p_z$ orbital allows hyperconjugation via π -network, similar to butadiene or acrolein (Figures 4.10 and 4.11).

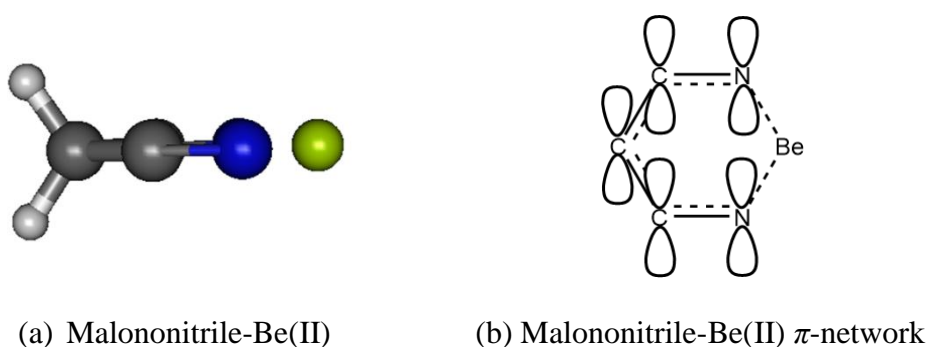
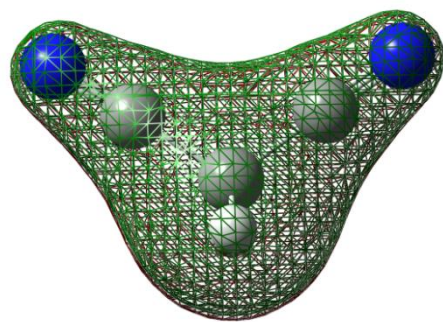
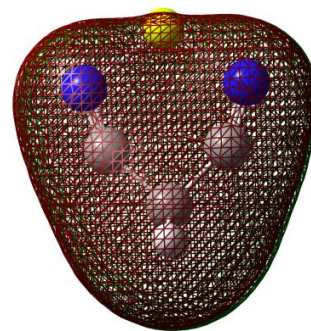


Figure 4.10 (a) Planar optimized structure of Be(II) complex with malononitrile; (b) conjugated π -network in malononitrile-Be(II).

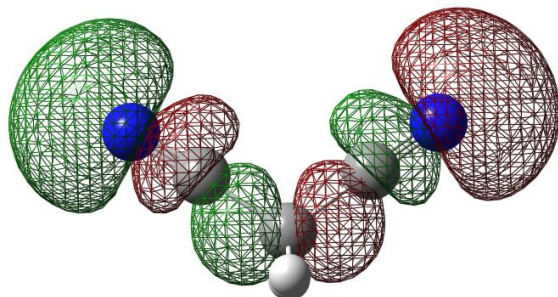
Beryllium cation binds to both cyano nitrogen atoms in malononitrile and reducing the N-N distance from 4.413 \AA to 2.766 \AA , putting the Be(II) in the middle between the two nitrogen with 1.761 \AA N-Be bond distance. The C-N bond distances in malononitrile and its Be(II) complex are the same (1.179 \AA). Likewise, the C1-H bond distances in both cases are also the same (1.094 \AA). The C1-C2 bond distance is noticeably longer in the complex (1.483 \AA versus 1.466 \AA).



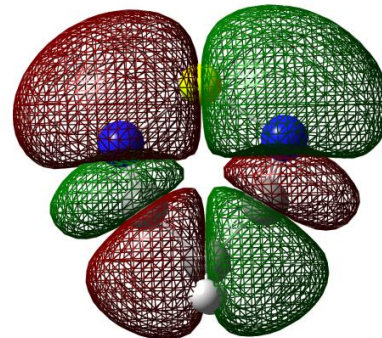
i) HOMO-6 of malononitrile



ii) HOMO-5 of Malononitrile-Be(II)



iii) HOMO-4 of malononitrile



iv) HOMO-4 of Malononitrile-Be(II)

Figure 4.11 Selected molecular orbitals of malononitrile (i) and (iii); malononitrile-Be(II) complex (ii) and (iv)

Malononitrile-Be(II) affords distinct vibrational frequencies at 374.0 cm^{-1} (sym. N-Be-N bending), 578.4 cm^{-1} (antisym. N-Be-N stretch) and 715.3 cm^{-1} (sym. N-Be-N stretch). The symmetric C-C stretch occurs at 977.7 cm^{-1} and C-N stretches occur at 2517.0 and 2540.0 cm^{-1} (asymm. and sym. stretches, respectively) (Table 4.11). ^{13}C NMR GIAO (*versus* TMS B3LYP/6-311+G(2d,p)) at B3LYP in water medium shows that the cyano carbon and the methylene carbons are both significantly deshielded compared to uncomplexed malononitrile; 152.57 and 15.21 ppm, respectively (Table 4.11). The increase in the cyano carbon shift is very large (56 ppm), presumably attributed to the ring current in the conjugated planar structure of the complex. Likewise, the two ^1H nuclei bonded to C1 are also apparently deshielded (5.30 ppm, compared to 3.91 ppm in malononitrile). The deshielding of the ^1H nuclei presumably is similar to the ^1H nuclei

at the periphery and perpendicular to the delocalized network or ring current in aromatic rings such as benzene, furan and imidazole.

4.2.9. Carbonitrile Reactivity and Binding Energies

The interactions of carbonitriles with cations involve the cyano nitrogen lone-pair electrons, leaving the π -electrons alone in order to avoid forming unstable vinyl cation (Apeloig & Stanger, 1982; Kobayashi *et al.*, 1993; Müller *et al.*, 2004; Winter & Falvey, 2009; Yates *et al.*, 1973). The driving force towards complex formation can be rationalized in terms of stabilization effect or energy lowering on the carbonitrile receptor.

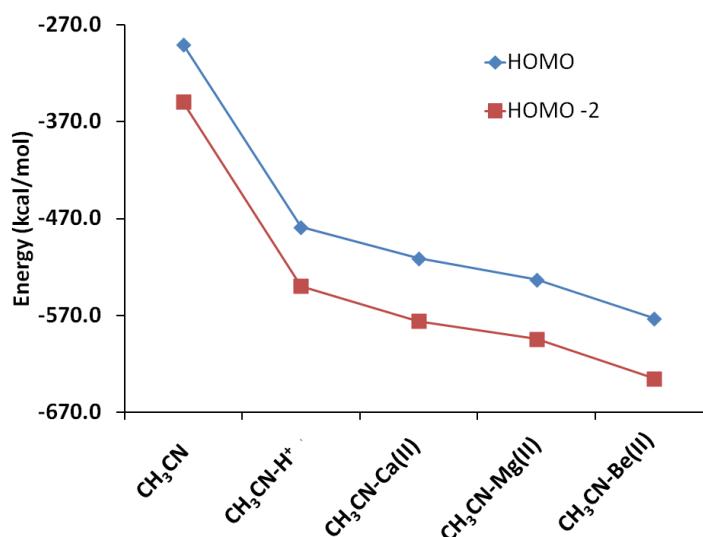


Figure 4.12 Lowering of acetonitrile MO energies due to interaction with cations

As highlighted by Purcell and Drago, interactions of Lewis acids with acetonitrile significantly reduce the energies of the π -molecular orbitals in the complexes (Purcell *et al.*, 1966). This work (Figure 4.12) confirms their results. The MO energies of HOMO and HOMO-2 orbitals in the three complexes are much lower than those in acetonitrile. In keeping with the observations discussed earlier (*i.e.* Figure 4.6), the HOMO energies follow the general trend of Be(II) < Mg(II) < Ca(II).

4.2.10 Sensor cell signals

Cyclopentane carbonitrile is commercially available and used in this work as the cation recognition agent in chemical sensor array application. In a potentiometry transduction measurement, target analyte and interfering cations produce voltage signal when the chemical sensor is connected to a reference electrode (typically a double junction silver-silver chloride electrode) (Heng & Hall, 2001). In order to convert analyte concentration to voltage signal and to maintain a stable signal, the sensor is equipped with its own internal reference (such as silver-silver chloride or doped conductive polymer). Potential difference between the internal reference and sensing membrane produces electrical signal according to the Nernst equation (Daniel, 1987). Figure 4.13 shows the signal patterns of different concentrations of magnesium ion without any interfering ion and with low and high concentrations of potassium ions. The mixture of magnesium-potassium with one to one ratio causes the sensor signal to increase by 40 mV (in comparison to signals from pure Mg(II)) for logarithmic of 1×10^{-2} M and 1×10^{-3} M but only 20 mV increases for 1×10^{-4} M. Similar trend has been observed when the proportion of potassium is increased such that in the magnesium to potassium ratio of 1:10, a signal increase of 40 mV for logarithmic of 1×10^{-2} M and an increase of 20 mV for logarithmic of 1×10^{-3} and 1×10^{-4} M, due to addition of K^+ . With the observed consistent and predictable signal patterns the carbonitrile receptor molecules can be exploited for detection of cations in sensor array applications.

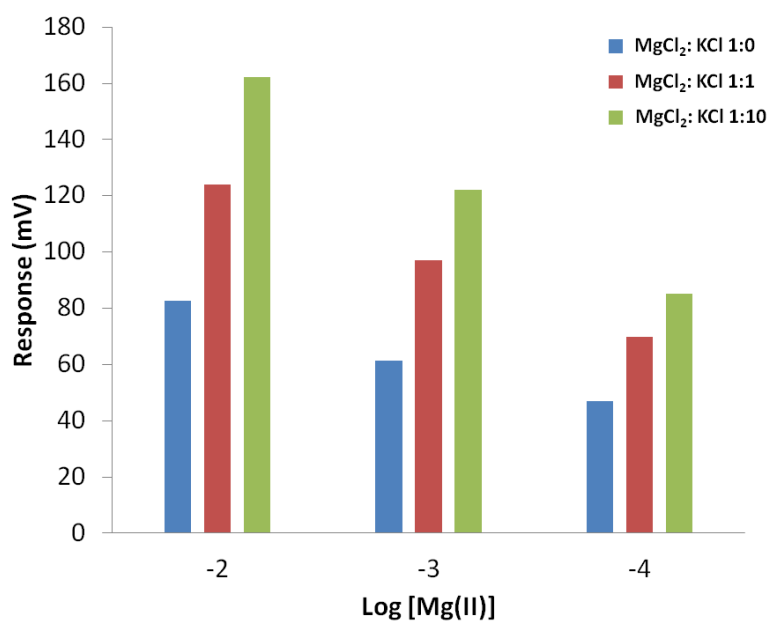


Figure 4.13 Response of fabricated chemical sensor with cyclopentane carbonitrile immobilized in acrylic copolymer membrane.

4.2.11 IR Measurement

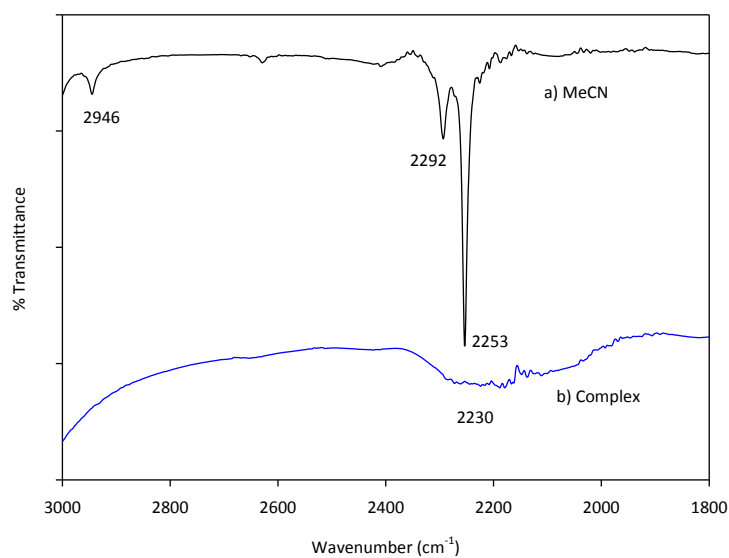


Figure 4.14 The IR spectra of acetonitrile and acetonitrile-Mg(II) complex

As described earlier, our simulation using the G3 method reveals that uncomplexed acetonitrile shows a vibrational frequency at 2586.1 cm^{-1} that can be attributed to C-N stretching. Likewise, as expected based on earlier experimental results, binding with cations increase the frequencies of the cyano group; Mg(II), Be(II) and H^+ afford the

following C-N stretches 2620.8, 2623.0 and 2609.0 cm^{-1} , respectively. Purcell and Drago have reported facile preparations of acetonitrile complexes with boron trifluoride and tin tetrachloride (Purcell & Drago, 1966). However, when we tried to prepare magnesium complex with acetonitrile using the method described in the next section, we only observed a broad peak at the 2300 to 2000 cm^{-1} region (Figure 4.14). However, using the same characterization setup, neat acetonitrile affords a strong cyano C-N stretching frequency at 2253 cm^{-1} .

4.3 Conclusions

A systematic theoretical study of cation recognition using carbonitriles as receptors for the design of chemical sensor array had been presented in this chapter. The B3LYP, G3, CBS-QB3, G4 and MQZVP methods had been employed in four benchmark cases relevant to chemical sensor design. The methods had been verified as accurate and diligently used for designing cation recognition molecules. The G3 method has been especially useful due to its accuracy and speed in evaluating the binding interactions between carbonitriles and Mg(II), Be(II) and H^+ . The G4 method has been specifically adopted to gain accurate energy calculations involving calcium(II). The G4 reproduces the earlier G3 results of Mg(II), Be(II) and H^+ . ^1H NMR study shows that H6 is deshielded by interaction with cation following the trend $\text{Be(II)} > \text{Mg(II)} > \text{Ca(II)}$. The results also show that H6 can be distinguished from H4 and H5 in the acetonitrile-analyte complexes, presumably due to σ - p hyperconjugation. The hydrogen atoms on C1 and N3 receive most of the positive charge from the analytes. NBO analysis shows that the cyano triple bond remains unchanged after interacting with the analytes.

n-Pentane carbonitrile lipophilic model shows no significant difference from acetonitrile when bound to Mg(II). The complex of Mg(II) with two acetonitrile molecules shows interesting 141.4° N-Mg(II)-N angle in striking contrast to linear MgCl_2 . Malononitrile-Be(II) is a planar complex exhibiting π -network with cationic methylene carbon as

evidenced by its strongly deshielded methylene protons. Frontier orbital analysis shows that interaction with cation lowers the energy of HOMO and HOMO-2 of the carbonitrile receptors. Reproducible sensor signals in Mg(II) separate solutions, and in mixtures of Mg(II) and K⁺ strongly suggest that carbonitrile recognition molecules can be exploited in sensor array applications.

Chapter 5 : Rational Design of Carbonitrile-Carboxaldehyde Cation

Receptor Models - Probing The Nature of Heteroatom-Metal

Interaction

Hybrid functional and G4 methods employed in rational design of carbonitrile-carboxaldehyde receptor models for cation recognition. Electron sharing *versus* ionic interaction has been analyzed utilizing overlap population, atomic valence, electrostatic potential and CHELPG charge in order to elucidate the nature of heteroatom-metal interaction, the N *versus* O disparity and pH effect. Receptor fragment models from Ionomycin have been employed to rationalize the choice of receptor models in discriminating Group I cations, in enhancing the selectivity of Mg(II) against Ca(II) and examining the effects of keto-enol forms and negatively charged sites. The optimized geometries revealed that interaction between Group II cations and the keto, enol and enolate forms of 2-cyanoethanal (1) caused 12% bending of the C-C-N angle from linearity. Overlap population showed that electron sharing interaction favours Group II cations but the same mechanism allows Li(I) to compete. The total spin of Li(I) is 17% greater than that of Ca(II) but the G4 binding energy of the two is separated by more than 50 kcal/mol, favouring Group II and could eliminate interference from Li(I). 1,2-Dicyanoethylene (2) having only one form shows similar characteristics. CHELPG analysis shows that Mg(II) transfers 25% and 18% of its positive charge to 2-cyanoethanal enolate and 1,2-dicyanoethylene, respectively. Hydrogen atoms receive

most of the positive charge in both receptors but the N terminals exhibit strikingly different characteristics. Electrostatic potential contour profiles are in good agreement with the atomic charge distribution. Uncharged 1,3-dicarbonyl and 2-cyano carbonyl receptors and judicious choice of polymeric membrane that suppresses Hofmeister effect could give high selectivity towards magnesium, whereas, multiple negatively charged ionophores favour calcium.

5.1 Introduction

Selective detection of calcium(II) and magnesium(II) are of significant interest in biological analysis. Ca(II) and Mg(II) are essential dietary nutrients for human body functions (Greene *et al.*, 1988; Ross *et al.*, 2011). In plant growth, the two divalent cations are among the most important ionic nutrients consumed by plant in large quantities (primary macronutrients) (He *et al.*, 2001; Maathuis, 2009).

Ionomycin (Figure 5.1) has often been used in detection of calcium (Erdahl *et al.*, 1994; Kauffman *et al.*, 1980). It does not always exist in an uncharged form. In slightly basic medium, the carboxylic acid terminal ionizes to carboxylate ion. At even higher pH, the acidic protons in 1,3-dicarbonyl and the carboxylate α -protons can be deprotonated to afford multiple charged form of ionomycin. Relating to Ca(II) determination using EDTA, deprotonated Ionomycin presumably increases its selectivity towards calcium(II). The pH effect on binding interaction between cations and carboxylic calcium ionophores such as Ionomycin and Calcimycin (ionophore A23187) has been reported (Erdahl *et al.*, 1995; Jyothi *et al.*, 1994; Kauffman *et al.*, 1980; Reed *et al.*, 1972). Hofmeister effect has been suggested in explaining the preferential bindings towards weakly hydrated monovalent cations having low surface charge density (Kherb *et al.*, 2012; Zhang, Jenny, *et al.*, 2000; Zhang & Cremer, 2006)

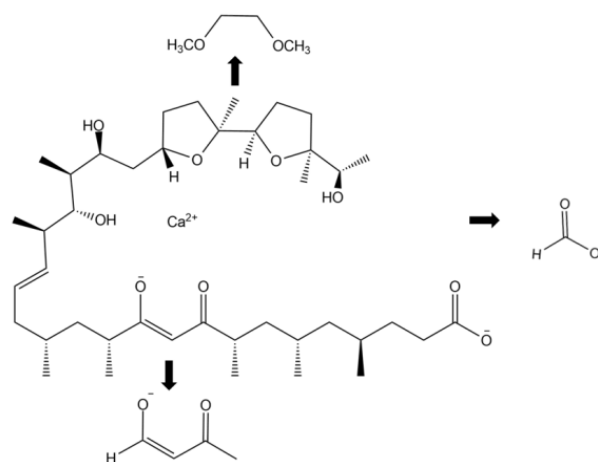


Figure 5.1. Ionomycin and extracted fragment models

This work is interested to utilize the natural binding characteristics between carbonitrile-carboxaldehyde receptor models and Group I and II cations (March, 1992). Three functional fragments had been extracted in Ionomycin, namely, ethylene glycol methyl ether, butanal-3-one and formic acid as simple models for Ionomycin and investigate its interaction with Group I and II cations in general, and calcium(II), magnesium(II), lithium(I) and potassium(I) in particular. In addition, density functional theory is adopted to optimize structures of interest, and extensively used G4 theories to evaluate comparative binding strength. In order to facilitate computational efforts but without losing essential information, 2-cyano ethanal (1) and 1,2-dicyanoethylene (2) were focussed as working models for the cation receptors.

Malonodiamide lipophilic neutral molecules have been reported to exhibit selectivity towards Mg(II) (Zhang, Jenny, *et al.*, 2000). Discrimination against Ca(II) and Group I cations are satisfactory (100 to 1000 times) when three malonodiamides ligands are used *i.e.* tripodal malonodiamides (ETH 5504, ETH 5506) (O'Donnell *et al.*, 1993; Zhang & Spichiger, 2000) or aza-crown and two malonodiamides (ETH 2022, ETH22B5) (Siswanta *et al.*, 1997). The nature of polymeric membrane, the lipophilic agent (tetraphenyl borate) to ionophore ratio and choice of plasticizer have often been

considered as contributing factors towards cation selectivity (Bakker *et al.*, 1994; Bakker *et al.*, 2000).

Probing the nature of metal-heteroatom (Rao *et al.*, 1988) is the main focus of this work, and the electron sharing versus ionic interaction (Pauling, 1960b) analysis is extensively employed to elucidate the binding strength and basis for sensor selectivity. Overlap population between metal and heteroatom, atomic valence of metals, binding energy and structural changes were analyzed in order to deduce critical design parameters (Mayer, 1983, 1984; Wiberg *et al.*, 1984). Structural changes in three-dimensional optimized geometries in the metal cation complexes, especially Ca(II) and Mg(II), with the fragment models extracted from Ionomycin and carbonitrile-carboxaldehyde models are critically examined in selectivity rational design. Electrostatic potential contours (Dykstra, 1993; Murray *et al.*, 1992; Rick *et al.*, 1994) and CHELPG (Breneman *et al.*, 1990; Kelly *et al.*, 2005; Martin *et al.*, 2005) of atomic charges are utilized to rationalize the significance of ionic interaction.

5.2 Results and Discussion

5.2.2 Optimized Structures of Receptor Models

2-Cyanoethanal (1) has three forms of interest for cation recognition analysis; uncharged transoid keto (1a), cisoid enol (1b) forms and a negatively charge enolate (1c). Interaction between 1 and cation can be envisioned to form a six-membered cyclic complex wherein the two ends of the receptor; the carbonitrile N and carbonyl O in forming covalent or ionic type interactions with Group I and II cations are of significant interest in this work. The N *versus* O predominance in cation binding involving these forms of 1 with different cation analytes will be studied extensively.

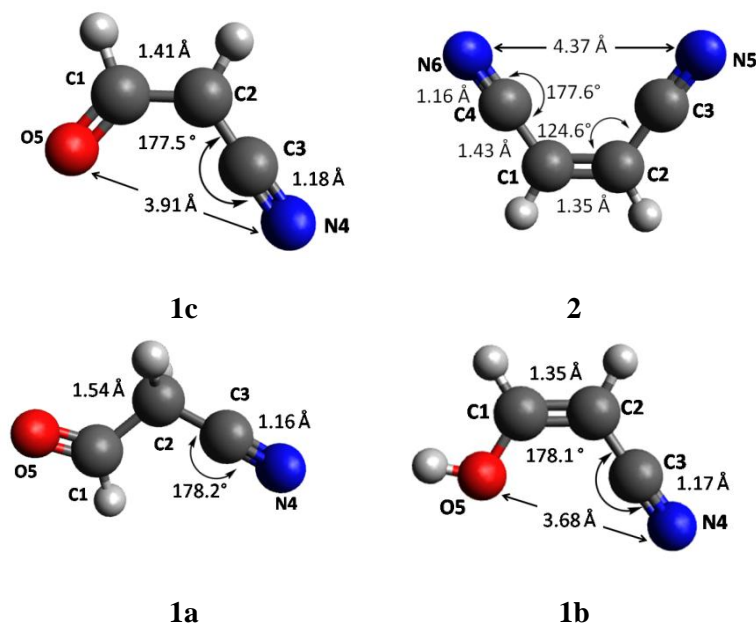


Figure 5.2. Optimized geometries of 2-cyanoethanal keto form (1a) 2-cyanoethanal enol form (1b), 2-cyanoethanal enolate (1c) and 1,2-dicyanoethylene (2) calculated using B3LYP/6-31+G(d,p).

The relative importance of charge neutral forms, keto *versus* enol will also be highlighted. Distribution of electron density in the three forms of 1 will also be elucidated from population analysis view point. The significant change in the C1-C2 bond distances in the three forms of 1 is noteworthy. While the keto form 1a exhibits the longest C1-C2 bond length (1.54 Å), those in enol 1b and enolate 1c are strikingly different (Figure 5.2).

The C1-C2 bond in 1c (1.41 Å) is 4.4% longer than that in 1b (1.35 Å). This observation suggests that the C1-C2 bond order in 1c is only slightly higher than those in 1a. The electron density presumably is distributed over the entire π -framework. Elongation of the C3-N bond in 1c (1.18 Å) supports this arguments.

On the contrary, the C1-C2 bond in 1b more closely resembles that in ethylene, lacks conjugation and doesn't affect the cyano bond. Interaction with cation requires significant pulling of the N and O terminals closer together, thus resulting in severe distortion of the complex structure, *i.e* the unusual C2-C3-N bending from almost perfect linearity (178°). 1,2-Dicyanoethylene (2) on the contrary has only one form to be considered. Likewise, the two N terminals are quite far apart from each other (4.37 \AA) and the C-C-N angle is almost perfectly linear (177.6°). Binding with Group I and II cation would require pulling the two ends significantly nearer to each other and presumably bending of the C-C-N bond (Figure 5.3).

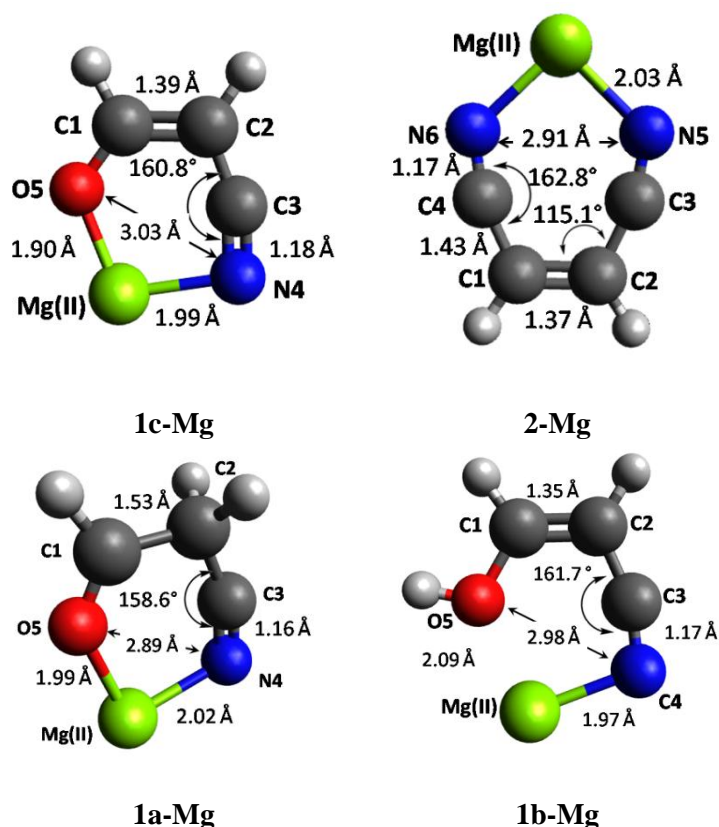


Figure 5.3. Optimized geometries of 1a-Mg, 1b-Mg, 1c-Mg and 2-Mg calculated using B3LYP with 6-31+G(d,p) basis sets for non-metals and QZVP for metals.

5.2.3 Optimized Structures of Complexes

Binding with Mg(II) causes pulling of the N and O terminals in 1a to be closer together (2.89 Å), significantly bending the C-C-N angle from linearity to 158.6°. The N-Mg and O-Mg bond distances are 2.02 Å and 1.99 Å, respectively – the cation center making N-Mg-O angle of 92.3°. Interestingly, in 1c-Mg both N-Mg and O-Mg bond distances are longer, but the N-O distance increases to 3.03 Å. Furthermore, the enol complex 1b-Mg had shown the shortest N-Mg bond length while the O-Mg significantly elongated to 2.09 Å. It is apparent that the diminishing interaction in O-Mg gives rise to more effective N-Mg bonding. It should be pointed out that the presence of H atom in the enol 1b reduces the availability of O electron density for binding with Group I and II cations. Figure 5.3 and supplementary data shows that the N *versus* O disparity in carbonitrile-carboxaldehyde cation receptors could be detected simply by structural inspection. On the contrary, 2-Mg is a symmetric and perfectly planar complex exhibiting 2.03 Å N-Mg bond distance, with the center making a 91.6° N-Mg-N angle, and distorting the C-C-N to 162.8° angle from perfect linearity. Electrostatic potential contours (Figure 5.4) of uncomplexed receptor models 1a, 1b, 1c and 2 have been analyzed in order to examine the availability of negative charge density for complex formation. The graphical potential gradient plots are then linked to the CHELPG atomic charges described later. Transoid keto form of 2-cyanoethanal (1) exhibits almost equal negative charge densities around N and O terminals. Likewise, the center point of 1a around C2 has apparent positive charge density.

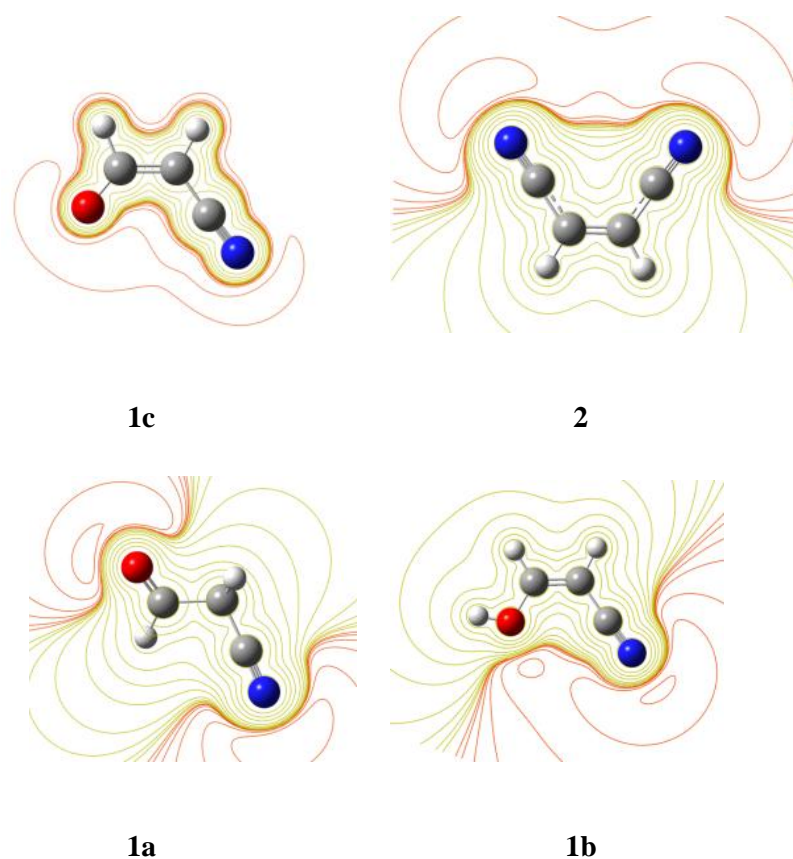


Figure 5.4. Electrostatic Potential contours of 2-cyanoethanal keto form (1a), 2-cyanoethanal enol form (1b), 2-cyanoethanal enolate (1c) and 1,2-dicyanoethylene (2). The red contour indicates the negative electrostatic potential.

On the contrary, the enol form 1b, having a hydrogen atom at O completely loses the negative charge density around O, and all the negative charge density concentrates on N, and the negative density contours widens to half of the molecule. In enolate 1c, the negative charge density covers the entire anion, presumably via π -conjugation, with very high density concentrates on O and N and the negative contour fields combined at one side in the cisoid enolate (1c).

Table 5.1. CHELPG charges for 1a, 1b, 1c, 2, 1c-Mg and 2-Mg

	1a	1b	1c	2	1c-Mg	2-Mg
C1	0.555	0.302	0.696	-0.144	0.355	-0.216
C2	-0.200	-0.494	-0.884	-0.144	-0.734	-0.216
C3	0.351	0.618	0.762	0.441	0.752	0.637
N	-0.457	-0.559	-0.810	-0.445	-0.702	-0.572
O	0.468	-0.524	-0.751	NA	-0.710	NA
Mg	NA	NA	NA	NA	1.525	1.645

The uncomplexed 1,2-dicyanoethylene (2) receptor has very dense negative contours on both N terminals, and the negative fields overlap on one side and extended to a long distance away from the terminals. CHELPG charge analysis is performed to examine how metal cation analytes impart its positive charge to the carbonitrile-carboxaldehyde receptor models, and to relate the atomic charges to the observed charge density contours in the electrostatic potential plots observed earlier.

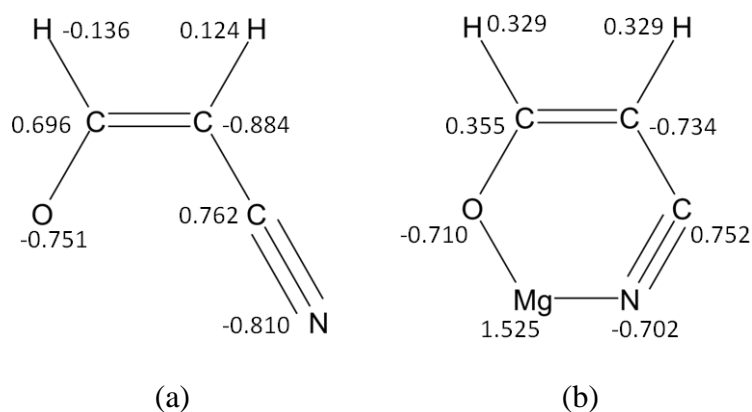
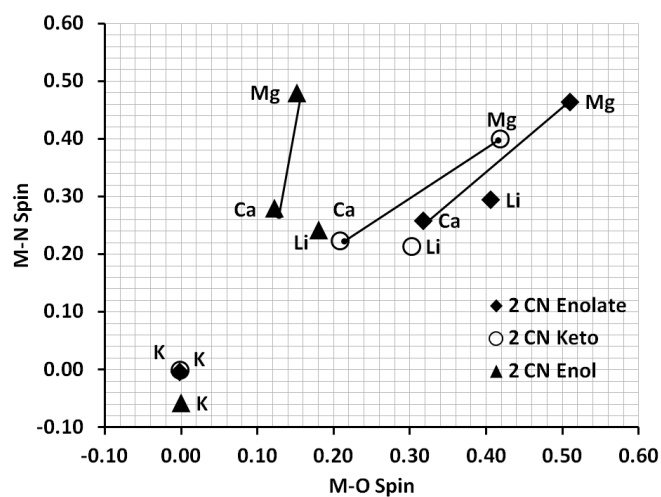
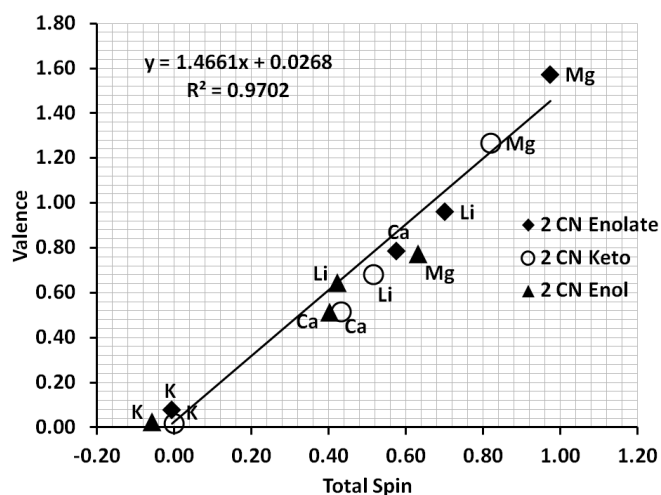


Figure 5.5 CHELPG charges of (a) 2-cyanoethanal enolate (1c) (b) 1c-Mg

Table 5.1 and Figure 5.5 show that Mg(II) transfers 24.4% of its positive charge to 2-cyanoethanal enolate (1c) and 1.525 of its positive charge remains on the cation. The results also show that the N terminal loses more (13.7% loss) of its negative charge due to interaction with Mg(II), compared to the O terminal (6% loss). Moreover, in the 1c-Mg complex the C1 atom becomes strikingly less positive by 49%, while both hydrogen atoms and C2 receive most of the negative charge. The charge of cyano carbon remains unchanged. Mg(II) transfers 18% of its positive charge to 1,2-dicyanoethylene. The N terminal becomes noticeably more negative (3%), while the positive charge is mainly transferred to hydrogen atoms (0.330) and the cyano carbons (0.637).



(a)



(b)

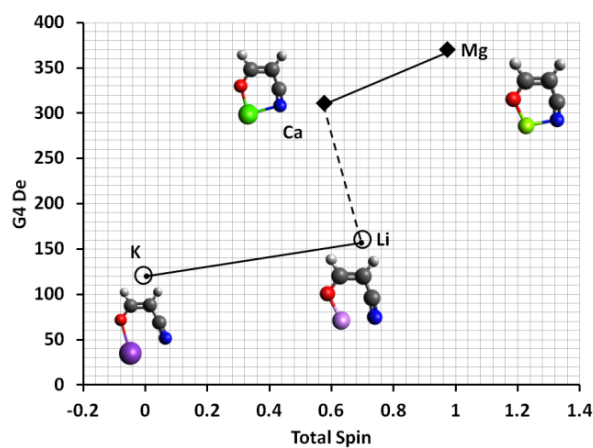
Figure 5.6 Population overlap and metal atomic valence plots obtained from AOmix calculations.:
(a) M-N Spin vs M-O Spin(b) Metal Valence vs Total Spin.

5.2.4 Deduction of Design Parameters for 2-Cyanoethanal

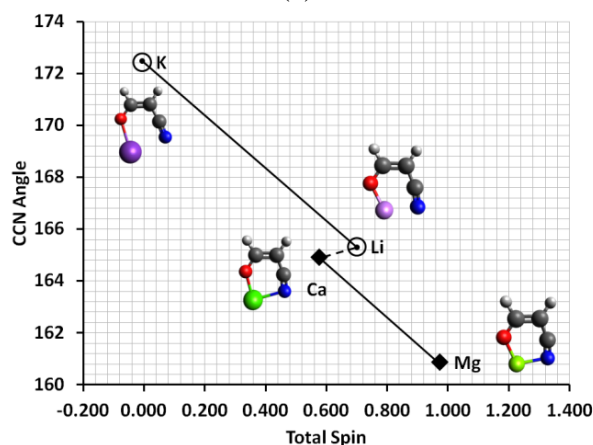
The strength of interaction between cation and heteroatom receptor can be deduced from the efficiency in the overlap between bonding orbitals and thus the electron population in the overlapping area. Likewise, the availability of electron density for sharing-type interaction can be examined from the atomic valence population. Figure

5.6a shows the disparity in the M-N *versus* M-O overlap population in the interactions between Group I and II cations with the keto, enol and enolate forms of 2-cyanoethanal. Magnesium(II) consistently shows the highest overlap population and even distribution between M-N and M-O interaction. Calcium(II) exhibits significantly less overlap population compared to Mg(II) while Li(I) shown similar levels of overlap as that of Ca(II) while K(I) indicates negligible sharing-type interaction. The results indicate that on electron sharing ground Group II cations are favored but Li(I) could compete due to the same mechanism. The keto form (1a) shows that the lone-electron pairs on carbonyl and the carbonitrile terminal give rise to the same extent of heteroatom-metal overlap electron densities. On the contrary, when M-O interaction in enol 1b diminishes, the M-N becomes more efficient (compared to keto 1a). In good accordance with electron distribution over the entire π -framework, the negative charge in enolate 1c causes proportional increases in the M-N and M-O populations. In the 2-cyanoethanal model Mg(II) and Ca(II) are best separated by the keto form, and the least by the enol form (almost halved). Similar trend is true for discrimination between Ca(II) and Li(I) – Li(I) encroaches the most to Group II in the enol form.

Figure 5.6b shows that the total of overlap population (sum of M-N and M-O spins) is linearly related to the atomic valence of metal cation analyte. It is more apparent in this plot that the average population with Li(I) is significantly higher than that with Ca(II). This observation suggests that while valence-type interaction favours Mg(II) against Ca(II), this type of interaction allows Li(I) to compete with Group II cation and can interfere in ion selective potentiometry measurement.



(a)



(b)

Figure 5.7 G4 dissociation energy and total spin plots for complexes of cations with 2-cyanoethanal enolate
 (a) G4 Dissociation energy vs Total spin
 (b) The C-C-N bond angle vs Total Spin

However, the G4 binding energy calculations (Figure 5.7a) indicate that although Li(I) and Ca(II) show comparable total overlap population, the binding of Li I to **1c** is more than 150 kcal/mol weaker and presumably would not cause interference problem. The bending of the C-C-N angle from linearity also seems to be linearly related to total overlap population (Figure 5.7b). Mg(II) causes the largest bending while Ca(II) and Li(I) show comparable pulling strength. Energetics data could be more meaningful for more complete picture on binding preference between receptor models and metal cations. All contributing factors presumably are added to afford the dissociation energies. Figure 5.7a shows that while the difference in dissociation energies for K(I) and Li(I) is relatively small, the two cations are well separated by total

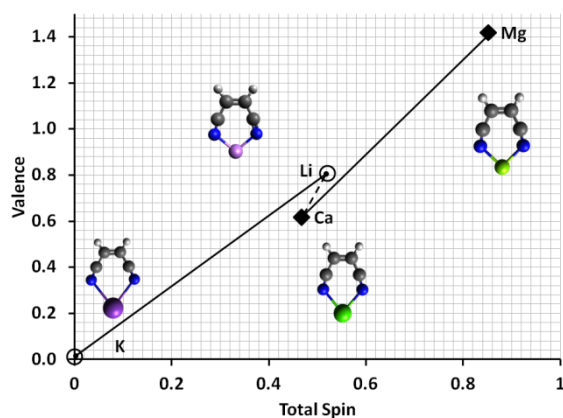
spin. On the contrary, while Ca(II) and Li(I) has similar total spin, the two are well discriminated energetically (De) by more than 150 kcal/mol. Total spin and dissociation energy appear to have similar importance in separating Mg(II) from Ca(II), and considering both design parameters it is obvious that it is possible to design recognition molecules that gives very high selectivity towards Group II, and not worrying interference signal from Li(I). Figure 5.7b indicates that the total spin is linearly related to the bending of the C-C-N angle from linearity. Likewise, this plot shows similar effect of Ca(II) and Li(I) on C-C-N bending, but good discriminations between Mg(II) and Ca(II), and between K(I) and Li(I).

Table 5.2 Overlap population, M-N spin, M-O spin, total spin and metal atomic valence for 2-cyanoethanal enolate (1c), 2-cyanoethanal keto form (1a) and 2-cyanoethanal enol form (1b)

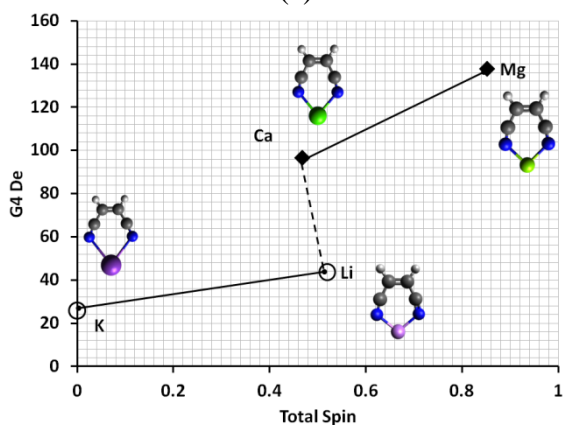
2-cyanoethanal enolate (1c)					
	O-M spin	N-M spin	Total spin	Valence	CCN angle
Li	0.406	0.294	0.700	0.960	165.3
K	-0.002	-0.004	-0.006	0.079	172.4
Mg	0.510	0.464	0.974	1.573	160.9
Ca	0.318	0.258	0.576	0.785	164.9
2-cyanoethanal keto form (1a)					
	O-M spin	N-M spin	Total spin	Valence	CCN angle
Li	0.302	0.214	0.516	0.681	165.0
K	-0.002	0.000	-0.002	0.018	171.4
Mg	0.418	0.400	0.818	1.267	159.0
Ca	0.208	0.224	0.432	0.518	162.2
2-cyanoethanal enol form (1b)					
	O-M spin	N-M spin	Total spin	Valence	CCN angle
Li	0.180	0.242	0.422	0.644	166.6
K	0.000	-0.058	-0.058	0.024	178.4
Mg	0.152	0.480	0.632	0.773	161.7
Ca	0.122	0.280	0.402	0.513	166.2

5.2.5 Deduction of Design Parameters for 1,2-Dicyanoethylene

The complexes between 1,2-dicyanoethylene (2) and Group I and II cations are perfectly symmetrical and planar (Figure 5.3). Therefore there is no problem of disparity between the two terminals of the neutral receptor. Figure 5.8a shows that metal cation atomic valence is directly proportional to total overlap population. Similar to the observation in 2-cyanoethanal, Mg(II) shows significantly higher electron-sharing interaction compared to Ca(II). Likewise, Li(I) appears to have significant valence interaction with 2 (stronger compared to calcium), and higher total spin compared to Ca(II), and thus could potentially cause signal interference in potentiometry measurement.



(a)



(b)

Figure 5.8 Metal valence, G4 dissociation energy and total spin plots for complexes of cations with 2-cyanoethanal enolate (a) Metal valence vs Total Spin (b) G4 Dissociation energy vs Total Spin.

However, the discrimination between Mg(II) and Ca(II), and between K(I) and Li(I) can be conveniently achieved by 1,2-dicyanoethylene receptor. Energetics parameter appears to allow discrimination between Group I and II using the dicyano neutral receptor. While K(I) and Li(I) are separated by less than 20 kcal/mol, Mg(II) and Ca(II) are separated by about 140 kcal/mol. While Ca(II) and Li(I) have very similar total spin, the two cations are separated energetically by more than 50 kcal/mol (Figure 5.8b).

Table 5.3 Design parameters for 1,2-dicyanoethylene

	1,2-Dicyanoethylene					
	Valence	Total Spin	CCN Angle	N-M-N	M NPA	N-N BD Å
Li	0.81	0.26	166.3	99.4	0.906	3.133
K	0.013	0	172.2	76.8	0.957	3.551
Ca	0.616	0.234	164.8	79.6	1.858	3.014
Mg	1.418	0.426	162.9	91.7	1.823	2.907

Table 5.3 shows that Mg(II) exhibits the strongest pulling strength – causing the two N terminal to be at 2.907 Å from each other, and causing a C-C-N bending of 17° from linearity. Ca(II), Li(I) and K(I) show diminishing strength in bending the C-C-N angle. In general, 2-cyanoethanal and 1,2-dicyanoethylene receptor models consistent characteristics in providing design rationale in terms of electron sharing, metal atomic valence and G4 complex dissociation energies.

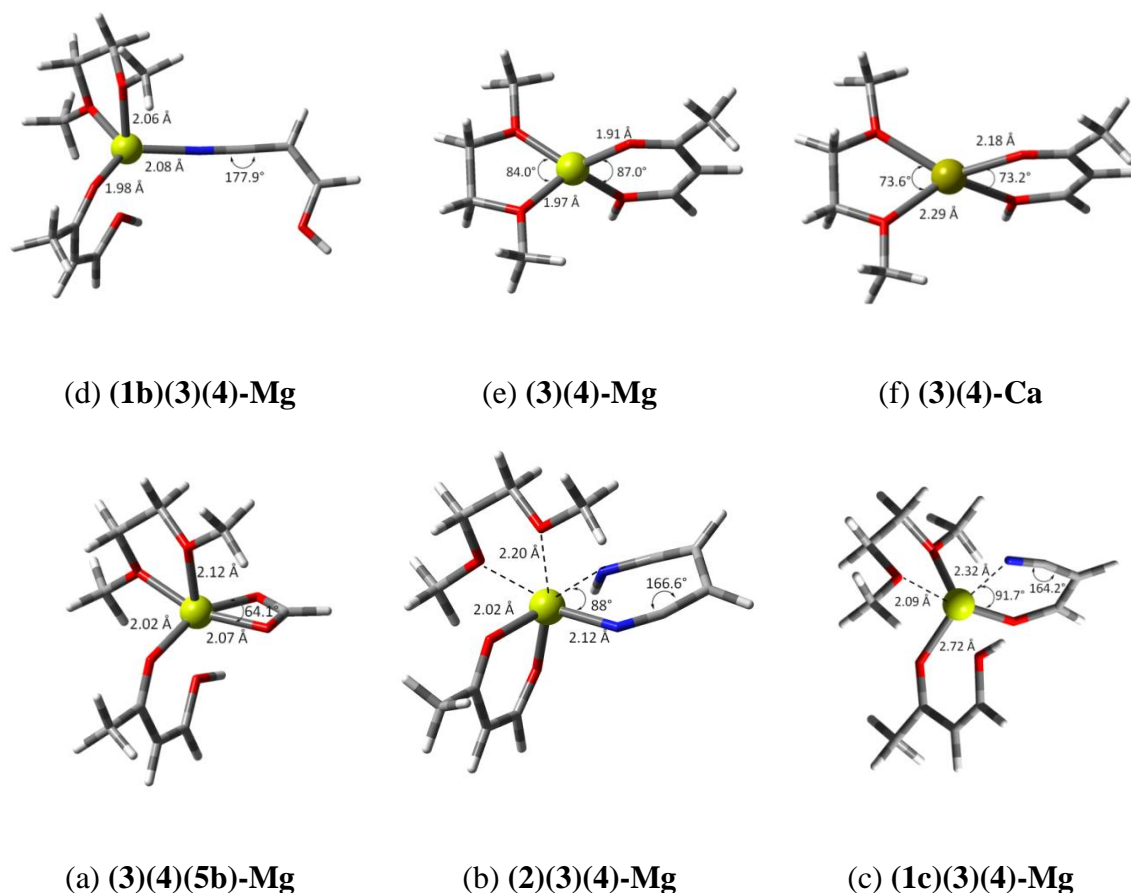


Figure 5.9 . Optimized geometries 3-dimensional rational design calculated using B3LYP with 6-31+G(d,p) basis sets for non-metals and QZVP for metals (a) complex of Mg(II) with ethylene glycol methyl ether (3), butanal-3-one enol (4) and formate (5b), (b) complex of Mg(II) with ethylene glycol methyl ether (3), butanal-3-one enol (4) and 1,2-dicyanoethylene (2), (c) complex of Mg(II) with ethylene glycol methyl ether (3), butanal-3-one enol (4) and 2-cyanoethanal enolate (1c), (d) complex of Mg(II) with ethylene glycol methyl ether (3), butanal-3-one enol (4) and 2-cyanoethanal enol (1b) form, (e) complex of Mg(II) with ethylene glycol methyl ether (3), butanal-3-one enol (4) and (f) complex of Ca(II) with ethylene glycol methyl ether (3), butanal-3-one enol

5.2.6 3-Dimensional Rational Design with Carbonitrile-Carboxaldehyde Receptor Models and Ionomycin Fragment Models

Three-dimensional rational design attempts to elucidate interactions between carbonitrile-carboxaldehyde receptor models with Group I and II cations, utilizing the fragment models from Ionomycin as case studies. Initially interactions between the three fragments from Ionomycin with Mg(II) and Ca(II) are examined. Ethylene glycol methyl ether and butanal-3-one fragments are fixed throughout but the third ligand is changed. Interactions between metal cations with the two fixed ligands serve as

reference points, and the effects of formic acid and formate as the third ligand demonstrate the application of this approach to understand heteroatom-metal interaction in neutral and negatively charged Ionomycin (Figure 5.1). The different forms of 2-cyanoethanal and 1,2-dicyanoethylene then replace formate as the third ligand. It should be highlighted that three-dimensional interactions involving Group I cations are not significant. It is apparent that the single charged positive metal cations exhaust its binding capability with the fixed fragment models from Ionomycin and thus fail to interact with the third ligand.

Figure 5.9a shows that the O-Mg with butanal-3-one receptor is the shortest hetroatom-metal bond (2.02\AA), shorter than the O-Mg bond (2.07\AA) with formate ligand. The O-Mg bond with ethylene glycol methyl ether is 2.12\AA . The O-Mg bonds with two fixed ligands (Figure 5.9e) are much shorter; 1.91\AA in butanal-3-one and 1.97\AA in ethylene glycol methyl ether. The O-Ca bonds are much longer when Ca(II) replaces Mg(II) in the fixed ligands (Figure 5.9f); 2.18\AA with butanal-3-one and 2.29\AA in the diether. Substituting the third ligand with 2-cyanoethanal enolate causes the O-Mg bonds to increase to 2.09\AA and 2.72\AA , in diether and dicarbonyl ligands, respectively. The N-Mg bond distance is 2.32\AA and Mg(II) strongly pulls the two terminals to make N-Mg-O angle of 91.7° and bringing the two ends close together to 3.099\AA .

When 2-cyanoethanal enol (1b) replaces the third ligand, the O terminal, now becomes too electropositive thus completely fails to bind with Mg(II) in Figure 5.9(d) – the C-C-N angle widens to linearity. The electron density in 1b concentrates on the N terminal causing a strong N-Mg interaction and a short bond of 2.08\AA . Likewise, the binding strength of Mg(II) towards the two fixed ligands increases causing short O-Mg bonds of 1.98\AA and 2.06\AA with dicarbonyl and diether, respectively. Replacing the third

ligand with 1,2-dicyanoethylene in Figure 5.9b causes the dicarbonyl enol hydrogen atom to migrate to one of the N terminal in 2, but Mg(II) retains bonding (2.12 Å N-Mg bond distance) with both the N terminals. Mg(II) strongly pulls the two N terminals to make a 88° N-Mg-N bond and brings the two ends to 3.049 Å from each other.

Table 5.4 CHELPG charges of metal and heteroatoms in Mg(II) complexes with ethylene glycol methyl ether (3), butanal-3-one enol (4), 2-cyanoethanal enolate (1c) and 1,2-dicyanoethylene (2 or DCNE)

	Complexes		
	(3)(4)-Mg	(1c)(3)(4)-Mg	(2)(3)(4)-Mg
Ether O1	-0.399	-0.284	-0.371
Ether O2	-0.422	-0.296	-0.256
Carbonyl O1(enol)	-0.643	-0.326	-0.673
Carbonyl O2	-0.606	-0.629	-0.756
Mg	1.257	1.123	1.274
Receptor O	NA	-0.665	-0.325
Receptor N	NA	-0.673	-0.737

CHELPG atomic charges (Table 5.4) show that Mg(II) transfers 37%, 44% and 36% of its positive charge to its complexes with ethylene glycol methyl ether (diether)-butanal-3-one (dicarbonyl), diether-dicarbonyl-1c and diether-dicarbonyl-2, respectively. The negative charges on the oxygen atoms in butanal-3-one (dicarbonyl) are consistently higher than those on diether oxygen atoms. The dicarbonyl O-Mg bond distances are consistently shorter than those in the Mg(II)-diether complexes. This seems to indicate that the heteroatom-metal interaction in the former, with higher negative charge on oxygen atom, is stronger. The N and O terminals of 2-cyanoethanal enolate (1c) in the 3-dimensional design show comparable level of negative charge. The lack of charge disparity on the N and O terminals indicates efficient charge delocalization throughout the π -network, observed earlier in the CHELPG analysis on 1c-Mg. It is surprising that 1,2-dicyanoethylene does not contribute to reduce positive charge on Mg(II), compared to the 37% transferred to the two fixed ligands. When 2 is added as the third ligand, Mg(II) appears to interact more poorly and the heteroatom-Mg

interactions reoptimized among the three receptor models, in striking contrast to that when 1c is used as the third ligand. This indicates that 2 is a weak Group II receptor and it can be used as an advantage in discriminating divalent cations.

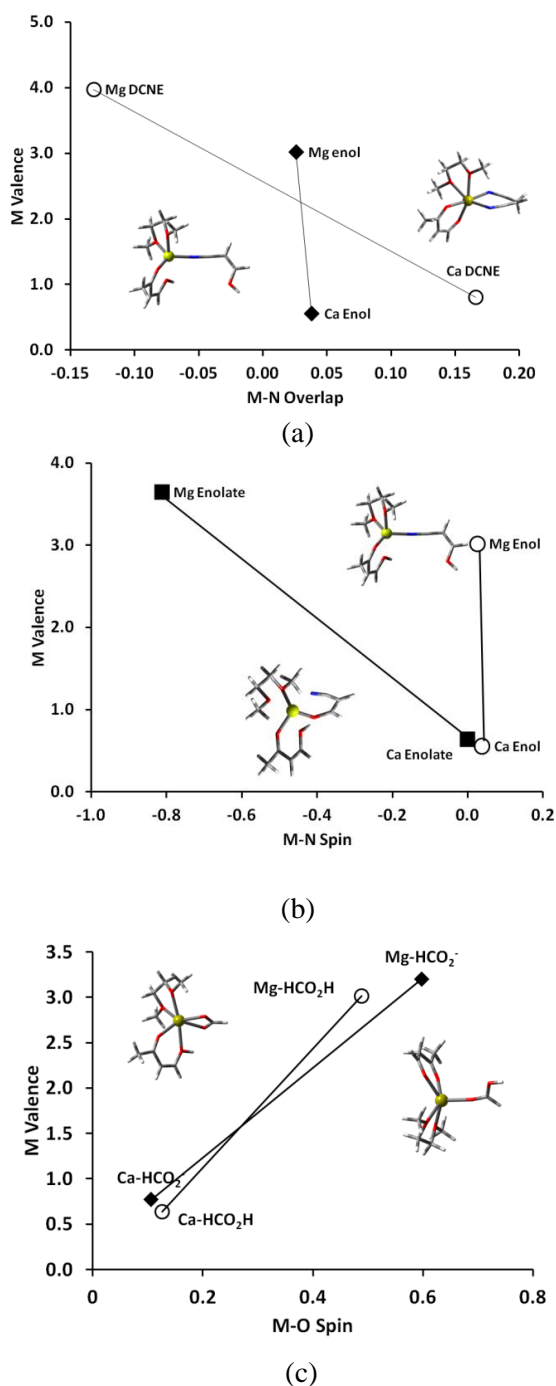


Figure 5.10 Design parameter plots from complexes of Mg(II) and Ca(II) with Ionomycin fragment models, 2-cyanoethanal (1) and 1,2-dicyanoethylene (2) receptors: (a) Metal valence vs M-N Overlap for (1b)(3)(4) and (2)(3)(4), (b) Metal valence vs M-N overlap for (1b)(3)(4) and (1c)(3)(4), (c) M valence vs M-O Spin for HCO₂H and HCO₂⁻.

Overlap population analysis in Table 5.5 shows the striking contrast between the atomic valence of Mg(II) and Ca(II). While the atomic valences of Mg(II) are greater than 3, indicating a very strong electron sharing tendency, the Ca(II) valence of less than 1 suggests that ionic interaction is significantly more important for the latter. Therefore, enolizable receptors that form multiple negatively charged sites can discriminate magnesium in favour of calcium.

Figure 5.10a shows that while the overlap population between 2-cyanoethanal enol 1b both divalent cations (magnesium and calcium) are very similar, the M-N spin with 1,2-dicyanoethylene as the third receptor separate the two cations by more than two folds. Likewise, metal valence and M-N spin with 2-cyanoethanal enol form (1b) and enolate (1c) separate Mg(II) and Ca(II) by more than two folds (Figure 5.10b). The enormous difference in atomic valence between the two Group II cations, and the significant increase in overlap population due to negatively charged site are essential design parameters towards Mg(II) *versus* Ca(II) discrimination. Although prior reports suggest that pH effect could favour Ca(II) against Mg(II) in calcium determination using Ionomycin ionophore, the result in Figure 5.10c shows that the difference between formic acid and formate, deduced from metal valence and O-M spin, only marginally favors formate.

Table 5.5 Metal atomic valence and overlap population design parameters for Mg(II) and Ca(II) complexes with ethylene glycol methyl ether (3), butanal-3-one enol (4), 2-cyanoethanal enol (1b) and 1,2-dicyanoethylene (2 or DCNE)

	M Valence	M-N Spin	Total Spin
(1b)(3)(4)-Mg	3.016	0.026	0.026
(1b)(3)(4)-Ca	0.557	0.038	0.038
(2)(3)(4)-Mg	3.974	-0.132	-0.264
(2)(3)(4)-Ca	0.804	0.166	0.332

Highly selective calcium determination involving enolizable and multiple negatively charged calcium ionophores presumably is caused by ionic interaction. The G4 dissociation energies (Table 5.6) utilizing the formic acid or formate receptor model alone show that the discrimination between Mg(II) and Ca(II) in the formic acid case is 30.3 kcal/mol, favouring magnesium. On the contrary the formate receptor separate further the two divalent cations by 55.1 kcal/mol, *i.e* there is 24.8 kcal/mol additional discrimination against Ca(II). This indicates that if the ionic interaction mechanism needs to be optimized in order to favour Ca(II) some other factors need to be considered such as the use of more than one equivalent of ligand to each calcium cation, optimization of the lipophilic tetraphenylborate weight percent, suitable polymeric membrane, proper plasticizer choice and solvation effect by water molecules.

Table 5.6 G4 Dissociation energies of HCO₂H and HCO₂⁻

Complex	G4 ΔH_{rxn} (kcal/mol)
Mg-HCO ₂ H \rightarrow Mg ²⁺ + HCO ₂ H	109.3
Ca- HCO ₂ H \rightarrow Ca ²⁺ + HCO ₂ H	79.0
Mg- HCO ₂ ⁻ \rightarrow Mg ²⁺ + HCO ₂ ⁻	368.4
Ca- HCO ₂ ⁻ \rightarrow Ca ²⁺ + HCO ₂ ⁻	313.3

5.2.7 Rationale for Magnesium *versus* Calcium Selectivity and Discrimination of Group I Cations

G4 calculations reveal that in the absence of water solvation Mg(II) binds 259.1 kcal/mol more strongly to formate than it does to the uncharged form, formic acid (Table 5.6). Likewise, Ca(II) interacts more strongly by 234.3 kcal/mol to formate than to formic acid. In both uncharged and anion forms, Mg(II) binds more strongly to the receptor model compared to Ca(II), by 30.3 and 55.1 kcal/mol, respectively. The negatively charged formate favors Mg(II) by additional 24.8 kcal/mol. All the energetics data and overlap population plots seem to be in favour of magnesium. CHELPG and

metal atomic valence could be the links that rationalize the observed selectivity towards calcium against magnesium and Group I cations. The apparent preference of calcium towards ionisable ionophores, at higher pH and with multiple negatively charged recognition molecules such as EDTA, Ionomycin and carboxylic ionophore A23187, strongly suggests the role of ionic interaction in calcium recognition. While Mg(II) shows atomic valence of significantly greater than 3, Ca(II) does not appear to gain electron into its valence during interaction with electron donor receptors such as the carbonitrile-carboxaldehyde models.

The CHELPG data suggests that the extent of positive charge transfer from the metal cations to the receptor models is strongly related to the ability of the recognition molecule to stabilize the analytes. Striking contrast between 2-cyanoethanal enolate (1c) and 1,2-dicyanoethylene (2) towards removing positive charge from Mg(II) clearly seen in the CHELPG data. After binding to two fixed receptor models from Ionomycin fragments, ethylene glycol methyl ether (diether) and butanal-3-one (dicarbonyl), adding 1,2-dicyanoethylene as the third ligand does not reduce the positive charge on Mg(II). However, hydrogen atom transfer from the dicarbonyl enol to one of the N terminal in 2 could complicate the observation. In this particular case the dicarbonyl “fixed” receptor from Ionomycin fragment now is formally an enolate, thus changing the whole scenario, and the protonated 2 could be expected to be deactivated towards cation binding. Overlap population, metal atomic valence, charge distribution and energetics data indicate that Group I cations can be discriminated in the rational design towards highly selective divalent cation ionophores.

Nevertheless, two factors should be highlighted regarding potential potentiometry interference signal from competing cations; (i) Hofmeister effect (Kherb *et al.*, 2012; Zhang, Jenny, *et al.*, 2000; Zhang & Cremer, 2006) favours weakly hydrated cations having low surface charge density and highly polarizable monovalent ions in the following order; $\text{Li}^+ > \text{Cs}^+ > \text{Rb}^+ > \text{NH}_4^+ > \text{K}^+ > \text{Ca}^{2+} > \text{Mg}^{2+} > \text{Zn}^{2+}$, and the presence of lipophilic tetraphenylborate as ion exchanger or anionic sites in the sensing membrane increases this effect, and (ii) Based on electron sharing ground, lithium(I) encroaches deep into the Group II design parameter region and Li(I) overcomes calcium in this type of interaction.

Therefore, the reported highly selective detections of magnesium using tripodal lipophilic malonodiamide and other malonodiamide receptors presumably have been achieved by judicious optimization of polymeric membrane components, and in good accordance with the proposed rationale. The effect of hydration on Mg(II), Ca(II) and Group I cations in aquatic environment may not be over emphasized. Although the effect of solvation by water molecules has been accounted for in the observed Hofmeister series, in actual sensing membranes, the potentiometry signal transduction occurs in almost exclusively lipophilic environment, wherein the extent of cation hydration could be minimal, and different from the aqueous medium.

5.3 Conclusions

Density functional method using B3LYP hybrid functionals having three Becke parameters, fitted to G1 test set has successfully been employed to obtain optimized geometries of receptor models and its complexes with Group I and II cations. Pople's split valence, polarized and diffused basis sets and Ahlrich's QZVP basis functions have been utilized throughout. The optimized geometries have been used in the following

CHELPG, electrostatic potential contour and overlap population calculations. Energetics data were obtained using G4 composite method that utilizes Dunning's correlation consistent basis sets that include reliable extrapolation to the basis set limit for potassium and calcium. CHELPG data reliably account for transfer of positive charge from metal cations and redistribution of the imparted charge within the receptor models. In all cases the CHELPG data is consistent with the charge density gradient obtained from electrostatic potential plots. The computational model for Ionomycin has been adopted in elucidating the rational carbonitrile-carboxaldehyde heteroatom-metal interaction, deduction of design parameters and pH effect. Ethylene glycol methyl ether (diether), butanal-3-one (dicarbonyl) and formate fragment models have been extracted from Ionomycin, and the first two have been used as fixed ligands, while formate has been replaced with three forms of 2-cyanoethanal (1) and 1,2-dicyanoethylene (2).

Overlap population analysis shows that divalent cations are favoured in the electron sharing type interaction. This mechanism indicates that lithium encroaches deep into Group II region and competes seriously with calcium. Metal atomic valence is linearly related to heteroatom-metal spin and total spin. Energetics data show that preferential bindings between carbonitrile-carboxaldehyde receptors or three receptor models extracted from Ionomycin and divalent cation could discriminate Group I cations. G4 calculations and overlap population data are in favour of higher selectivity towards magnesium. The striking difference between atomic valence in Mg(II) and Ca(II) most probably is the rationale in highly selective calcium ionophore. Judicious choice of polymeric membrane and optimization of sensing membrane components could overcome Hofmeister effect and afford the desired selectivity, either in favour of magnesium or calcium, in good agreement with the proposed rationale.

Chapter 6 : Computational Evaluation of Unsaturated Carbonitriles as Neutral Receptor Model for Beryllium(II) Recognition

Design of neutral receptor molecules (ionophores) for beryllium(II) using unsaturated carbonitrile models had been carried out using Density Functional Theory, G3 and G4 calculations. The first part of this work focuses on gas phase binding energies between beryllium(II) and 2-cyano butadiene (2-CN BD), 3-cyano propene (3-CN P) and simpler models with two separate fragments; acrylonitrile and ethylene. Interactions between beryllium(II) and cyano nitrogen and terminal olefin in the models have been examined in terms of geometrical changes, distribution of charge over the entire π -system and rehybridization of vinyl carbon orbitals. NMR shieldings and vibrational frequencies probed charge centers and strength of interactions. The six-membered cyclic complexes have planar structures with the rehybridized carbon slightly out of plane (16° in 2-CN BD). G3 results show that in 2-CN BD complex participation of vinyl carbon further stabilizes the cyclic adduct by 16.3 kcal/mol, whereas, in simpler models, interaction between beryllium(II) and acetonitrile is favourable by 46.4 kcal/mol compared with that of ethylene. The terminal vinyl carbon in 2-CN BD rehybridizes to sp^3 with an increase of 7% of s character to allow interaction with beryllium(II). G4 calculations show that the Be(II) and 2-CN BD complex is more strongly bound than those with Mg(II) and Ca(II) by 98.5 and 139.2 kcal/mol respectively. QST2 method shows that the cyclic and acyclic forms of Be(II)-2-CN BD complexes are separated by 12.3 kcal/mol barrier height. Overlap population analysis reveals that Ca(II) can be discriminated based on its tendency to form ionic interaction with the receptor models.

6.1 Introduction

The chemistry of beryllium compounds can be explained in terms of charge to radius ratio, electronegativity and electron deficiency of beryllium atom and its charged species. In keeping with these reasoning the structure and reactivity of beryllium (I and II) compounds closely resemble those of aluminium and boron, and untypical to its Group II neighbours (Everest, 1964). Beryllium use in daily life owes to its light weight and mechanical strength especially the beryllium-copper alloy (Mooradian, 1952; Wang *et al.*, 2011; Watanabe *et al.*, 1995). The electron deficient nature of divalent beryllium compounds can be exploited as catalyst in polymerization process and synthesis (Kobetz *et al.*, 1974; Swinnen *et al.*, 2010; Wang *et al.*, 2011).

Schleyer, Schaefer and their co-workers have demonstrated earlier the use of computational methods in estimating stabilities of organometallic systems involving beryllium (Binkley *et al.*, 1977; Lao *et al.*, 1967; Swope *et al.*, 1976). Clark, Frenking and their co-workers have exploited advanced *ab initio* and DFT methods in investigating beryllium-ligand interaction (Alex *et al.*, 2006; Parameswaran *et al.*, 2009). DFT (Hirai *et al.*, 1999, 2000) method has widely been utilized in obtaining reliable molecular geometries and properties.

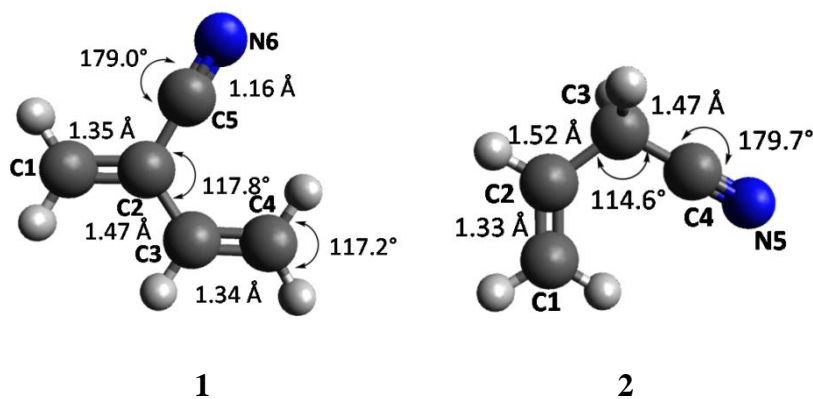


Figure 6.1 Computed B3LYP/6-31+G(d,p) geometries of 1 (2-CN BD) and 2 (3-CN P).

Computational methods had been adopted in order to gain insights on the interaction of doubly charged beryllium cation (Be(II)) with unsaturated carbonitriles in our attempt to design neutral receptor molecule or ionophore for beryllium(II). This work focusses on 2-cyanobutadiene (2-CN BD) and 3 cyanopropene (3-CN P) to represent unsaturated carbonitriles (Figure 6.1). Eventually, this investigation is desired to reveal the viable options of beryllium ionophore having high selectivity towards beryllium - against magnesium(II), calcium(II) and aluminium(III).

Structure 1 is employed in order to evaluate the binding of beryllium(II) with lone electron pair in the cyano group, direct participation of a carbon-carbon double bond in cation-receptor interaction and stabilization of the Be(II)-receptor complex due to π -conjugation. A carbonitrile receptor model that lacks conjugation, *i.e* structure 2 elucidates the participation of carbonitrile and olefin moieties but without π -system. Simpler models have been evaluated for comparison - these are small molecule fragments of structures 1 and 2 (ethylene, acetonitrile and acrylonitrile) that give useful information with much less computation time. It is insightful to confirm that metal cations could actually form strong interaction with vinyl moieties, and this finding could extend the applications of beryllium in chemical sensor, preparative procedure and polymerisation.

We have reported earlier the interactions of unsaturated carbonitriles with metal cations (Rosli, Ahmad, *et al.*, 2013; Rosli, Bakar, *et al.*, 2013). We have highlighted that in the absence of conjugation, the imparted positive charge from the cation is mainly transferred to the α -protons and the cyano bond remains intact. On the contrary, in conjugated carbonitriles such as acrylonitrile, the transferred positive charge is distributed over the entire π -network and the cyano bond broken to afford a ketenimine

structure (Woi *et al.*, 2014). During the preparation of this report we have also investigated the possibility of employing carbonitrile-carboxaldehyde receptors as selective recognition molecules for Group II divalent cations. We have proposed that electron sharing *versus* ionic type interaction could elucidate the nature of heteroatom-metal binding and provide rationale in discrimination of Group I cations and explanation in the experimentally determined selectivity.

6.2 Results and Discussion

6.2.1 Optimized Geometries

The interaction of beryllium(II) species with 2-cyanobutadiene (1) presumably is initiated by sharing of cyano nitrogen lone electron pair to beryllium(II) empty orbital. In the acyclic complex the immediate product is destabilized due to repulsion between positively charged neighbouring nitrogen and beryllium cation. Stabilization can be achieved if the positive charge on nitrogen is distributed over the entire π -network. Results in Table 6.1 show that beryllium(II) has donated 52% of its charge (reduced to 0.963) to structure 1 in the acyclic complex. Beryllium(II) imparts further its positive charge to the diene moiety by interacting with C4 resulting in only 23% of its positive charge (reduced to 0.454) remains on beryllium. Distribution of positive charge over the π -network in the acyclic complex moves positive centre further from beryllium atom, and resulting in 4% shortening of the C2-C5 bond and 2 to 3% elongation of C5-N6 (the cyano bond) and C1-C2 bonds (Figure 6.2). This result indicates that what had been observed earlier in acrylonitrile-metal complexes, the cyano bond in 1-Be is broken and a bent ketenimine moiety is formed. There is no significant change in the C3-C4 bond other than the out-of-plane (57.8° C1-C2-C3-C4 dihedral angle) twist of the olefin moiety. The C3-C4 bond is elongated by about 6% due to the interaction of beryllium(II) with the π -bond orbitals on C3-C4 for the formation of Be-C4 bond. The

2-cyanobutadiene-metal interaction is the strongest in Cyclic 1-Be compared to those with magnesium(II) and calcium(II), inspected based on the structural changes to the receptor induced by the interactions with divalent cations. Beryllium pulls the terminal vinyl atom and the cyano nitrogen atom closer together at 2.89 Å and making a 117.0° N6-Be-C4 angle. Likewise, the metal-C4, the metal-N6 bonds and the C4-N6 distance are the shortest with beryllium(II). The Ca-C4 (2.93 Å) and the Mg-C4 (2.30 Å) bond distances are 65% and 29% longer, respectively, compared to Be-C4. Moreover, the Ca-N6 bond length is 48% longer than Be-N. Weaker interactions give smaller N6-metal-C4 angles; N6-Ca-C4 and N6-Mg-C4 affords 76° and 35% smaller N6-metal-C4 angle, compared to N6-Be-C4. The C1-C2 only experiences minor structural changes due to its position being further away from the the receptor-metal binding sites, and not significantly affected by the complex π -network.

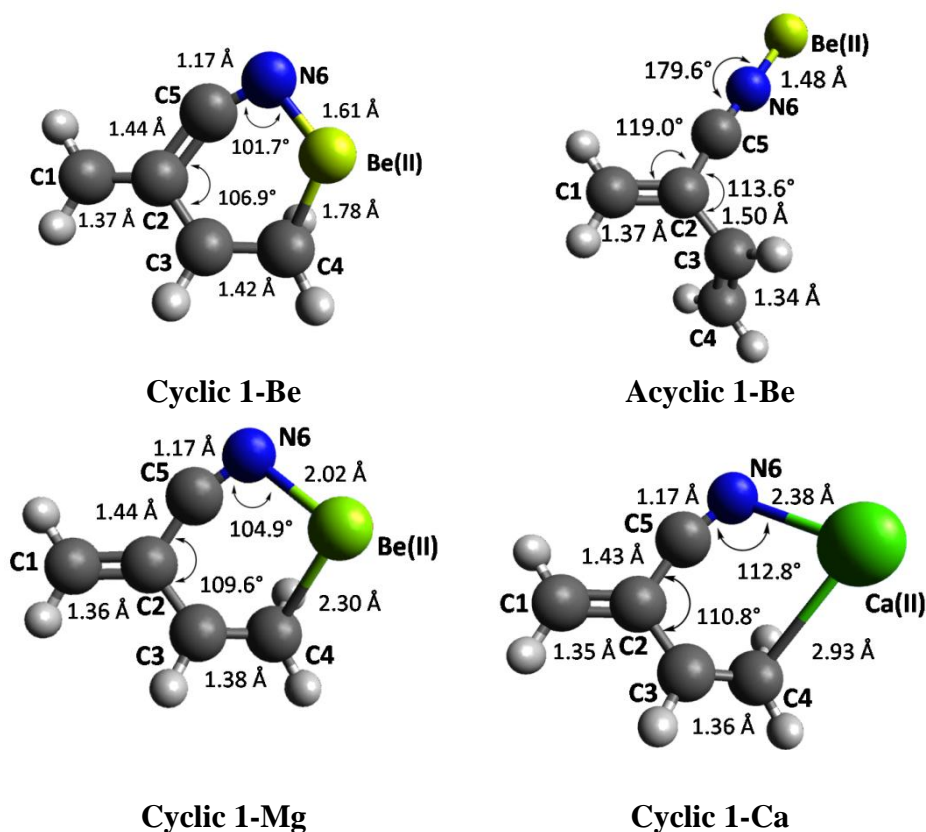


Figure 6.2. Optimized geometries of Be(II)-2-CN BD cyclic complex, Be(II)-2-CN BD acyclic complex, Mg(II)-2 CN BD cyclic complex and Ca(II)-2 CN BD cyclic complex.

Mulliken charge analysis indicates that the interaction of beryllium(II) ion with 1 results in reduction of 77.3% of the positive charge on beryllium (Table 6.1). The cyano nitrogen experiences the largest increase in positive charge by 0.66, followed by C3 with increase by 0.22. This accounts for most of the positive charge donated from beryllium(II) analyte. Due to interaction with Be(II), the cyano carbon (C5) is expected to be more reactive and electrophilic, having a vinyl cation characteristic. Bending of the C2-C5-N6 bond from linearity to allow interaction between Be(II) and C5 is balanced with avoidance of forming C2-C5 allenic double bond and vinyl cation. This balancing act results in almost a full covalent bond between Be(II) and C4 with 1.78 Å bond length, and the biggest accumulation of negative charge on C2 and C4, the latter is directly favourable to the highly electronegative beryllium atom (Table 6.1).

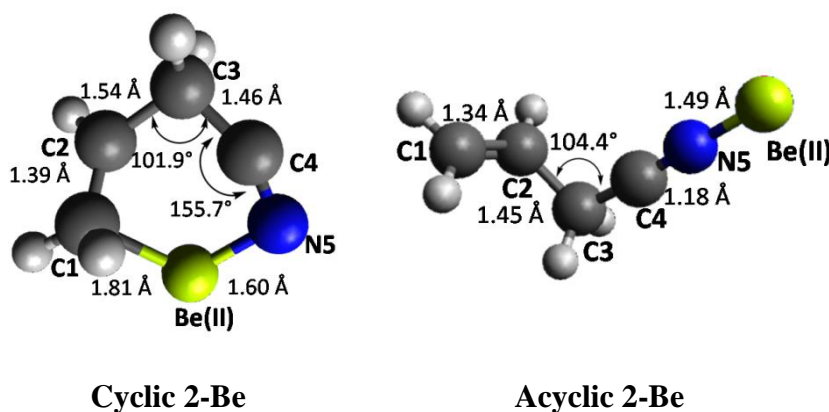


Figure 6.3 Optimized geometries of Be(II)-3-CN P cyclic complex and Be(II)-3-CN P acyclic complex.

The six-membered Cyclic 1-Be complex is best viewed as an almost flat structure except for the 16° out of plane involving C5-C2-C3-C4 atoms (Table 6.2). The carbon and beryllium centres involved in the new C4-Be bond exhibit significant sp^3 -like character. The p orbital in C4, initially forms π -bond between C3 and C4, rehybridizes to sp^3 hybrid orbital, taking the two π -electrons with it to the beryllium empty orbitals (Figure 6.2). This leaves C3 as a positively charged centre, sharing the positive charge over the entire π -system. Natural Bond Orbital (NBO) analysis shows

18% decrease in *s* character in the rehybridized *p* orbital in C4. This is in keeping with the observed decrease in the H10-C4-H11 bond angle from 117° to 111° (Table 6.3). This explanation is consistent with the observed GIAO NMR shieldings described in the following section.

Table 6.1 Mulliken atomic charges for 2-CN BD, 3-CN P and its complexes with beryllium(II)

	2-CN BD			3-CN P		
	1	Acyclic 1-Be	Cyclic 1-Be	2	Acyclic 2-Be	Cyclic 2-Be
C1	-0.153	-0.032	-0.097	-0.278	-0.176	-0.258
C2	0.753	0.223	0.852	-0.034	-0.029	0.191
C3	-0.138	0.119	0.078	-0.240	-0.189	-0.305
C4	-0.174	-0.229	-0.330	0.221	0.150	0.267
C5	-0.532	-0.154	-0.487	NA	NA	NA
N	-0.514	-0.017	0.150	-0.496	-0.007	0.128
Be	NA	0.963	0.454	NA	1.02	0.466

In the absence of π -conjugation (diene moiety), interaction of beryllium(II) with 3-cyanopropene (receptor model 2) results in longer C_{vinyl}-Be (1.82 Å) and only slightly shorter Be-N_{cyano} bond (1.60 Å, compared to 1.61 Å in Cyclic 1-Be)(Figure 6.3). This is consistent with the above reasoning that weaker interaction (longer C_{vinyl}-Be bond) between beryllium and vinyl carbon results from the absence of π -conjugation. Likewise, in the absence of conjugation, the C-C bond adjacent to the cyano group is longer in structure 2 (1.46 Å), as compared to that in structure 1 (1.44 Å). Despite the apparent differences in bond distances, the C-N-Be and C-C-N bond angles in both receptor models are very similar (about 100° and 155°, respectively)(Table 6.3). As predicted, in the absence of conjugation the remaining positive charge on beryllium is higher in Cyclic 2-Be (0.466) compared to that in Cyclic 1-Be (0.454). Moreover, the positive charge on carbon atom (C2) adjacent to C-Be bond is higher in Cyclic 2-Be (0.191), whereas in Cyclic 1-Be, after distributing to three carbon atoms, only 0.078 of Mulliken charge remains on the respective carbon (C3). The Cyclic 2-Be complex also

exhibits an almost flat structure with 30° dihedral angle for C1-C2-C3-C4 (Table 6.2). Meanwhile, the interaction of beryllium(II) with acyclic form of 3-CN P showed similar trend with the acyclic 2-CN BD with only 50% of Be(II) charge transferred to the unconjugated receptor 2 resulting in 1.02 of Mulliken charge remains on beryllium atom. The Acyclic 2-Be complex lacks interaction between C1 vinyl carbon with Be(II). Consequently, the greater extent of positive charge retained by beryllium atom is confirmed by the negligible change in C1 Mulliken charge (in Acyclic 2-Be). The C1 of Cyclic 2-Be complex had been proposed to undergo rehybridization from sp^2 to sp^3 as indicated by the decrease in the H7-C1-H8 angle from 117.2° to 113.8°.

Table 6.2 Dihedral angles of 2-CN BD, 3-CN P and its complexes with Be(II)

2-CN BD			
Dihedral Angles	1 (°)	Cyclic 1-Be (°)	Acyclic 1-Be (°)
C1-C2-C3-C4	180	169.8	58
C2-C4-N-Be	NA	5.7	178.8
C5-C2-C3-C4	0	-16.1	-119.7
N-C5-C1-C2	180	165.6	-179.7
C1-C2-C5-N	180	165.6	178.6
3-CN P			
Dihedral Angles	2 (°)	Cyclic 2-Be (°)	Acyclic 2-Be (°)
C1-C2-C3-C4	-0.02	30.5	-99.3
C1-C3-N-Be	NA	11.3	-99.9
C3-C4-N-Be	NA	-5.8	-164.0
C1-C2-N-Be	NA	25.9	-70.4

Table 6.3 Bond angle in 2-CN BD , 3-CN P and its complexes with Be(II)

2-CN BD			
Bond angles	1 (°)	Cyclic 1-Be (°)	Acyclic 1-Be (°)
C5-N-Be	NA	101.7	179.6
C2-C5-N	179.0	153.4	174.4
H10-C4-H11	117.2	110.8	117.0
C3-C2-C5	117.8	106.9	113.6
C1-C2-C5	119.1	127.0	119.0
3-CN P			
Bond angles	2 (°)	Cyclic 2-Be (°)	Acyclic 2-Be (°)
C4-N-Be	NA	100.3	177.5
C3-C4-N	179.9	155.5	175.2
H7-C1-H8	117.2	113.8	116.7
C2-C3-C4	114.6	102.0	104.0
C1-C2-C3	126.2	125.5	122.0

6.2.2 NMR Shifts and Vibrational Frequencies

Nuclei experiencing deshielding effect due to lack of electron density or localization of positive charge are probed using ^{13}C NMR shifts where increased chemical shifts are predicted for these nuclei. Cyclic 1-Be GIAO studies (Table 6.4) show that C3 and C1 experience the highest deshielding effects, with 88% and 57% increase in carbon chemical shifts, respectively, indicating the largest accumulation of positive charge on these nuclei. Moreover, consistent with the proposed rehybridization of C4 to sp^3 -like, this carbon atom experiences 52% decrease in chemical shift from 107.8 to 56.3 ppm due to shielding. Likewise, build-up of positive charge increases the chemical shift in C5 by 45% (from 98.7 to 142.7 ppm) due to deshielding effect. Moreover, the Cyclic 2-Be complex also experiences similar deshielding effect due to localization of positive charge only on one carbon nucleus (C2, adjacent to C1-Be), instead of two carbon nuclei observed in Cyclic 1-Be, with 74% (from 135.0 to 235.1 ppm) increase in chemical shift. As predicted, the C1 vinyl carbon in Cyclic 2-Be, shows the chemical shift decreases by 60% (from 124.3 to 73.9 ppm) due to shielding.

Table 6.4. GIAO ^{13}C NMR shifts (ppm) with TMS reference of 2-CN BD, 3-CN P and its complexes with Be(II).

	2-CN BD			3-CN P		
	1	Cyclic 1-Be	Acyclic 1-Be	2	Cyclic 2-Be	Acyclic 2-Be
C1	116.3	182.6	182.8	124.3	73.9	146.6
C2	113.1	106.2	93.2	135.0	235.1	98.0
C3	121.1	228.2	103.8	24.3	27.4	15.0
C4	107.8	56.3	143.1	120.2	151.4	154.3
C5	98.7	142.7	149.5	NA	NA	NA
N	272.3	230.3	130.1	297.3	220.3	127.3
Be	NA	97.4	93.9	NA	99.1	95.8

This observation supports the proposed rehybridization of the C1 vinyl carbon from sp^2 to sp^3 -like to allow covalent type interaction with beryllium. The two complexes, Cyclic 1-Be and Cyclic 2-Be exhibit similar trend in nitrogen chemical shifts. The nitrogen nuclei are shielded due to interaction with Be(II), and the cyclic complexes show significantly greater extents of this effect. The absence of π -network in Cyclic 2-Be does not influence the shielding on nitrogen nuclei.

Vibrational frequency analysis (Table 6.5) shows that Be-N bond in the Acyclic 1-Be complex stretch at 884.3 cm^{-1} and the Be-N and C5-Be in the Cyclic 1-Be complex stretch at 892.5 cm^{-1} and 665.0 cm^{-1} , respectively. These are comparable to the vibrational frequencies obtained at the same level of theory in hydrogen cyanide-Be(II) and ethylene-Be(II) complexes (970.7 cm^{-1} and 721.5 cm^{-1}).

Table 6.5 Vibrational frequencies of Be-N and Be-Cvinyl

a) Be-N_{ciano} Bond Stretch (cm⁻¹)	
CH3-CN---Be	792.4
H-CN---Be	970.7
CH2=CHCN---Be	816.7
acyclic 2-Be(II)	800.5
cyclic 2-Be(II)	880.2
acyclic 1-B (II)	884.3
cyclic 1-Be(II)	892.5
cyclic 1-Mg(II)	481.6
cyclic 1-Ca(II)	390.4
b) Be-C_{vinyl} Bond Stretch (cm⁻¹)	
cyclic 1-Be(II)	665.0
cyclic 1-Mg(II)	359.1
cyclic 1-Ca(II)	109.6
cyclic 2-Be(II)	595.0
CH2=CH2---Be	721.5
CH2=CH=CH=CH2---Be	781.9

The observed frequencies are consistent with the reasoning that lower energies (lower frequencies) are needed to stretch weaker bonds and more weakly bound interactions. The Be-N stretch in Cyclic 1-Be is higher compared to that in Cyclic 2-Be (892.5 and 880.2 cm^{-1} , respectively), consistent with a stronger interaction in the former. Likewise the C-Be stretch is higher in Cyclic 1-Be compared to the analogous stretch in Cyclic 2-Be (665 and 595 cm^{-1} , respectively). In olefin and conjugated models without carbonitrile functionality, similar trend is observed, the C-Be bond stretch in Be(II)-ethylene (721.5 cm^{-1}) is 60 cm^{-1} lower (weaker interaction) compared with that in butadiene (781.9 cm^{-1}) conjugated model. The Mg-N and Ca-N bond stretches much weaker compared to Be-N (481.6 and 390.4 cm^{-1} respectively) that contributed to low dissociation energy obtained later.

6.2.3 Electron Population Analysis

The C4 atom in 2-cyanobutadiene (receptor 1) utilizes its 2s, $2p_x$ and $2p_y$ orbitals to form sp^2 hybrid orbitals used to form covalent bonds with C3 and two hydrogen atoms. The $2p_z$ orbitals remain for formation of π -bond with C3. The electron population of the $2p_x$ and $2p_y$ orbitals in C4 are greater than one due to contributions from neighbouring C3 and two hydrogen atoms. Interaction with Be(II) causes migration of electron density from the C3-C4 π -bond to the C4 carbon centre, rehybridizes the carbon orbitals to sp^3 -like and significantly increased the C4 $2p_y$ and $2p_z$ population by 25% and 28%, respectively. This observation is in keeping with a significant reduction in C3 population upon formation of Cyclic 1-Be, the whole population of C3 is reduced by about 10%, and the C3 $2p_z$ orbital alone experiences a 35% reduction in population and thus becomes a cationic centre (Table 6.6). The observed electron population data are in good accordance with the GIAO NMR shieldings data described earlier.

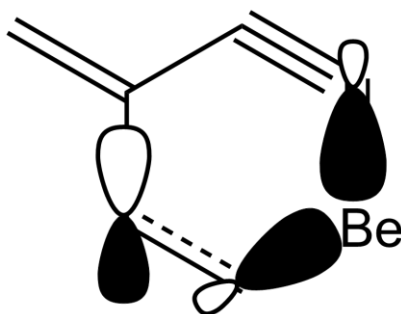


Figure 6.4. Interaction between C4 and Be.

The *s* versus *p* characters by percentage in **Table 6.7** further support the rehybridization arguments. The C4 center significantly exhibits reduced *s* character and increased *p* character in **Cyclic 1-Be** and the interaction between C4 and Be(II) involve sp^3 -like orbital.

Table 6.6 NBO populations of 2-CN BD and Be(II)- 2-CN BD

	2-CN BD			
	2s	2p _x	2p _y	2p _z
C3	0.976	1.054	1.191	1.013
C4	1.066	1.214	1.145	0.963
C5	0.854	0.945	0.965	0.925
N	1.594	1.231	1.363	1.094
	Be(II)- 2-CN BD			
	2s	2p _x	2p _y	2p _z
C3	1.028	1.060	1.083	0.658
C4	1.172	1.168	1.433	1.232
C5	0.883	0.880	0.784	0.817
N	1.518	1.455	1.298	1.236

The C3 center experience a slight increase in *p* character presumably to better stabilize the positively charge carbon. On the contrary, the C3 and C4 atoms show negligible changes in the Acyclic 1-Be complex.

Table 6.7 Percentages of *s* versus *p* characters in C3-C4 and C5-N6 σ -bonds in 2-CN BD and Be(II)- 2-CN BD.

C3-C4 σ-bond <i>s</i> and <i>p</i> characters by percentage				
	C3 <i>s</i>	C3 <i>p</i>	C4 <i>s</i>	C4 <i>p</i>
2-CN BD (1)	38.9	61.0	38.3	61.7
Cyclic 1-Be	37.1	62.9	31.2	68.8
Acyclic 1-Be	39.4	60.6	37.3	62.6
C5-N6 σ-bond <i>s</i> and <i>p</i> characters by percentage				
	C5 <i>s</i>	C5 <i>p</i>	N6 <i>s</i>	N6 <i>p</i>
2-CN BD (1)	47.6	52.4	45.3	54.4
Cyclic 1-Be	45.7	54.3	45.9	53.8
Acyclic 1-Be	43.0	56.9	59.2	40.7

6.2.4 Frontier Molecular Orbital (FMO) Analysis

The Cyclic 1-Be complex requires interactions between Be(II) with carbonitrile N6 and C4 atoms (Figure 6.4). The frontier orbital analysis indicates the HOMO-3 in 2-cyanobutadiene (receptor 1) most probably is utilized in forming the Cyclic 1-Be complex. This MO has suitable orbital to be occupied by lone electron pair on the cyano nitrogen atom (N6), and a 2*p* orbital on C4 that can be utilized to form interactions with beryllium cation. Furthermore, the same phase of the orbitals are pointing towards Be(II). The cyano N6 atom presumably exhibits significant 2*s* orbital and initially interacts with Be(II). In the next step, due to stabilization gained in further transfer of positive charge from Be(II) to the receptor, the 2*p* orbital on C4, having the same phase as that in N6, forms a bridge with the vinylic carbon terminal and thus affords the six-membered ring. The low-lying unoccupied molecular orbitals are of interest in nucleophilic addition to the cyclic complex by Lewis bases and in polymerization process involving beryllium catalysts. The FMO of the Cyclic 1-Be complex shows that the energies of the low-lying unoccupied MO's in ascending order are assigned to those in C3-C4, C1-C2 and C5-N6, respectively (Figure 6.5). Therefore, nucleophilic addition to the C3 cation center is energetically favorable based on FMO argument.

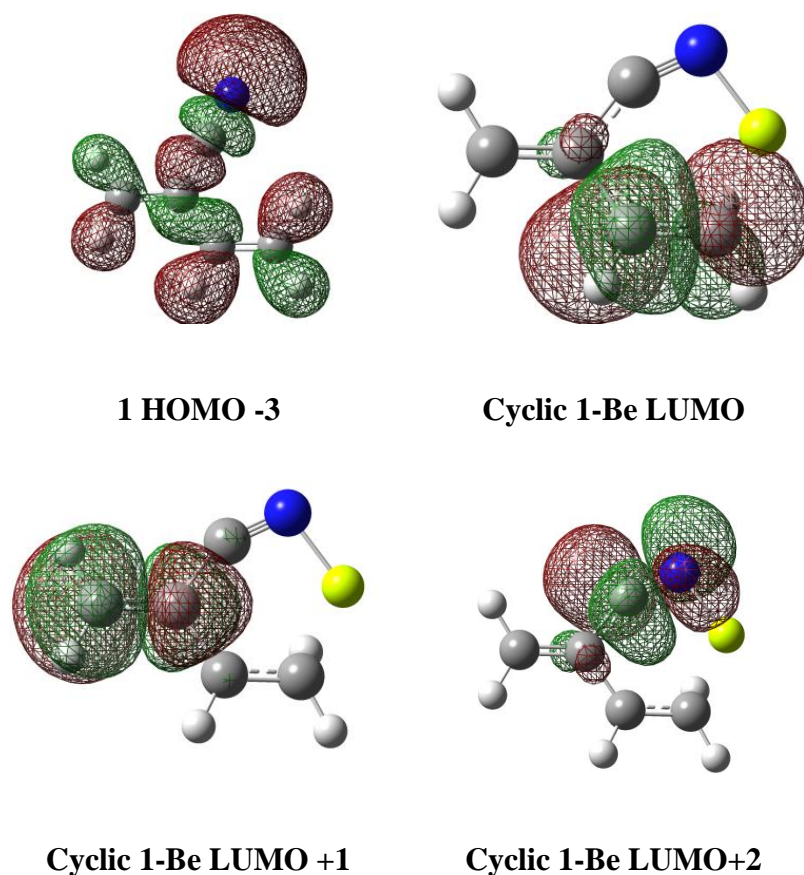


Figure 6.5 Frontier Molecular orbitals(FMO) of 1 and its cyclic complex with Be(II).

6.2.5 Energetics of Divalent Complexes

Accuracy on calculated G3 energies used to deduce relative stability of beryllium(II) adducts with unsaturated carbonitrile receptor models have first been verified using experimental (NIST) heats of formation (Namazian *et al.*, 2008). The following reactions involving hydrogenation of beryllium(II) oxide and fluorination of beryllium(I) hydride and beryllium atom are employed to determine G3 error in calculating energies of beryllium compounds (Table 6.8).

Table 6.8 Benchmark reactions involving beryllium compounds
(G3 and NIST energies in kcal/mol)

	NIST ΔH	G3 ΔH_{rxn}	Error
$\text{BeO} + \text{H}_2 \rightarrow \text{Be} + \text{H}_2\text{O}$ rxn 1	-13.0	-17.8	4.8
$\text{BeH} + \text{F}_2 \rightarrow \text{BeF} + \text{HF}$ rxn 2	-187.4	-185.5	1.9
$\text{Be} + \text{F}_2 \rightarrow \text{BeF}_2$ rxn 3	-267.7	-266.2	1.5

The results show that G3 reproduces the experimental heats of reaction for reactions 1, 2 and 3 within experimental error (4.8, 1.9 and 1.5 kcal/mol, respectively). It should be noted that experimental data for beryllium compounds are old and limited in number and could be inaccurate. The effectiveness of interactions between beryllium(II) and the carbonitrile receptor models and simpler models are estimated by the relative stabilization of doubly charged and naked beryllium cation by the ligands. Stabilization of beryllium(II) by one molecule of water in Be(II)-H₂O is used as a reference for zero energy. Roughly this reflects the ability of the neutral model molecules in stabilizing doubly charged beryllium.

G3 results (Table 6.9) show that individual contribution of one ethylene is negligible (destabilization by 2 kcal/mol) and comparable to one water molecule. Quite on the contrary, one molecule of acetonitrile model affords 44.4 kcal/mol stabilization. Conjugation effect in acrylonitrile gives 52.1 kcal/mol stabilization or 7.7 kcal/mol additional stability when compared to Be(II)-CH₃CN. Likewise, in unsaturated carbonitrile models 2-CN BD when there is no vinyl participation (in the acyclic complex) the stabilization energy is reduced by 9.7 kcal/mol. The presence of conjugation due to one diene moiety in 2-CN BD gives additional stability of 6.6 kcal/mol compared to the analogous cyclic Be(II)-3- CN P complex.

Table 6.9 Beryllium(II) dissociation energies involving Be(II) complexes as measure of stabilization by receptor models; using one water molecule as reference.

	Complex	G3 ΔH_{rxn} (kcal/mol)
1	$(\text{H}_2\text{O})\text{-Be}^{2+} \rightarrow \text{Be}^{2+} + \text{H}_2\text{O}$	-142.8
2	$(\text{H}_2\text{O})_2\text{-Be}^{2+} \rightarrow \text{Be}^{2+} + 2\text{H}_2\text{O}$	-260.3
3	$\text{CH}_2=\text{CH}_2\text{-Be}^{2+} \rightarrow \text{Be}^{2+} + \text{CH}_2=\text{CH}_2$	-140.8
4	$\text{CH}_3\text{-CN-Be}^{2+} \rightarrow \text{Be}^{2+} + \text{CH}_3\text{-CN}$	-187.2
5	$\text{CH}_2=\text{CHCN-Be}^{2+} \rightarrow \text{Be}^{2+} + \text{CH}_2=\text{CHCN}$	-194.9
6	$\text{CH}_3\text{-CN-Be}^{2+}\text{-CH}_2=\text{CH}_2 \rightarrow \text{Be}^{2+} + \text{CH}_3\text{-CN} + \text{CH}_2=\text{CH}_2$	-280.7
7	$3\text{-CN P-Be}^{2+} \text{ (cyclic)} \rightarrow \text{Be}^{2+} + 3\text{-CN P}$	-208.8
8	$3\text{-CN P-Be}^{2+} \text{ (cyclic)} \rightarrow \text{Be}^{2+} + 3\text{-CN P}$	-194.8
9	$2\text{-CN BD-Be}^{2+} \text{ (acyclic)} \rightarrow \text{Be}^{2+} + 2\text{-CN BD}$	-199.1
10	$2\text{-CN BD-Be}^{2+} \text{ (cyclic)} \rightarrow \text{Be}^{2+} + 2\text{-CN BD}$	-215.4

The results reveal that cyclic complexes between 2-cyanobutadiene (receptor 1) and Be(II), Mg(II) and Ca(II) are all bound in the gas phase (Table 6.10). We initially thought that only the cyclic adduct of Be(II) is important.

In later part of this work comparison in binding strengths between carbonitrile receptor and Group II divalent cations became more critical. Consequently, the G4 method that covers calcium utilizing Dunning's correlation consistent aug-cc-pVnZ basis sets, were employed to determine binding energies for complexes involving Be(II), Mg(II) and Ca(II). G4 calculations show that formation of the Cyclic 1-Be is 46% more exothermic than that of Cyclic 1-Mg. Likewise, while the formation of Cyclic 1-Ca is still exothermic by -76.9 kcal/mol, but it is 35% less exothermic compared to the Mg(II) complex.

Table 6.10 G4 dissociation energies of 2-cyanobutadiene complexes with Be(II), Mg(II) and Ca(II).

Complexes	G4 ΔH_{rxn} (kcal/mol)
$2\text{-CN BD-Be}^{2+} \rightarrow \text{Be}^{2+} + 2\text{-CN BD (cyclic)}$	-216.1
$2\text{-CN BD-Mg}^{2+} \rightarrow \text{Mg}^{2+} + 2\text{-CN BD (cyclic)}$	-117.6
$2\text{-CN BD-Ca}^{2+} \rightarrow \text{Ca}^{2+} + 2\text{-CN BD (cyclic)}$	-76.9

6.2.6 Overlap Population Analysis

Overlap population between two interacting centers and atomic valence on the central atoms in molecular fragments indicate the importance of valence type interaction or electron-sharing type chemical bonding as opposed to ionic interaction. AOMix program by S. Gorelsky was utilized to obtain individual atom-metal spin, total spin and metal atomic valence populations (Gorelsky, 2013).

Table 6.11. Metal valence and overlap population analysis

	M Valence	C-M Spin	N-M Spin	Total spin
Cyclic 1-Be	1.870	0.462	0.140	0.602
Cyclic 1-Mg	1.570	0.396	0.462	0.858
Cyclic 1-Ca	0.673	0.124	0.274	0.398
Cyclic 2-Be	1.838	0.454	0.278	0.732
Cyclic 2-Mg	1.543	0.352	0.428	0.780
Cyclic 2-Ca	0.707	0.142	0.262	0.404

Although the C4-Be bond distance (1.78 Å) in Cyclic 1-Be is longer than that in N6-Be (1.61 Å), the former shows significantly higher overlap population (0.462) compared to the later (0.140). This observation presumably due to high electronegativity of nitrogen atom that keeps its lone electron pair close to its nuclei and not in the overlap area. On the contrary, the rehybridized C4 (from sp^2 to sp^3 -like) shows significant migration of electron population from the C3-C4 π -bond to the covalent-type C4-Be overlap area. The interaction between Be(II) and 3-cyanopropene (receptor 2) shows similar pattern of carbon *versus* nitrogen overlap population.

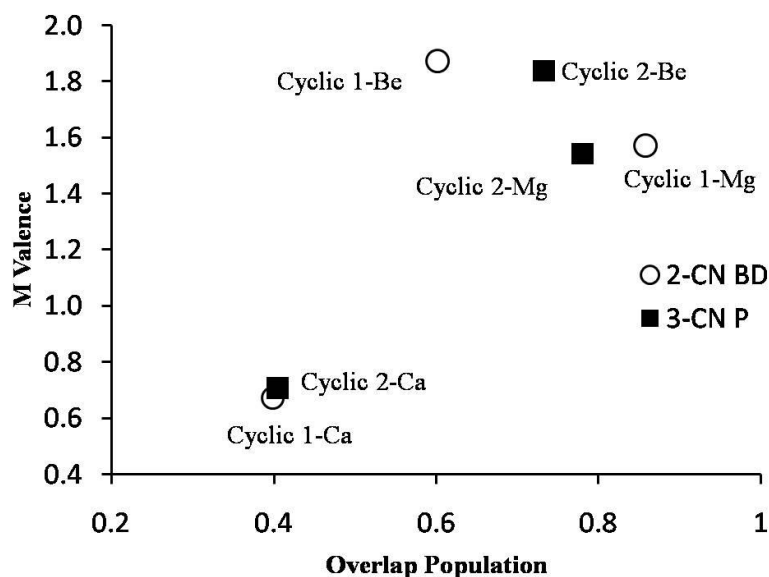


Figure 6.6. Plot of metal atomic valence *versus* overlap population in complexes between Be(II), Mg(II) and Ca(II) with 2-CN BD and 3-CN P.

Mg(II) shows more balanced overlap population with carbon and nitrogen terminals in both unsaturated carbonitrile receptor models 1 and 2. Ca(II) exhibits predominantly ionic type interaction and has only less than one electron in its atomic valence (Table 6.11). Both Be(II) and Mg(II) show consistently high atomic valence (greater than 1.5) involved in formation of cyclic complexes (Figure 6.6).

6.2.7 Transition Structure

In order to locate the structures of the transition states we use the Synchronous Transit-Guided Quasi-Newton method utilizing Gaussian 09 QST2 keyword, wherein the acyclic structure (Acyclic 1-Be) had been designated as the reactant and the cyclic structure (Cyclic 1-Be) as the product. One imaginary frequency at -220.8 cm^{-1} has been located that corresponds to the transition state. Formation of the acyclic complex between Be(II) and 1 in the gas phase is exothermic by 213.3 kcal/mol. Interaction between Be(II) and C4 gives additional stabilization by 12.5 kcal/mol and thus gives rise to the cyclic complex (Figure 6.7).

Intrinsic Reaction Coordinate (IRC) result confirms that the transition structure which has a forward activation barrier of 12.3 kcal/mol connects the two optimized minima. In further solvent effect studies utilizing the IEFPCM continuum model, that are not described in details in this work, we found that the cyclic complex (Cyclic 1-Be) survives in non-polar solvents such as heptane, benzene and dichloromethane. However, polar solvents such as diethyl ether and tetrahydrofuran were found to stabilize Be(II) and break the Be(II)-C4 bond, and the cyclic complex ring opens to the acyclic form.

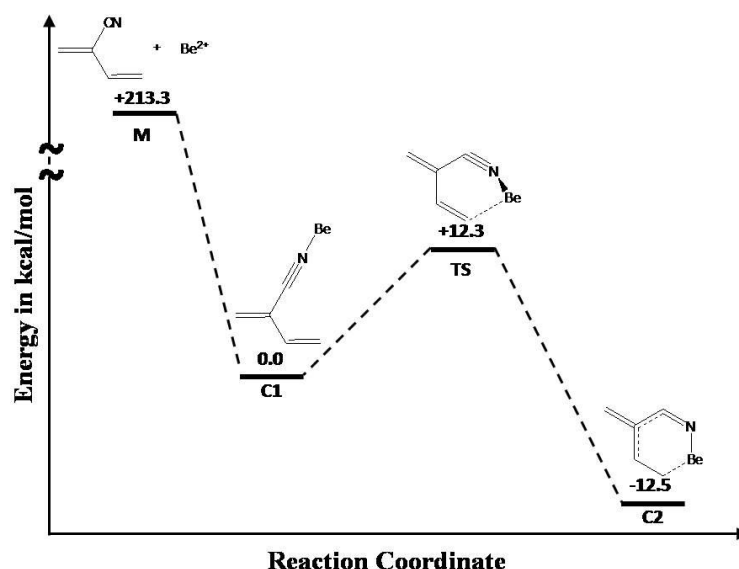


Figure 6.7 Energy profile of 2-CN BD and its complexes with Be(II)(M) Uncomplex (C1) Reactant, (TS) Transition Structure and (C2) Product.

6.2.8 Rationale for Beryllium(II) Recognition using Unsaturated Carbonitriles

Our results suggest that beryllium cation interacts with unsaturated carbonitrile initially by forming N-Be bond. The interaction between Be(II) and the cyano nitrogen atom is more than 45 kcal/mol stronger than that with vinyl carbons, using the acetonitrile and ethylene simple models and examined separately (Table 6.9). Moreover, the energetics data reveal that interaction with the vinyl carbon to form Cyclic 1-Be further the complex by 12 kcal/mol. Furthermore, G4 results show that Mg(II) and Ca(II) are also capable of making interaction with vinyl carbon, after forming acyclic complexes

through N-Be bonding. Consequently, it is important to investigate if a complex between Be(II) and a conjugated carbonitrile could still form another interaction with a separate vinyl moiety. For this purpose we investigate the complex between Be(II) and two separate fragments; acrylonitrile and ethylene (Figure 6.8), and the results confirm that Be(II) complexes with fragmented conjugated carbonitrile and vinyl moiety are bound.

The optimized structures show that the Be-C bond distance in the simple model (1.777 Å) is very similar to that in Cyclic 1-Be (1.78 Å). On the contrary, the Be-N bond length in the fragmented simpler model (1.54 Å) is significantly shorter than that in Cyclic 1-Be (1.61 Å). This presumably is due to the ring strain in the Acyclic 1-Be six-membered complex. The π -network results in a strained planar structure, except for the dihedral angle involving the sp^3 -like C4 center, that could not adopt a less strained chair conformation. The Acyclic 1-Be exhibits even shorter Be-N bond distance (1.48 Å). This could be explained in terms of more efficient interaction between Be(II) and only one ligand, the imparted positive charge delocalized by the conjugated carbonitrile receptor, and the resulting acyclic complex free from ring strain. The C4 in Cyclic 1-Be exhibits more significant rehybridization to sp^3 -like centre having H-C4-H bond angle of 110.8° compared to 116.7° in the fragmented simple models.

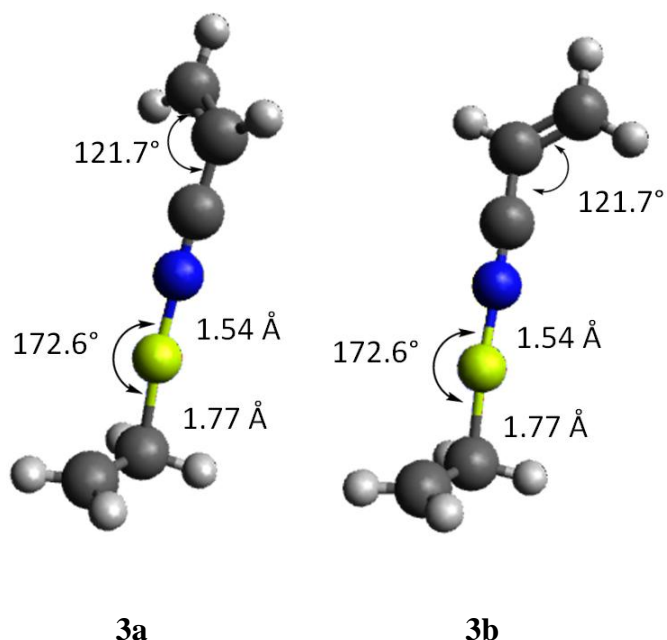


Figure 6.8 Optimized geometries of simple models

Optimized geometries indicate that in unconjugated carbonitriles, interaction with cations leaves the cyano bond unaffected. However, stabilization due to π -network in conjugated carbonitriles strongly suggests formation of ketenimine reactive functionality and significant reduction of the C-N bond order (Woi *et al.*, 2014). In a yet unpublished work, the interactions between carbonitrile-carboxaldehyde receptor models and Group I and II cations can be elucidated using electron sharing *versus* ionic interaction approach. The results reveal that electron sharing by uncharged heteroatom receptors favours divalent cations, and Group I cations can be effectively discriminated utilizing this approach. Moreover, magnesium exhibits significantly higher atomic valence compared to calcium. Therefore, calcium can be discriminated in highly selective magnesium determination based on electron sharing ground (Zhang & Spichiger, 2000). However, lacking in valence electron but retaining its positive charge, calcium can be selectively determined using multiple negatively charged receptors. In addition, being more weakly hydrated, calcium is favored by the Hofmeister effect (Kherb *et al.*, 2012; Zhang & Cremer, 2006). Beryllium recognition follows similar line of reasoning as that described for magnesium. In all cases it exhibits similar

nature of interactions with receptor models; carbonitriles, carboxaldehyde, polyether and vinyl carbon (Marynick *et al.*, 1988) in particular. Preferential recognition towards beryllium is expected with uncharged ionophores, having multiple ligands and having suppressed Hofmeister effect (Kherb *et al.*, 2012; Zhang & Cremer, 2006). Judicial choice of polymeric sensing membrane, lipophilic borate and plasticizer that reduces ion exchanging characteristics can further favour beryllium (Bakker *et al.*, 1994).

6.3 Conclusions

Beryllium(II) recognition molecules have been designed using DFT and G3 computational methods. 2-Cyanobutadiene and 3-cyanopropene represent unsaturated carbonitrile models, with and without π -system. Small molecule models such as ethylene, acetonitrile and acrylonitrile elucidate individual participation and cumulative effect of vinyl and cyano functionalities in critical design parameters especially the strengths of the $C_{\text{vinyl}}\text{-Be}$ and $\text{Be-N}_{\text{cyano}}$ interactions. GIAO NMR shifts probed centers of positive charges in the models and beryllium(II) complexes. In all cases the changes in the degree of carbon nuclei shielding is consistent with the reasoning on how doubly charged beryllium imparts and distributes the donated positive charge. NBO analysis examined orbital occupancies that suggest rehybridization at the terminal vinyl carbon to sp^3 , forming interaction with beryllium atom and at the carbon and nitrogen atoms, adjusting to the positively charged centers. Beryllium(II) cyclic complexes with 2-CN BD and 3-CN P exhibits almost perfect planar, except for slight out of plane dihedral angle at one atom of the six membered ring. This and numerous other evidence suggest that both cyano and vinyl groups participate in binding with beryllium, and π -system conjugation in 2-CN BD affords 16.3 kcal/mol stabilization. Relative stabilization by one water molecule, ethylene alone has negligible effect, whereas stabilization of unconjugated carbonitrile model (acetonitrile) gives rise to 44.4 kcal/mol stabilization.

The interaction of Be (II)-2 CN BD is the strongest compared against Mg(II) and Ca(II) complexes, proven by the dissociation energy obtained from G4 calculation. The Be(II)-2-CN BD complexes of cyclic and acyclic forms separated by 12.3 kcal/mol barrier height as shown by the QST2 method. Discrimination of Ca(II) from Be(II) and Mg(II) can be based on the overlap population analysis that showed Ca(II) prefers ionic interaction with the receptor models.

Chapter 7 : Conclusion

7.1 Major Achievements

DFT/B3LYP method is the best method to study the electronic structures of the receptor molecules. This includes the study on optimized geometries and vibrational frequencies. Other specialized tools can help provide more information such as nuclear magnetic shielding, electrostatic charge distribution, bond orders and overlap populations from the optimized geometry.

The Gn theory had proven itself as the most accurate compound method to obtain energies. The benchmark against NIST data showed remarkable performance for relevant cases and had been comprehensively used in this work.

Polymeric membrane based sensor cell had been successfully fabricated by incorporating carbonitrile molecule into acrylic membrane. The fabricated sensor cell shown distinctive signal pattern that can be utilized by sensor array approach.

7.2 Limitations

The main drawback for this work is to maintain the accuracy of the method utilized within the molecules size limit. The G3 and G4 theory can only guarantee accuracy for the energy obtained from small system (less than 10 large atoms). Meanwhile, DFT/B3LYP can optimize large molecule system (such as Ionomycin) but it can take up to few days to complete. Certain desired method such as CBS-APNO can only covers certain elements (first and second row elements as in periodic table) and limited to less than six atoms. Those are not computationally feasible with current method and hardware.

Beryllium(II) had been studied intensively on chapter 6, but due to the toxic nature of beryllium(II), no experimental works were able to carry out to evaluate the sensing ability of carbonitrile on beryllium(II).

7.3 Future Works

Although the result presented in this dissertation showed the ability of DFT/B3LYP and G_n theory, a few recommendations for future works can be implemented to raise the quality of this research. This includes the access to superior computing machines such as supercomputer or dedicated workstation, where both can handle highly expensive methods such as W1, M1, CBS-APNO and Full CI with moderate time compared with the current hardware.

More comprehensive and exhaustive study on the sensor itself can be done to further characterize the sensor. The test includes drift test, temperature effect, accuracy test, pH stability and limit of detection. Improvement on materials, carbon quality, nanomaterials

in transducer (polythiophene). Different sensor platform can be explored such as state of the art tungsten(W) IDE based platform on roger board. This platform can improve consistency and reliability over current screen printed platform.

Sensor array approach is deemed to be suitable for this work. The signal pattern produced by the sensor array can be further processed to gain selectivity for magnesium(II) or calcium(II). Extra work and different expertise required for the development of this platform that covers the algorithm for pattern recognition, neural network and signal processing.

References

- Adam, H., Stanisław, G., & Folke, I. (1991). Chemical sensors definitions and classification. *Pure and Applied Chemistry*, 63, 1274-1250.
- Afeefy, H. F., Liebmann, J. F., & Stein, S. E. (2005). Neutral Thermochemical Data., from NIST
- Agarwal, A., & Lang, J. (2005). *Foundations of Analog and Digital Electronic Circuits*: Elsevier Science.
- Alex, A., Hänsele, E., & Clark, T. (2006). The ethylene/metal (0) and ethylene/metal (I) redox system: model ab initio calculations. *Journal of Molecular Modeling*, 12(5), 621-629.
- Ambrose, T. M., & Meyerhoff, M. E. (1996). Characterization of photopolymerized decyl methacrylate as a membrane matrix for ion - selective electrodes. *Electroanalysis*, 8(12), 1095-1100.
- Antonisse, M. M. G., Snellink-Ruel, B. H. M., Yigit, I., Engbersen, J. F. J., & Reinhoudt, D. N. (1997). Neutral anion receptors: synthesis and evaluation as sensing molecules in chemically modified field effect transistors. *The Journal of Organic Chemistry*, 62(26), 9034-9038.
- Apeloig, Y., & Stanger, A. (1982). α -Silicon-substituted vinyl cations. A theoretical *ab initio* investigation. *The Journal of Organic Chemistry*, 47(8), 1462-1468.
- Armstrong, R., & Horvai, G. (1990). Properties of PVC based membranes used in ion-selective electrodes. *Electrochimica Acta*, 35(1), 1-7.
- Arnold, M. A., & Meyerhoff, M. E. (1984). Ion-selective electrodes. *Analytical Chemistry*, 56(5), 20R-48R.
- Arquitt, S., & Johnstone, R. (2004). A scoping and consensus building model of a toxic blue - green algae bloom. *System Dynamics Review*, 20(2), 179-198.
- Bakker, E., Bühlmann, P., & Pretsch, E. (1997). Carrier-based ion-selective electrodes and bulk optodes. 1. General characteristics. *Chemical Reviews*, 97(8), 3083-3132.
- Bakker, E., Meruva, R., Pretsch, E., & Meyerhoff, M. (1994). Selectivity of polymer membrane-based ion-selective electrodes: Self-consistent model describing the potentiometric response in mixed ion solutions of different charge. *Analytical Chemistry*, 66(19), 3021-3030.
- Bakker, E., Pretsch, E., & Bühlmann, P. (2000). Selectivity of potentiometric ion sensors. *Analytical Chemistry*, 72(6), 1127-1133.
- Barone, V., & Cossi, M. (1998). Quantum calculation of molecular energies and energy gradients in solution by a conductor solvent model. *The Journal of Physical Chemistry A*, 102(11), 1995-2001.

- Bausells, J., Carrabina, J., Errachid, A., & Merlos, A. (1999). Ion-sensitive field-effect transistors fabricated in a commercial CMOS technology. *Sensors and Actuators B: Chemical*, 57(1), 56-62.
- Becke, A. D. (1988). Density-functional exchange-energy approximation with correct asymptotic behavior. *Physical Review A*, 38(6), 3098.
- Becke, A. D. (1993a). Density - functional thermochemistry. III. The role of exact exchange. *The Journal of Chemical Physics*, 98, 5648.
- Becke, A. D. (1993b). A new mixing of Hartree-Fock and local density - functional theories. *The Journal of Chemical Physics*, 98(2), 1372-1377.
- Bhasin, S. K. (2012). *Pharmaceutical Physical Chemistry: Theory and Practices*: Pearson Education India.
- Binkley, J. S., Seeger, R., Pople, J. A., Dill, J. D., & Schleyer, P. v. R. (1977). Carbon-beryllium binding in CH₂ Be. *Theoretica Chimica Acta*, 45(1), 69-72.
- Boyd, J. W., Cobb, G. P., Southard, G. E., & Murray, G. M. (2004). Development of molecularly imprinted polymer sensors for chemical warfare agents. *Johns Hopkins APL technical digest*, 25(1), 44-49.
- Boyes, W. (2002). *Instrumentation Reference Book*: Elsevier Science.
- Boys, S. F. (1950). Electronic wave functions. I. A general method of calculation for the stationary states of any molecular system. *Proceedings of the Royal Society of London. Series A. Mathematical and Physical Sciences*, 200(1063), 542-554.
- Breneman, C. M., & Wiberg, K. B. (1990). Determining atom - centered monopoles from molecular electrostatic potentials. The need for high sampling density in formamide conformational analysis. *Journal of Computational Chemistry*, 11(3), 361-373.
- Brzózka, Z., Dawgul, M., Pijanowska, D., & Torbicz, W. (1997). Durable NH₄⁺-sensitive CHEMFET. *Sensors and Actuators B: Chemical*, 44(1), 527-531.
- Buck, R. P. (1978). Ion selective electrodes. *Analytical Chemistry*, 50(5), 17R-29R.
- Cadogan, D. F., & Howick, C. J. (1996). Plasticizers. *Kirk-Othmer Encyclopedia of Chemical Technology*.
- Carey, F. A., & Sundberg, R. J. (2007). *Advanced Organic Chemistry: Part A: Structure and Mechanisms*. New York: Springer.
- Cazes, J. (2004). *Analytical Instrumentation Handbook, Third Edition*: Taylor & Francis.
- Cheeseman, J. R., Trucks, G. W., Keith, T. A., & Frisch, M. J. (1996). A comparison of models for calculating nuclear magnetic resonance shielding tensors. *The Journal of Chemical Physics*, 104(14), 5497-5509.

- Chiang, J. L., Chou, J. C., & Chen, Y. C. (2001). Study of the pH-ISFET and EnFET for Biosensor Application. *Journal of Medical and Biological Engineering*, 21(3), 135-146.
- Comeau, B., & Chemistry, T. U. (2008). *Plasticizer Alternatives for Use in Polymer Membrane Ion Selective Electrodes*: Tufts University.
- Craggs, A., Moody, G., & Thomas, J. (1974). PVC matrix membrane ion-selective electrodes. Construction and laboratory experiments. *Journal of Chemical Education*, 51(8), 541.
- Cramer, C. J., & Gladfelter, W. L. (1997). *Ab Initio* Characterization of $[\text{H}_3\text{N}-\text{BH}_3]_2$, $[\text{H}_3\text{N}-\text{AlH}_3]_2$, and $[\text{H}_3\text{N}-\text{GaH}_3]_2$. *Inorganic Chemistry*, 36(23), 5358-5362.
- Cremer, M. (1906). *Über die Ursache der elektromotorischen Eigenschaften der Gewebe, zugleich ein Beitrag zur Lehre von den polyphasischen Elektrolytketten*: R. Oldenbourg.
- Cristea, C., Bodoki, E., Sima, V., & Sandulescu, R. (2009). Modified Screen Printed Electrodes for the Development of Biosensors. In S. Vlad, R. Ciupa & A. Nicu (Eds.), *International Conference on Advancements of Medicine and Health Care through Technology* (Vol. 26, pp. 89-92): Springer Berlin Heidelberg.
- Curtiss, L. A., & Raghavachari, K. (2002). Gaussian-3 and related methods for accurate thermochemistry. *Theoretica Chimica Acta*, 108(2), 61-70.
- Curtiss, L. A., Raghavachari, K., Redfern, P. C., Rassolov, V., & Pople, J. A. (1998). Gaussian-3 (G3) theory for molecules containing first and second-row atoms. *The Journal of Chemical Physics*, 109, 7764-7776.
- Curtiss, L. A., Raghavachari, K., Trucks, G. W., & Pople, J. A. (1991). Gaussian - 2 theory for molecular energies of first - and second - row compounds. *The Journal of Chemical Physics*, 94(11), 7221-7230.
- Curtiss, L. A., Redfern, P. C., & Raghavachari, K. (2007). Gaussian-4 theory. *The Journal of Chemical Physics*, 126, 084108-084119.
- Curtiss, L. A., Redfern, P. C., & Raghavachari, K. (2011). Gn theory. *Wiley Interdisciplinary Reviews: Computational Molecular Science*, 1(5), 810-825.
- Daniel, C. H. (1987). *Quantitative Chemical Analysis*. New York: W. H. Freeman and Company.
- Davidson, E. R., & Feller, D. (1986). Basis set selection for molecular calculations. *Chemical Reviews*, 86(4), 681-696.
- Dirac, P. A. (1928). The quantum theory of the electron. *Proceedings of the Royal Society of London. Series A, Containing Papers of a Mathematical and Physical Character*, 610-624.

- Domanský, K., Baldwin, D. L., Grate, J. W., Hall, T. B., Li, J., Josowicz, M., & Janata, J. (1998). Development and calibration of field-effect transistor-based sensor array for measurement of hydrogen and ammonia gas mixtures in humid air. *Analytical Chemistry*, 70(3), 473-481.
- Dror, M., Bergs, E., & Rhodes, R. (1987). Potassium ion-selective electrodes based on valinomycin/PVC overlayered solid substrates. *Sensors and Actuators*, 11(1), 23-36.
- Duarte, L., Jutten, C., & Moussaoui, S. (2009). Ion-Selective Electrode Array Based on a Bayesian Nonlinear Source Separation Method. In T. Adali, C. Jutten, J. Romano & A. Barros (Eds.), *Independent Component Analysis and Signal Separation* (Vol. 5441, pp. 662-669): Springer Berlin Heidelberg.
- Duarte, L. T., Jutten, C., Temple-Boyer, P., Benyahia, A., & Launay, J. (2010). A dataset for the design of smart ion-selective electrode arrays for quantitative analysis. *Sensors Journal, IEEE*, 10(12), 1891-1892.
- Duncan, D. M., & Cockayne, J. (2001). Application of calixarene ionophores in PVC based ISEs for uranium detection. *Sensors and Actuators, B: Chemical*, 73(2), 228-235.
- Dunning, T. H. (1989). Gaussian basis sets for use in correlated molecular calculations. I. The atoms boron through neon and hydrogen. *The Journal of Chemical Physics*, 90(2), 1007.
- Durst, R., Baumner, A., Murray, R., Buck, R., & Andrieux, C. (1997). Chemically modified electrodes: recommended terminology and definitions.
- Dykstra, C. E. (1993). Electrostatic interaction potentials in molecular force fields. *Chemical Reviews*, 93(7), 2339-2353.
- Erdahl, W. L., Chapman, C. J., Taylor, R. W., & Pfeiffer, D. R. (1994). Ca²⁺ transport properties of ionophores A23187, ionomycin, and 4-BrA23187 in a well defined model system. *Biophysical Journal*, 66(5), 1678-1693.
- Erdahl, W. L., Chapman, C. J., Taylor, R. W., & Pfeiffer, D. R. (1995). Effects of pH conditions on Ca²⁺ transport catalyzed by ionophores A23187, 4-BrA23187, and ionomycin suggest problems with common applications of these compounds in biological systems. *Biophysical Journal*, 69(6), 2350-2363.
- Everest, D. A. (1964). *The chemistry of beryllium*: Elsevier Pub. Co.
- Ewing, G. W. (1997). *Analytical Instrumentation Handbook, Second Edition*: Taylor & Francis.
- Fermi, E. (1928). A statistical method for the determination of some atomic properties and the application of this method to the theory of the periodic system of elements. *Zeitschrift für Physik*, 48, 73-79.
- Fleming, F. F., Gudipati, V., & Steward, O. W. (2002). Alkynenitriles: Chelation-Controlled Conjugate Additions. *Organic Letters*, 4(4), 659-661.

- Fleming, F. F., & Shook, B. C. (2002). Nitrile anions: Solvent-dependent cyclizations. *The Journal of Organic Chemistry*, 67(9), 2885-2888.
- Fleming, F. F., Wang, Q., & Steward, O. W. (2000). γ -Hydroxy Unsaturated Nitriles: Chelation-Controlled Conjugate Additions. *Organic Letters*, 2(10), 1477-1479.
- Fleming, F. F., Zhang, Z., Wang, Q., & Steward, O. W. (2002). Alkenenitriles: Annulations with ω -Chloro Grignard Reagents. *Organic Letters*, 4(15), 2493-2495.
- Fleming, I. (2011). *Molecular orbitals and organic chemical reactions: Reference Edition*: Wiley.
- Foresman, J. B., Frisch, A. E., & Gaussian, I. (1996). *Exploring chemistry with electronic structure methods*: Gaussian, Inc.
- Frisch, M., Trucks, G., Schlegel, H., Scuseria, G., Robb, M., Cheeseman, J., . . . D. J. Fox. (2010). Gaussian 09, Revision C. 01. *Gaussian, Inc., Wallingford CT*.
- Frisch, M. J., Krishnan, R., & Pople, J. A. (1980). A systematic study of the effect of triple substitutions on the electron correlation energy of small molecules. *Chemical Physics Letters*, 75(1), 66-68.
- Frisch, M. J., Pople, J. A., & Binkley, J. S. (1984). Self - consistent molecular orbital methods 25. Supplementary functions for Gaussian basis sets. *The Journal of Chemical Physics*, 80, 3265.
- Gagne, R. R., Koval, C. A., & Lisensky, G. C. (1980). Ferrocene as an internal standard for electrochemical measurements. *Inorganic Chemistry*, 19(9), 2854-2855.
- Glasoe, P. K., & Long, F. (1960). Use of glass electrodes to measure acidities in deuterium oxide1, 2. *The Journal of Physical Chemistry*, 64(1), 188-190.
- Gorelsky, S. I. (2013). AOMix: Program for Molecular Orbital Analysis (Version 6.85b). Retrieved from <http://www.sg-chem.net/>
- Greene, H. L., Hambidge, K., Schanler, R., & Tsang, R. C. (1988). Guidelines for the use of vitamins, trace elements, calcium, magnesium, and phosphorus in infants and children receiving total parenteral nutrition. *The American Journal of Clinical Nutrition*, 48(5), 1324-1342.
- Greer, F. R., & Shannon, M. (2005). Infant methemoglobinemia: the role of dietary nitrate in food and water. *Pediatrics*, 116(3), 784-786.
- Gustafsson, E. (1995). Swedish experiences of the ban on products containing mercury *Mercury as a Global Pollutant* (pp. 99-102): Springer.
- Haber, F., & Klemensiewicz, Z. (1909). Electric Forces at Phase Boundaries. *Zeitschrift fuer Physikalische Chemie (Muenchen, Germany)*, 67, 385.

- He, Z., Yang, X., Kahn, B. A., Stoffella, P. J., & Calvert, D. V. (2001). Plant nutrition benefits of phosphorus, potassium, calcium, magnesium, and micronutrients from compost utilization. *Compost Utilization in Horticultural Cropping Systems*, 307-317.
- Heng, L. Y., & Hall, E. A. (1996). Methacrylate-acrylate based polymers of low plasticiser content for potassium ion-selective membranes. *Analytica Chimica Acta*, 324(1), 47-56.
- Heng, L. Y., & Hall, E. A. H. (2001). Assessing a photocured self-plasticised acrylic membrane recipe for Na⁺ and K⁺ ion selective electrodes. *Analytica Chimica Acta*, 443(1), 25-40.
- Hirai, A., Nakamura, M., & Nakamura, E. (1999). Synergetic dimetallic effects in Gaudemar/Normant coupling between allylzinc and vinyl Grignard reagents. *Journal of the American Chemical Society*, 121(37), 8665-8666.
- Hirai, A., Nakamura, M., & Nakamura, E. (2000). Mechanism of Addition of Allylmetal to Vinylmetal. Dichotomy between Metallo-Ene Reaction and Metalla-Claisen Rearrangement. *Journal of the American Chemical Society*, 122(48), 11791-11798.
- Hoffmann, R. (1998). Qualitative thinking in the age of modern computational chemistry—or what Lionel Salem knows. *Journal of Molecular Structure: THEOCHEM*, 424(1), 1-6.
- Hohenberg, P., & Kohn, W. (1964). Inhomogeneous electron gas. *Physical Review*, 136(3B), B864.
- Hylander, L. D. (2001). Global mercury pollution and its expected decrease after a mercury trade ban. *Water, Air, and Soil Pollution*, 125(1), 331-344.
- Janz, G. J., & Ives, D. J. (1968). Silver, silver chloride electrodes. *Annals of the New York Academy of Sciences*, 148(1), 210-221.
- Jensen, F. (2013). Atomic orbital basis sets. *Wiley Interdisciplinary Reviews: Computational Molecular Science*, 3(3), 273-295. doi: 10.1002/wcms.1123
- Jyothi, G., Surolia, A., & Easwaran, K. (1994). A23187-Channel behaviour: fluorescence study. *Journal of Biosciences*, 19(3), 277-282.
- Kauffman, R. F., Taylor, R. W., & Pfeiffer, D. R. (1980). Cation transport and specificity of ionomycin. Comparison with ionophore A23187 in rat liver mitochondria. *Journal of Biological Chemistry*, 255(7), 2735-2739.
- Kelly, C. P., Cramer, C. J., & Truhlar, D. G. (2005). Accurate partial atomic charges for high-energy molecules using class IV charge models with the MIDI! basis set. *Theoretical Chemistry Accounts*, 113(3), 133-151.
- Keutsch, F. N., Braly, L. B., Brown, M. G., Harker, H. A., Petersen, P. B., Leforestier, C., & Saykally, R. J. (2003). Water dimer hydrogen bond stretch, donor torsion

- overtone, and “in-plane bend” vibrations. *The Journal of Chemical Physics*, 119, 8927-8937.
- Kherb, J., Flores, S. C., & Cremer, P. S. (2012). Role of carboxylate side chains in the cation Hofmeister series. *The Journal of Physical Chemistry B*, 116(25), 7389-7397.
- Klamt, A., & Schüürmann, G. (1993). COSMO: a new approach to dielectric screening in solvents with explicit expressions for the screening energy and its gradient. *Journal of the Chemical Society, Perkin Transactions 2*(5), 799-805.
- Klooster, W. T., Koetzle, T. F., Siegbahn, P. E. M., Richardson, T. B., & Crabtree, R. H. (1999). Study of the NH-HB Dihydrogen Bond Including the Crystal Structure of BH₃NH₃ by Neutron Diffraction. *Journal of the American Chemical Society*, 121(27), 6337-6343.
- Kobayashi, S., Matsumoto, T., Taniguchi, H., Mishima, M., Fujio, M., & Tsuno, Y. (1993). Substituent effect on gas phase basicity of 1-phenylpropyne. Thermodynamic stability and resonance demand of 1-phenylpropenyl cations. *Tetrahedron Letters*, 34(37), 5903-5906.
- Kobetz, P., Laran, R. J., & Johnson Jr, R. W. (1974). Washington, DC: Patent No. US Patent 3,832,456. U. S. P. a. T. Office.
- Kohn, W., & Sham, L. J. (1965). Self-consistent equations including exchange and correlation effects. *Physical Review*, 140(4A), A1133.
- Koryta, J. (1986). Ion-selective electrodes. *Annual Review of Materials Science*, 16(1), 13-27.
- Kosaki, Y., Takano, K., Citterio, D., Suzuki, K., & Shiratori, S. (2012). Quartz Crystal Microbalance Sensor Using Ionophore for Ammonium Ion Detection. *Journal of Nanoscience and Nanotechnology*, 12(1), 563-567.
- Lampman, G. M., Pavia, D. L., Krizz, G. S., & Vyvyan, J. R. (2009). Spectroscopy (4th ed., pp. 178-179). California: Brooks/Cole.
- Lao, R. C., & Riter Jr, J. R. (1967). Estimate of the total energy of the beryllium hydride molecule. *The Journal of Physical Chemistry*, 71(8), 2737-2739.
- Levichev, S. S., Bratov, A. V., & Vlasov, Y. G. (1994). New photocurable composition for ISFET polymer membranes. *Sensors and Actuators B: Chemical*, 19(1), 625-628.
- Lofrumento, D., La Piana, G., Abbrescia, D., Palmitessa, V., La Pesa, V., Marzulli, D., & Lofrumento, N. (2011). Valinomycin induced energy-dependent mitochondrial swelling, cytochrome c release, cytosolic NADH/cytochrome c oxidation and apoptosis. *Apoptosis*, 16(10), 1004-1013. doi: 10.1007/s10495-011-0628-7
- Maathuis, F. J. (2009). Physiological functions of mineral macronutrients. *Current Opinion in Plant Biology*, 12(3), 250-258.

- Malinowska, E., Gawart, L., Parzuchowski, P., Rokicki, G., & Brzózka, Z. (2000). Novel approach of immobilization of calix [4] arene type ionophore in 'self-plasticized' polymeric membrane. *Analytica Chimica Acta*, 421(1), 93-101.
- March, J. (1992). *Advanced organic chemistry: reactions, mechanisms, and structure* (3rd ed. Vol. 4). New York: John Wiley & Sons
- Martin, F., & Zipse, H. (2005). Charge distribution in the water molecule—A comparison of methods. *Journal of Computational Chemistry*, 26(1), 97-105.
- Marynick, D. S., & Kirkpatrick, C. M. (1988). Localized molecular orbitals of simple metal-olefin complexes. *Journal of Molecular Structure: THEOCHEM*, 169, 245-256.
- Mayer, I. (1983). Charge, bond order and valence in the ab initio SCF theory. *Chemical Physics Letters*, 97(3), 270-274.
- Mayer, I. (1984). Bond order and valence: Relations to Mulliken's population analysis. *International Journal of Quantum Chemistry*, 26(1), 151-154.
- McNaught, A. D., & Wilkinson, A. (1997). *IUPAC Compendium of chemical terminology* (Vol. 1669): Blackwell Science Oxford, UK.
- Miertuš, S., Scrocco, E., & Tomasi, J. (1981). Electrostatic interaction of a solute with a continuum. A direct utilization of AB initio molecular potentials for the prevision of solvent effects. *Chemical Physics*, 55(1), 117-129.
- Mikhelson, K. (2013). The Basics of the ISEs *Ion-Selective Electrodes* (Vol. 81, pp. 11-32): Springer Berlin Heidelberg.
- Mooradian, V. G. (1952). Washington, DC: Patent No. U.S. Patent No. 2,608,753. . U. S. P. a. T. Office.
- Moschou, E. A., & Chaniotakis, N. A. (2001). Potassium selective CHEMFET based on an ion-partitioning membrane. *Analytica Chimica Acta*, 445(2), 183-190.
- Müller, T., Juhasz, M., & Reed, C. A. (2004). The X - ray Structure of a Vinyl Cation. *Angewandte Chemie*, 116(12), 1569-1572.
- Murray, J. S., Seminario, J. M., Concha, M. C., & Politzer, P. (1992). An analysis of molecular electrostatic potentials obtained by a local density functional approach. *International Journal of Quantum Chemistry*, 44(2), 113-122.
- Namazian, M., Zakery, M., Noorbala, M. R., & Coote, M. L. (2008). Accurate calculation of the pKa of trifluoroacetic acid using high-level *ab initio* calculations. *Chemical Physics Letters*, 451(1), 163-168.
- . *National Recommended Water Quality Criteria*. (2002). (EPA-822-R-02-047). United States Environmental Protection Agency.

- O'Donnell, J., Li, H., Rusterholz, B., Pedrazza, U., & Simon, W. (1993). Development of magnesium-selective ionophores. *Analytica Chimica Acta*, 281(1), 129-134.
- Parameswaran, P., & Frenking, G. (2009). Chemical Bonding in Transition Metal Complexes with Beryllium Ligands [(PMe(3)) (2)M– BeCl(2)],[(PMe(3)) (2)M– BeClMe], and [(PMe(3)) (2)M– BeMe(2)](M= Ni, Pd, Pt)[†]. *The Journal of Physical Chemistry A*, 114(33), 8529-8535.
- Patko, T. A. D. (2009, April 2009). Understanding Ion Selective Sensors. from <http://www.astisensor.com/>
- Pauling, L. (1960a). *The Nature of the Chemical Bond and the Structure of Molecules and Crystals: An Introduction to Modern Structural Chemistry*. New York: Cornell Univ.
- Pauling, L. (1960b). The Nature of the Chemical Bond and the Structure of Molecules and Crystals: An Introduction to Modern Structural Chemistry (pp. 233, 512-514). New York: Cornell Univ.
- Pernites, R., Ponnampati, R., Felipe, M. J., & Advincula, R. (2011). Electropolymerization molecularly imprinted polymer (E-MIP) SPR sensing of drug molecules: Pre-polymerization complexed terthiophene and carbazole electroactive monomers. *Biosensors and Bioelectronics*, 26(5), 2766-2771.
- Pickard, F. C., Griffith, D. R., Ferrara, S. J., Liptak, M. D., Kirschner, K. N., & Shields, G. C. (2006). CCSD (T), W1, and other model chemistry predictions for gas - phase deprotonation reactions. *International Journal of Quantum Chemistry*, 106(15), 3122-3128.
- Polk, B. J. (2002). *ChemFET arrays for chemical sensing microsystems*. Paper presented at the Sensors, 2002. Proceedings of IEEE.
- Pople, J. A., Head - Gordon, M., Fox, D. J., Raghavachari, K., & Curtiss, L. A. (1989). Gaussian - 1 theory: A general procedure for prediction of molecular energies. *The Journal of Chemical Physics*, 90(10), 5622-5629.
- Purcell, K. F., & Drago, R. S. (1966). Studies of the Bonding in Acetonitrile Adducts. *Journal of the American Chemical Society*, 88(5), 919-924.
- Raatschen, N., Wenzel, M., Leichert, L. I. O., DÜchting, P., Krämer, U., & Bandow, J. E. (2012). *Effects of ionophores and aminosterol antibiotics on the proteome of Bacillus subtilis*.
- Rao, B., & Jena, P. (1988). Electronic structure and geometries of heteroatomic clusters. *Physical Review B*, 37(6), 2867.
- Rauk, A. (1994). *Orbital Interaction Theory of Organic Chemistry*. New York: Wiley.
- Reed, A. E., Curtiss, L. A., & Weinhold, F. (1988). Intermolecular interactions from a natural bond orbital, donor-acceptor viewpoint. *Chemical Reviews*, 88(6), 899-926.

- Reed, P. W., & Lardy, H. A. (1972). A23187: a divalent cation ionophore. *Journal of Biological Chemistry*, 247(21), 6970-6977.
- Reinhoudt, D. (1995). Durable chemical sensors based on field-effect transistors. *Sensors and Actuators, B: Chemical*, 24(1), 197-200.
- Richardson, T., de Gala, S., Crabtree, R. H., & Siegbahn, P. E. M. (1995). Unconventional Hydrogen Bonds: Intermolecular BH-HN Interactions. *Journal of the American Chemical Society*, 117(51), 12875-12876.
- Rick, S. W., Stuart, S. J., & Berne, B. J. (1994). Dynamical fluctuating charge force fields: Application to liquid water. *The Journal of Chemical Physics*, 101(7), 6141-6156.
- Rosli, A. N., Ahmad, M. R., Woi, P. M., Bakar, M. A. A., Manan, N. S. A., Zain, S. M., . . . Maluin, F. N. (2013). *Accurate Computational Approach for Designing Cation Recognition Molecules*. Paper presented at the The 6th International Conference on Sensors, Melaka.
- Rosli, A. N., Bakar, M. A. A., Manan, N. S. A., Woi, P. M., Lee, V. S., Zain, S. M., . . . Alias, Y. (2013). G3 Assisted Rational Design of Chemical Sensor Array Using Carbonitrile Neutral Receptors. *Sensors*, 13(10), 13835-13860.
- Ross, A. C., Manson, J. E., Abrams, S. A., Aloia, J. F., Brannon, P. M., Clinton, S. K., . . . Jones, G. (2011). The 2011 report on dietary reference intakes for calcium and vitamin D from the Institute of Medicine: what clinicians need to know. *Journal of Clinical Endocrinology and Metabolism*, 96(1), 53-58.
- Scott, A. P., & Radom, L. (1996). Harmonic vibrational frequencies: an evaluation of Hartree-Fock, Møller-Plesset, quadratic configuration interaction, density functional theory, and semiempirical scale factors. *The Journal of Physical Chemistry*, 100(41), 16502-16513.
- Scott, R. A., & Lukehart, C. M. (2007). *Applications of Physical Methods to Inorganic and Bioinorganic Chemistry*: Wiley.
- Selin, H. (2014). Global Environmental Law and Treaty-Making on Hazardous Substances: The Minamata Convention and Mercury Abatement.
- Senillou, A., Jaffrezic-Renault, N., Martelet, C., & Griffe, F. (1998). A miniaturized ammonium sensor based on the integration of both ammonium and reference FETs in a single chip. *Materials Science and Engineering: C*, 6(1), 59-63.
- Siswanta, D., Hisamoto, H., Koike, Y., Yamamori, S., Sato, S., & Matsumoto, Y. (1997). Magnesium Ion-Selective and a Lipophilic Cationic. *Science*, 13.
- Skoog, D. A. (2004). *Fundamentals of Analytical Chemistry*: Thomson-Brooks/Cole.
- Slater, J. C. (1930). Atomic shielding constants. *Physical Review*, 36(1), 57.
- Stibor, I., & Anslyn, E. V. (2005). *Anion Sensing*: Springer.

- Swinnen, S., Nguyen, V. S., & Nguyen, M. T. (2010). Catalytic generation of molecular hydrogen from hydrazine using lithium and beryllium hydrides. *Chemical Physics Letters*, 496(1), 25-31.
- Swope, W. C., & Schaefer III, H. F. (1976). Model organometallic systems. The interaction of 2S beryllium (1+) ion, 1S beryllium, and 3P beryllium atoms with acetylene and ethylene. *Journal of the American Chemical Society*, 98(25), 7962-7967.
- Taillades, G., Valls, O., Bratov, A., Dominguez, C., Pradel, A., & Ribes, M. (1999). ISE and ISFET microsensors based on a sensitive chalcogenide glass for copper ion detection in solution. *Sensors and Actuators B: Chemical*, 59(2), 123-127.
- Tajti, A., Szalay, P. G., Császár, A. G., Kállay, M., Gauss, J., Valeev, E. F., . . . Stanton, J. F. (2004). HEAT: High accuracy extrapolated ab initio thermochemistry. *The Journal of Chemical Physics*, 121(23), 11599-11613.
- Tan, L. L., Musa, A., & Lee, Y. H. (2011). Determination of ammonium ion using a reagentless amperometric biosensor based on immobilized alanine dehydrogenase. *Sensors*, 11(10), 9344-9360.
- Thomas, L. H. (1927). *The calculation of atomic fields*. Paper presented at the Mathematical Proceedings of the Cambridge Philosophical Society.
- Tomasi, J., Mennucci, B., & Cammi, R. (2005). Quantum mechanical continuum solvation models. *Chemical Reviews*, 105(8), 2999-3094.
- Tomasi, J., Mennucci, B., & Cances, E. (1999). The IEF version of the PCM solvation method: an overview of a new method addressed to study molecular solutes at the QM *ab initio* level. *Journal of Molecular Structure: THEOCHEM*, 464(1), 211-226.
- Trasatti, S. (1986). The absolute electrode potential: an explanatory note. *Pure and Applied Chemistry*, 58(7), 955-966.
- Umezawa, Y., Buhlmann, P., Umezawa, K., Tohda, K., & Amemiya, S. (2000). Potentiometric selectivity coefficients of ion-selective electrodes. Part I. Inorganic cations. *Pure and Applied Chemistry*, 72(10), 1851-2082.
- Umezawa, Y., Umezawa, K., & Sato, H. (1995). Selectivity coefficients for ion-selective electrodes : Recommended methods for reporting $K^{pota,b}$ values (A. C. DIVISION & C. O. E. CHEMISTRY, Trans.) *Pure and Applied Chemistry*. Great Britain: International Union of Pure and Applied Chemistry.
- Vosko, S. H., Wilk, L., & Nusair, M. (1980). Accurate spin-dependent electron liquid correlation energies for local spin density calculations: a critical analysis. *Canadian Journal of Physics*, 58(8), 1200-1211.
- Wang, S., Huang, Z., Liu, M., Liu, Y., & Ding, H. (2012). Application of Disposable Screen-printed Electrode as an Epirubicin Sensor and Relation among Whole Blood and Tissue Concentrations of Epirubicin. *International Journal of Electrochemical Science*, 7(2).

- Wang, X., Wang, R., Peng, C., Li, T., & Liu, B. (2011). Growth of BeO Nanograins Synthesized by Polyacrylamide Gel Route. *Journal of Materials Science & Technology*, 27(2), 147-152.
- Watanabe, F., & Kasai, A. (1995). Low outgassing residual gas analyzer with a beryllium-copper - alloy - flanged ion source. *Journal of Vacuum Science & Technology A*, 13(2), 497-500.
- Watanabe, H., Azuma, M., Igarashi, K., & Ooshima, H. (2005). Valinomycin Affects the Morphology of *Candida albicans*. *Journal of Antibiotics*, 58(12), 753-758.
- Weigend, F., & Ahlrichs, R. (2005). Balanced basis sets of split valence, triple zeta valence and quadruple zeta valence quality for H to Rn: Design and assessment of accuracy. *Physical Chemistry Chemical Physics*, 7(18), 3297-3305.
- Weigend, F., Furche, F., & Ahlrichs, R. (2003a). Gaussian basis sets of quadruple zeta valence quality for atoms H–Kr. *The Journal of Chemical Physics*, 119, 12753-12762.
- Weigend, F., Furche, F., & Ahlrichs, R. (2003b). Gaussian basis sets of quadruple zeta valence quality for atoms H–Kr. *The Journal of Chemical Physics*, 119, 12753.
- Weinhold, F. (2012). *Discovering chemistry with natural bond orbitals*: Wiley.
- Wiberg, K. B., & Wendoloski, J. J. (1984). Charge redistribution in the molecular vibrations of acetylene, ethylene, ethane, methane, silane and the ammonium ion. Signs of the MH bond moments. *The Journal of Physical Chemistry*, 88(3), 586-593.
- Wilson, D. M., Hoyt, S., Janata, J., Booksh, K., & Obando, L. (2001). Chemical sensors for portable, handheld field instruments. *Sensors Journal, IEEE*, 1(4), 256-274.
- Winter, A. H., & Falvey, D. E. (2009). Vinyl cations substituted with β π -donors have triplet ground states. *Journal of the American Chemical Society*, 132(1), 215-222.
- Woi, P. M., Bakar, M. A. A., Rosli, A. N., Lee, V. S., Ahmad, M. R., Zain, S. M., & Alias, Y. (2014). Does cation break the cyano bond? A critical evaluation of nitrile-cation interaction. *Journal of Molecular Modeling*, 20(5), 1-15.
- Wroblewski, W., Wojciechowski, K., Dybko, A., Brzózka, Z., Egberink, R. J. M., Snellink-Ruël, B. H. M., & Reinhoudt, D. N. (2001). Durability of phosphate-selective CHEMFETs. *Sensors and Actuators, B: Chemical*, 78(1), 315-319.
- Xu, X., & Goddard III, W. A. (2004). Bonding properties of the water dimer: A comparative study of density functional theories. *The Journal of Physical Chemistry A*, 108(12), 2305-2313.
- Yarkony, D. (1995). *Modern Electronic Structure Theory*: World Scientific.

- Yates, K., Schmid, G. H., Regulski, T. W., Garratt, D. G., Leung, H.-W., & McDonald, R. (1973). Relative ease of formation of carbonium ions and vinyl cations in electrophilic additions. *Journal of the American Chemical Society*, 95(1), 160-165.
- Yotter, R. A., & Wilson, D. M. (2004). Sensor technologies for monitoring metabolic activity in single cells-part II: nonoptical methods and applications. *Sensors Journal, IEEE*, 4(4), 412-429.
- Yu, Z.-H. (2012). The Restricted Geometry Optimization - A New Procedure to Accurately evaluate the aromatic stabilization energy *Questioning the Fundamental Principles of Organic Chemistry*. Beijing: Chinese Academy of Sciences.
- Zahran, E. M., New, A., Gavalas, V., & Bachas, L. G. (2014). Polymeric plasticizer extends the lifetime of PVC-membrane ion-selective electrodes. *Analyst*, 139(4), 757-763. doi: 10.1039/C3AN01963B
- Zhang, W., Jenny, L., & Spichiger, U. E. (2000). A Comparison of Neutral Mg^{2+} -Selective Ionophores in Solvent Polymeric Membranes: Complex Stoichiometry and Lipophilicity. *Analytical Sciences*, 16(1), 11-18.
- Zhang, W., & Spichiger, U. E. (2000). An impedance study of Mg^{2+} -selective membranes. *Electrochimica Acta*, 45(14), 2259-2266.
- Zhang, Y., & Cremer, P. S. (2006). Interactions between macromolecules and ions: the Hofmeister series. *Current Opinion in Chemical Biology*, 10(6), 658-663.
- Zhao, Y., Quick, M., Shi, L., Mehler, E. L., Weinstein, H., & Javitch, J. A. (2010). Substrate-dependent proton antiport in neurotransmitter: sodium symporters. *Nature Chemical Biology*, 6(2), 109-116.
- Zhao, Y., & Truhlar, D. G. (2008a). Density functionals with broad applicability in chemistry. *Accounts of Chemical Research*, 41(2), 157-167.
- Zhao, Y., & Truhlar, D. G. (2008b). The M06 suite of density functionals for main group thermochemistry, thermochemical kinetics, noncovalent interactions, excited states, and transition elements: two new functionals and systematic testing of four M06-class functionals and 12 other functionals. *Theoretical Chemistry Accounts*, 120(1), 215-241.
- Zhong, S., Barnes, E. C., & Petersson, G. A. (2008). Uniformly convergent n-tuple- ζ augmented polarized (nZaP) basis sets for complete basis set extrapolations. I. Self-consistent field energies. *The Journal of Chemical Physics*, 129, 184116-184127.
- Zhu, X., Gao, C., Kai, J., Do, J., Choi, J., & Ahn, C. (2003). *A Novel Dynamic Electrochemical Transduction Mechanism For Low Concentration Analyte Detection*. Paper presented at the Proceedings of the Seventh International Conference on Miniaturized Chemical and Biochemical Analysis System.
- Zoski, C. G. (2007). *Handbook of Electrochemistry*: Elsevier.

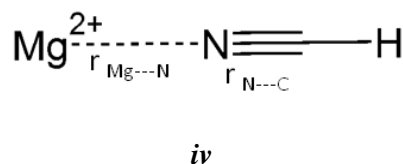
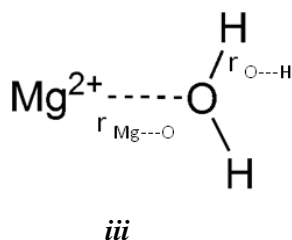
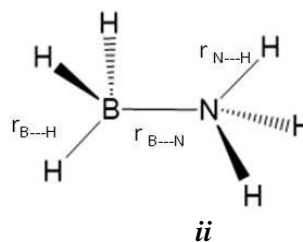
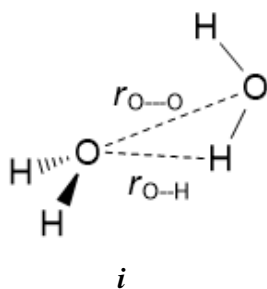
Appendix A

Supplementary Information for Chapter 4

Contents:

1. Benchmark Structures
2. Geometrical Structure
3. IR spectra
4. NMR GIAO spectra
5. Mulliken Charges
6. Molecular orbitals

1. Benchmark Structures



Benchmark Structures i. water dimer, ii. ammonia-borane, iii. Mg(II)-H₂O and iv. Mg(II)-HCN

HCN			
Symbol	X	Y	Z
C	0	0	-0.5117
N	0	0	0.664423
H	0	0	-1.58079

Mg(II)-H ₂ O			
Symbol	X	Y	Z
O	0	0	-1.00818
H	0	0.786319	-1.60806
H	0	-0.78632	-1.60806
Mg	0	0	0.940131

Mg(II)-HCN			
Symbol	X	Y	Z
Mg	0	0	1.441744
N	0	0	-0.57422
C	0	0	-1.74209
H	0	0	-2.82887

NH ₃ —BH ₃			
Symbol	X	Y	Z
N	-0.71562	0.000025	0.000009
B	0.910729	-1.2E-05	-9E-06
H	-1.09918	-0.27609	-0.90494
H	-1.09925	0.921743	0.213351
H	-1.09923	-0.6456	0.691599
H	1.25129	0.341064	1.114228
H	1.250837	-1.13564	-0.26173
H	1.251215	0.794417	-0.85252

Ethane			
Symbol	X	Y	Z
C	0	0	0.766238
C	0	0	-0.76624
H	-0.51028	0.883952	1.164521
H	-0.51039	-0.88389	1.164521
H	-1.02067	-0.00006	-1.16452
H	0.510281	0.883952	-1.16452
H	1.020666	-0.00006	1.164521
H	0.510385	-0.88389	-1.16452

2. Geometrical Structures

CH ₃ CN			
Symbol	X	Y	Z
C	0.273053	0.000036	0.000074
N	1.450787	-1.4E-05	-3.1E-05
C	-1.18659	-5E-06	-8E-06
H	-1.55806	0.578153	-0.84747
H	-1.55804	-1.023	-0.07707
H	-1.55821	0.44476	0.92436
Sum of electronic and thermal Enthalpies = -131.883190 hartrees			

Mg—CH ₃ CN			
Symbol	X	Y	Z
C	-0.98716	-0.04353	0.00006
N	0.1805	-0.11206	-1.8E-05
C	-2.43712	0.051242	-8E-06
Mg	2.306119	0.042253	-3E-06
H	-2.72551	1.103334	-0.01879
H	-2.83394	-0.45229	-0.88248
H	-2.83178	-0.41993	0.901111
Sum of electronic and thermal Enthalpies = -331.340853 hartrees			

Be—CH ₃ CN			
Symbol	X	Y	Z
C	0.202038	-0.02106	0.00021
N	-0.96325	-0.04274	0.000144
C	1.645698	0.018501	-9.6E-05
H	2.012613	-0.395	0.941093
H	2.017835	-0.57094	-0.83993
H	1.965726	1.057331	-0.10184
Be	-2.58497	0.055774	-0.00025
Sum of electronic and thermal Enthalpies = -146.253335 hartrees			

Malono nitrile			
Symbol	X	Y	Z
C	-1.20945	0.035464	0.000048
C	0	0.86391	0.000049
C	1.209446	0.035465	-4.3E-05
H	-3.2E-05	1.510394	-0.88341
H	0.000034	1.510297	0.883583
N	2.190386	-0.61641	-0.00012

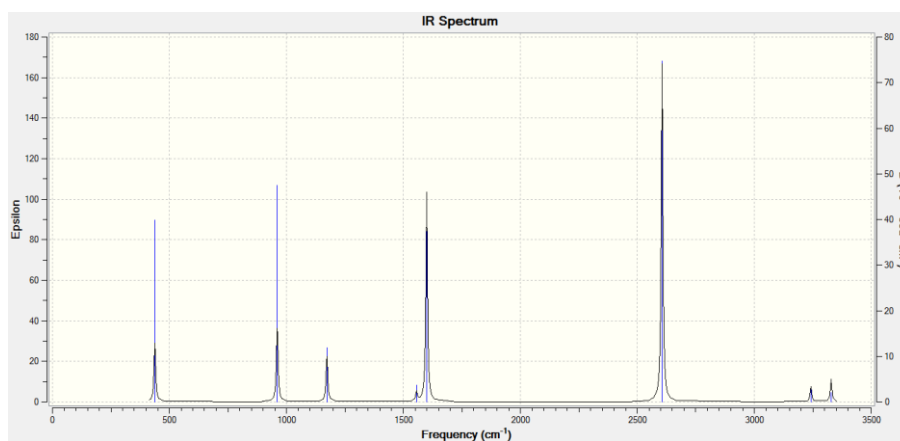
N	-2.19039	-0.61641	0.000047
Sum of electronic and thermal Enthalpies = -223.604231 hartees			

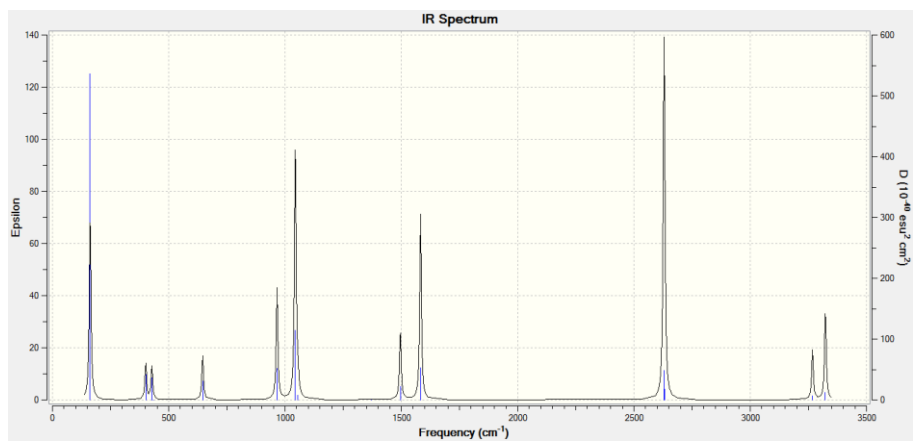
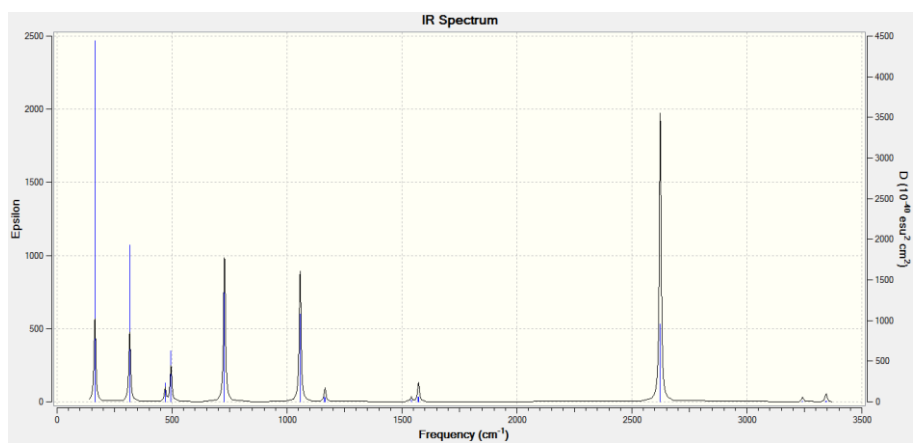
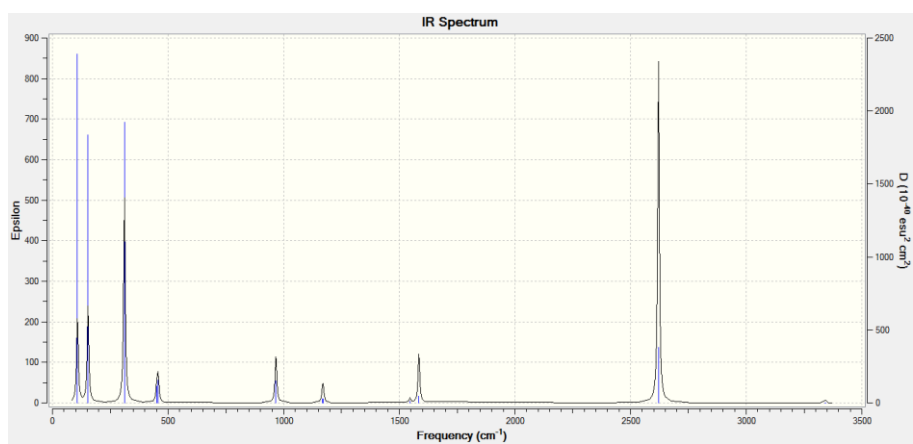
Be—Malono nitrile			
Symbol	X	Y	Z
C	1.072616	-0.38718	0
C	0	-1.4118	0.000003
C	-1.07262	-0.38718	0.000001
H	-1E-06	-2.02876	-0.90343
Be	0	1.735182	-2E-06
N	-1.44656	0.730978	-1E-06
N	1.446562	0.730977	-2E-06
H	0	-2.02876	0.903441
Sum of electronic and thermal Enthalpies = -237.904143 hartees			

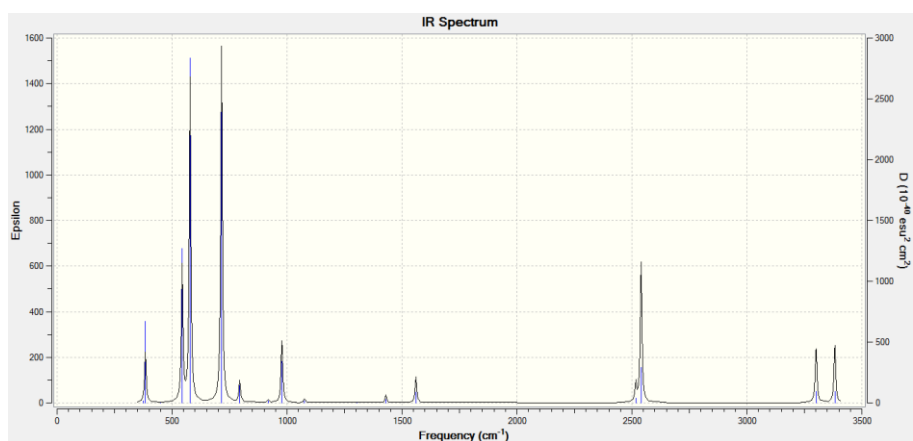
<i>n</i> -Pentane carbonitrile			
Symbol	X	Y	Z
C	-1.51004	0.698612	0.000025
C	-0.34329	-0.31358	-2E-06
C	1.018701	0.390409	-3E-06
C	2.198832	-0.59019	0.000031
C	3.562087	0.11097	-3.3E-05
C	-2.82349	0.051256	-0.00001
N	-3.85925	-0.47726	-2.4E-05
H	-1.45642	1.348367	0.881268
H	-1.45639	1.348435	-0.88117
H	-0.4295	-0.95983	0.881359
H	-0.42952	-0.95981	-0.88137
H	1.089979	1.044742	0.880264
H	1.090016	1.044713	-0.88029
H	2.124338	-1.24476	0.879088
H	2.124294	-1.24496	-0.87887
H	3.680138	0.746221	0.885851
H	3.679016	0.748205	-0.88465
H	4.381984	-0.61541	-0.00137
Sum of electronic and thermal Enthalpies = -289.875391 hartrees			

Mg-- <i>n</i> -Pentane carbonitrile			
Symbol	X	Y	Z
C	-0.35078	1.051676	-0.00016
C	0.661714	-0.12041	0.000039
C	2.106823	0.391662	0.000031
C	3.133631	-0.74925	-0.00014
C	4.582535	-0.2488	0.000091
C	-1.7287	0.585066	0.000074
N	-2.81294	0.181437	0.000177
H	-0.22021	1.687538	0.883119
H	-0.22029	1.687097	-0.88376
H	0.48477	-0.7446	0.882675
H	0.484807	-0.74484	-0.88244
H	2.268574	1.02775	0.881041
H	2.268527	1.027944	-0.88085
H	2.965515	-1.38574	0.878959
H	2.965642	-1.38533	-0.87955
H	4.788885	0.363893	0.885586
H	4.789054	0.36424	-0.88512
H	5.290031	-1.08485	-9E-06
Mg	-4.71717	-0.62857	-4.3E-05
Sum of electronic and thermal Enthalpies = -489.750237 hartrees			

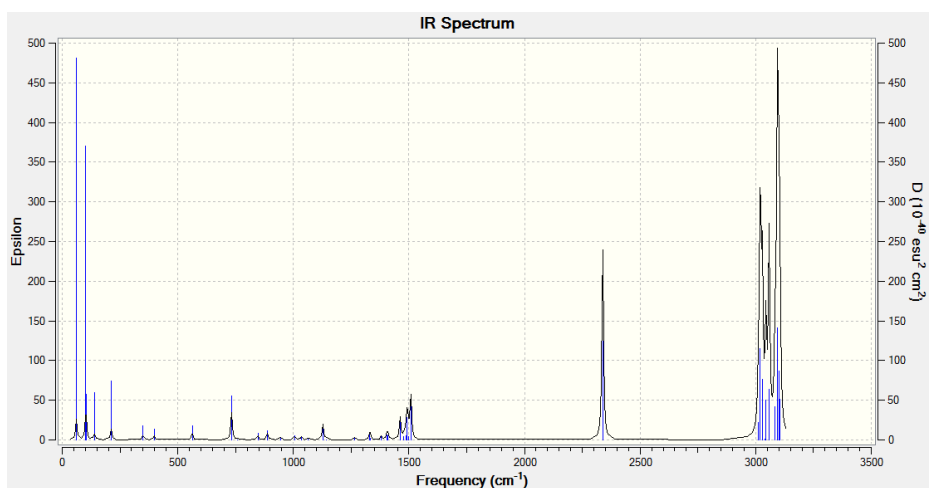
3. IR spectra



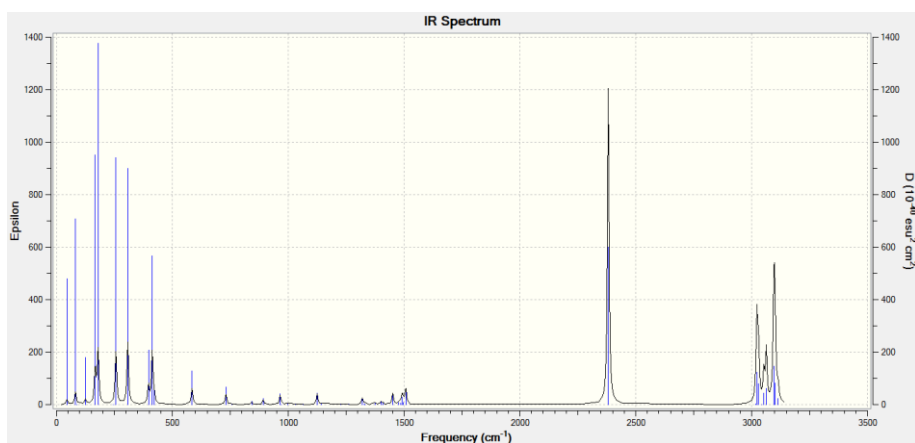




Be—Malono Nitrile

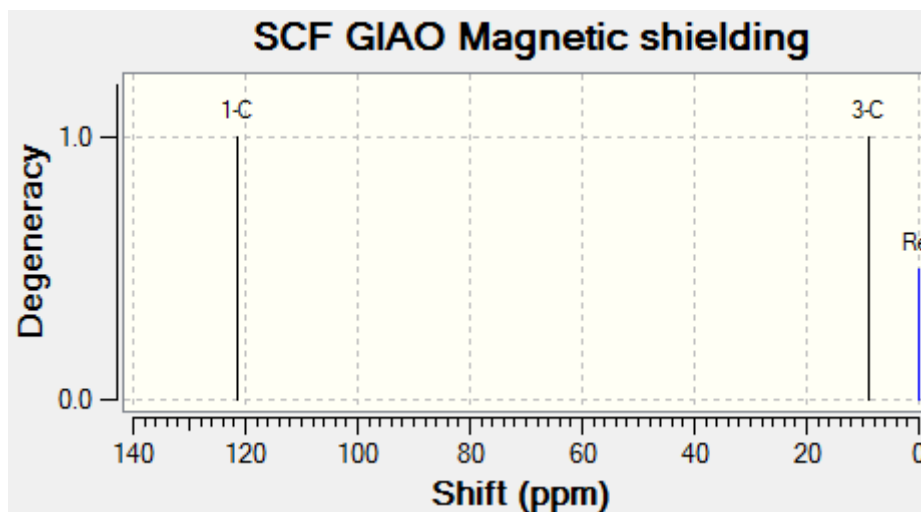


***n*-Pentane Carbonitrile**

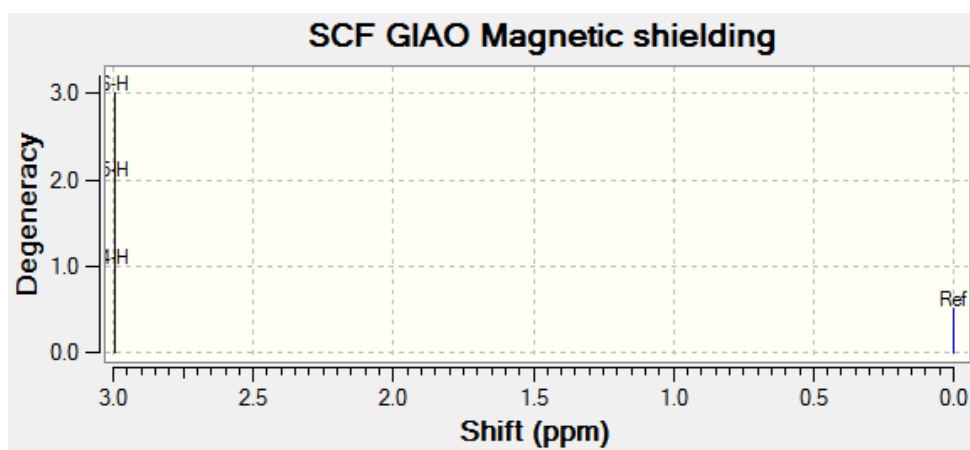


Mg--*n*-Pentane Carbonitrile

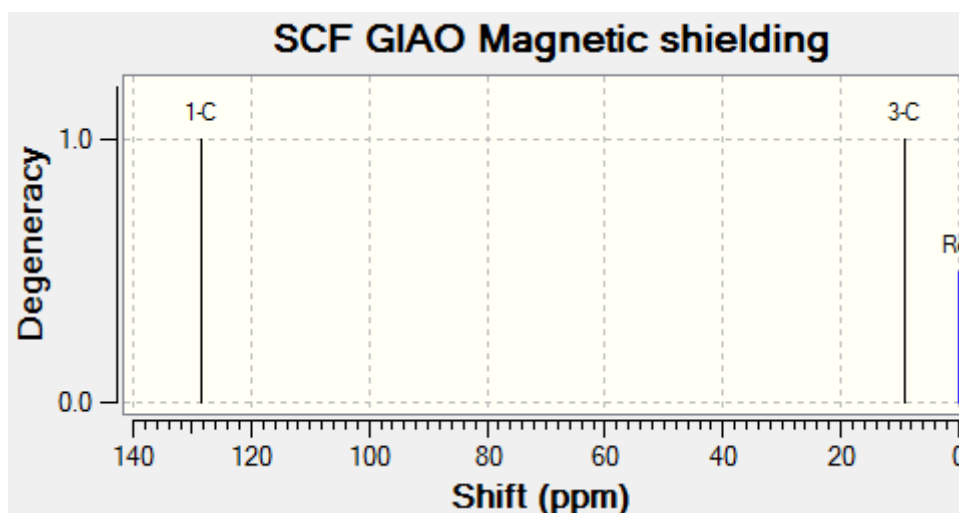
4. NMR GIAO Spectra



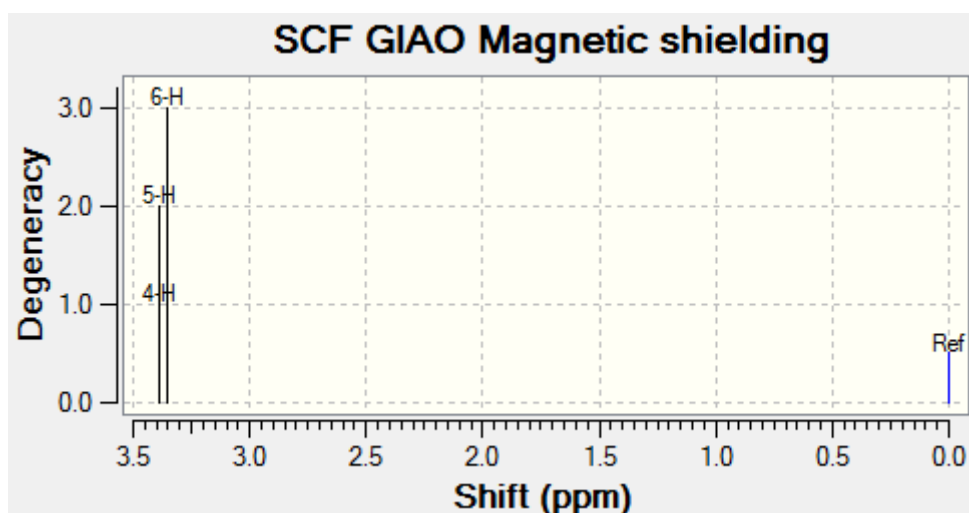
^{13}C NMR GIAO against reference TMS HF/6-31G(d) GIAO



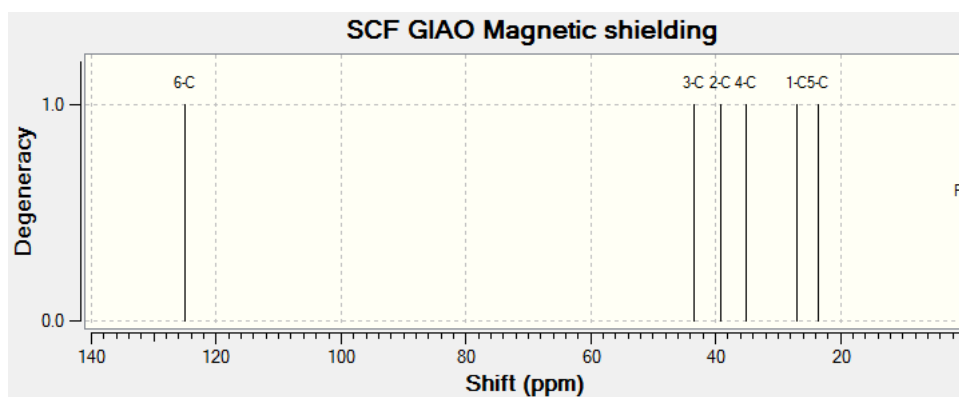
^1H NMR GIAO against reference TMS HF/6-31G(d) GIAO



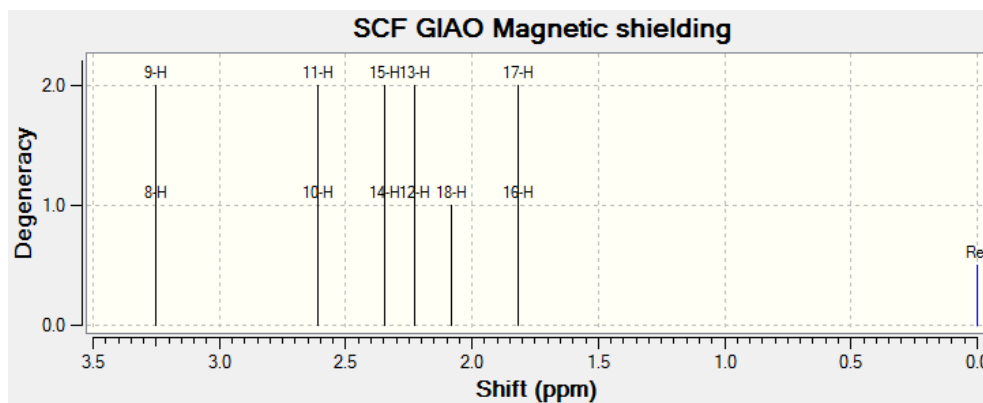
¹³C NMR GIAO against reference TMS HF/6-31G(d) GIAO



¹H NMR GIAO against reference TMS HF/6-31G(d) GIAO

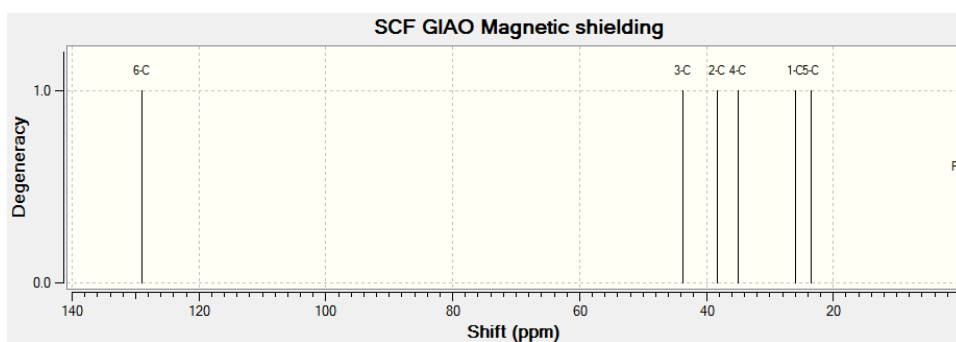


¹³C NMR GIAO against reference TMS HF/6-31G(d) GIAO

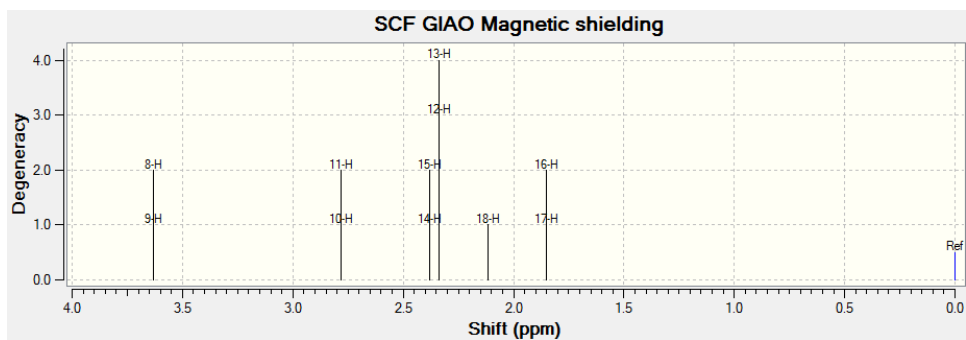


^1H NMR GIAO against reference TMS HF/6-31G(d) GIAO

Mg--*n*-Pentane Carbonitrile

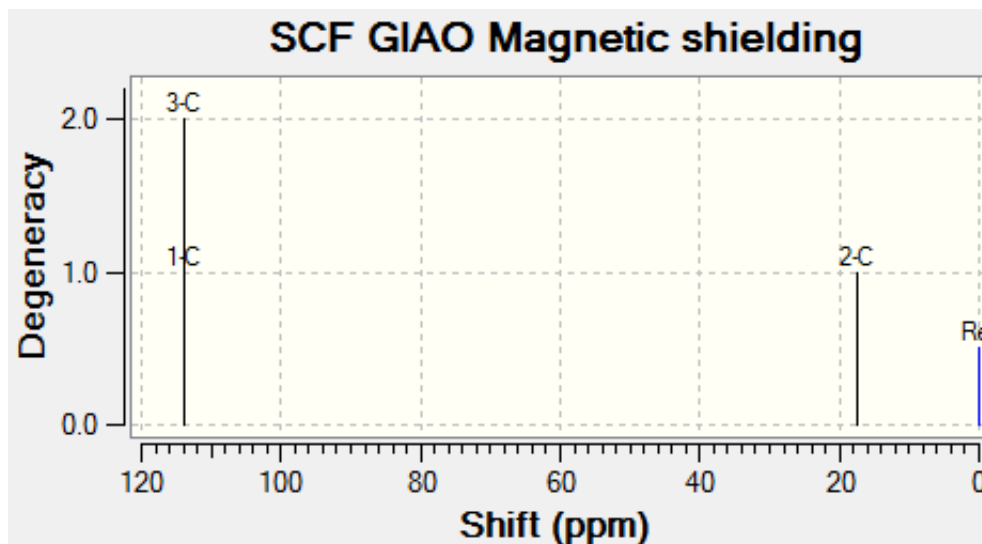


^{13}C NMR GIAO against reference TMS HF/6-31G(d) GIAO

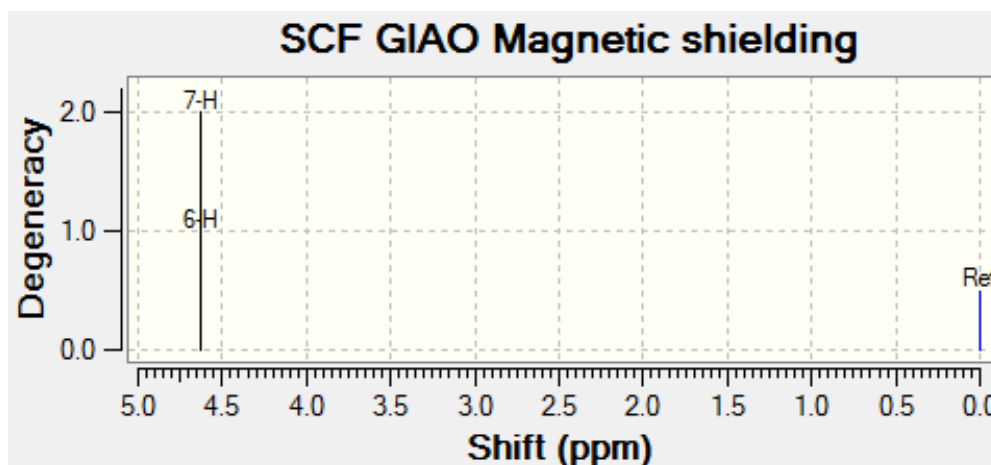


^1H NMR GIAO against reference TMS HF/6-31G(d) GIAO

Malono Nitrile

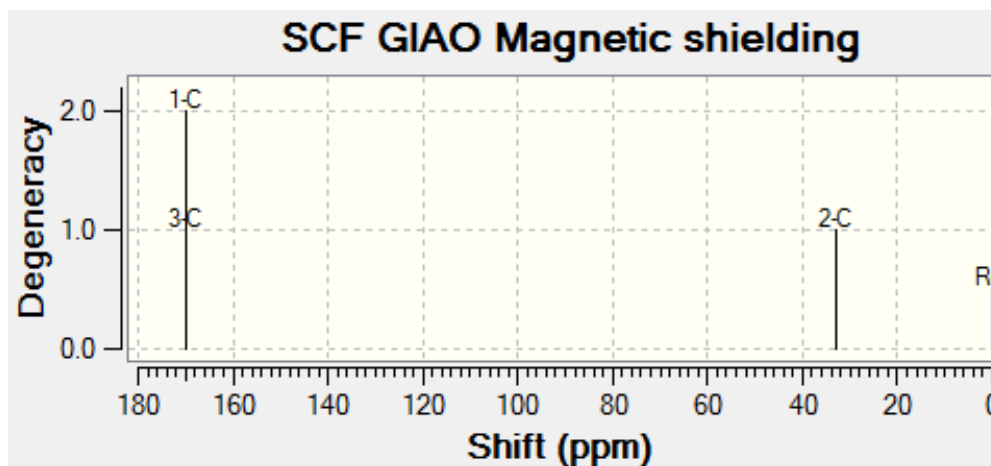


^{13}C NMR GIAO against reference TMS HF/6-31G(d) GIAO

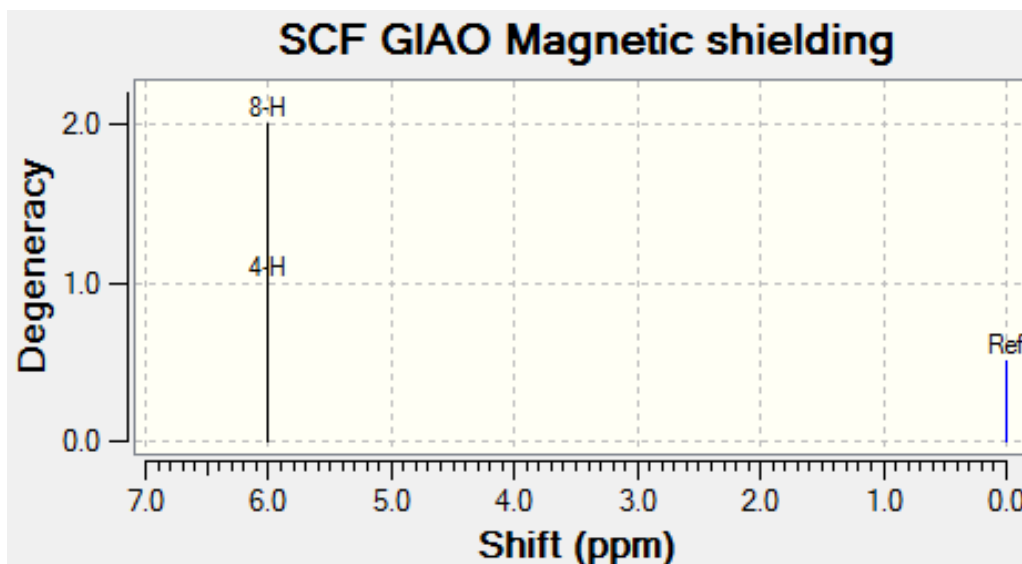


^1H NMR GIAO against reference TMS HF/6-31G(d) GIAO

Be—Malono Nitrile

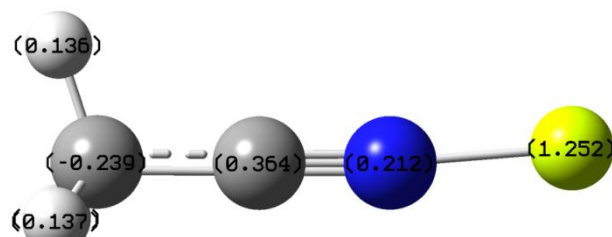
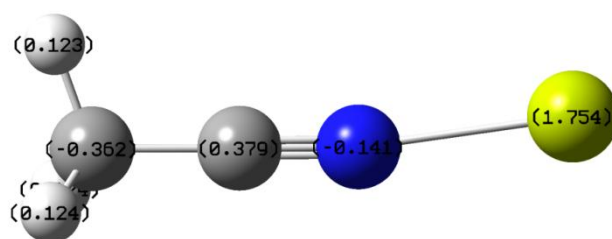
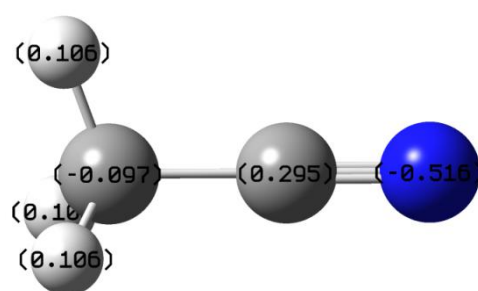


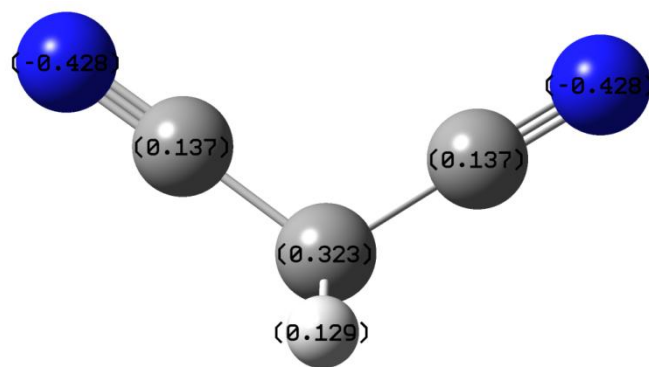
^{13}C NMR GIAO against reference TMS HF/6-31G(d) GIAO



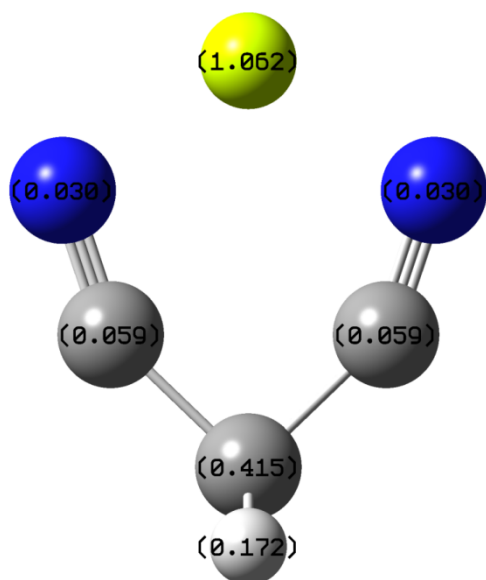
^1H NMR GIAO against reference TMS HF/6-31G(d) GIAO

5. Mulliken Charges

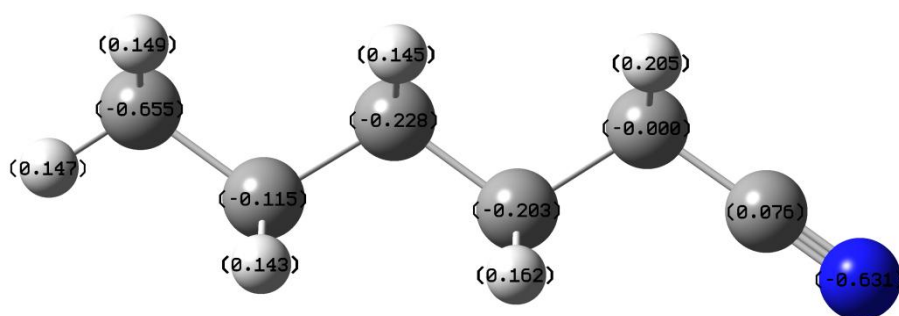




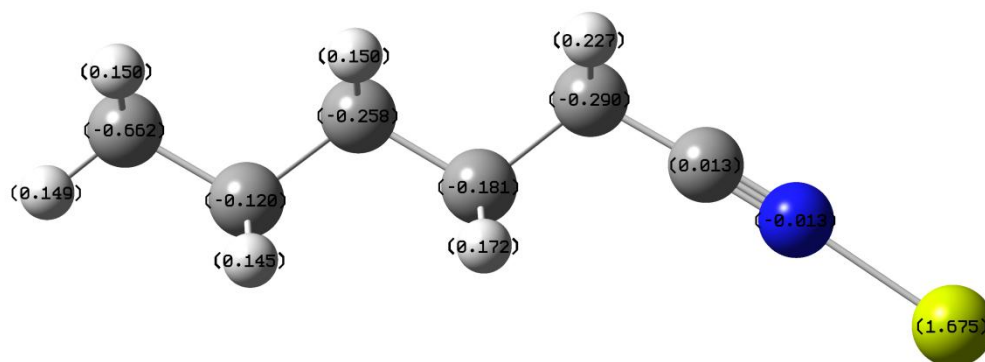
Malono nitrile



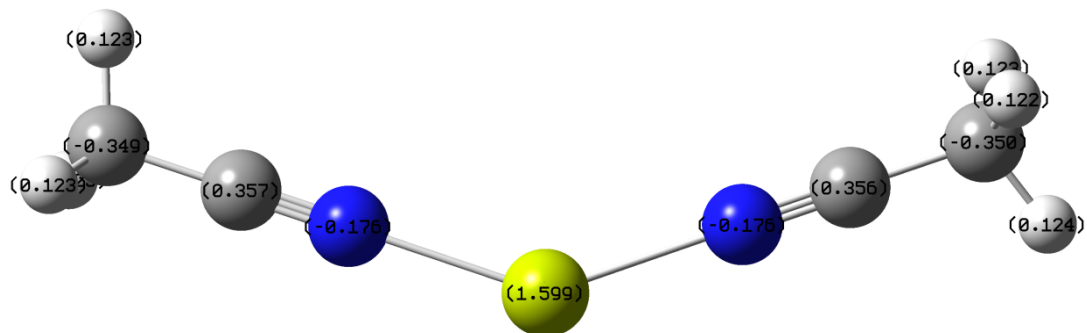
Be-Malono Nitrile



***n*-Pentane carbonitrile**

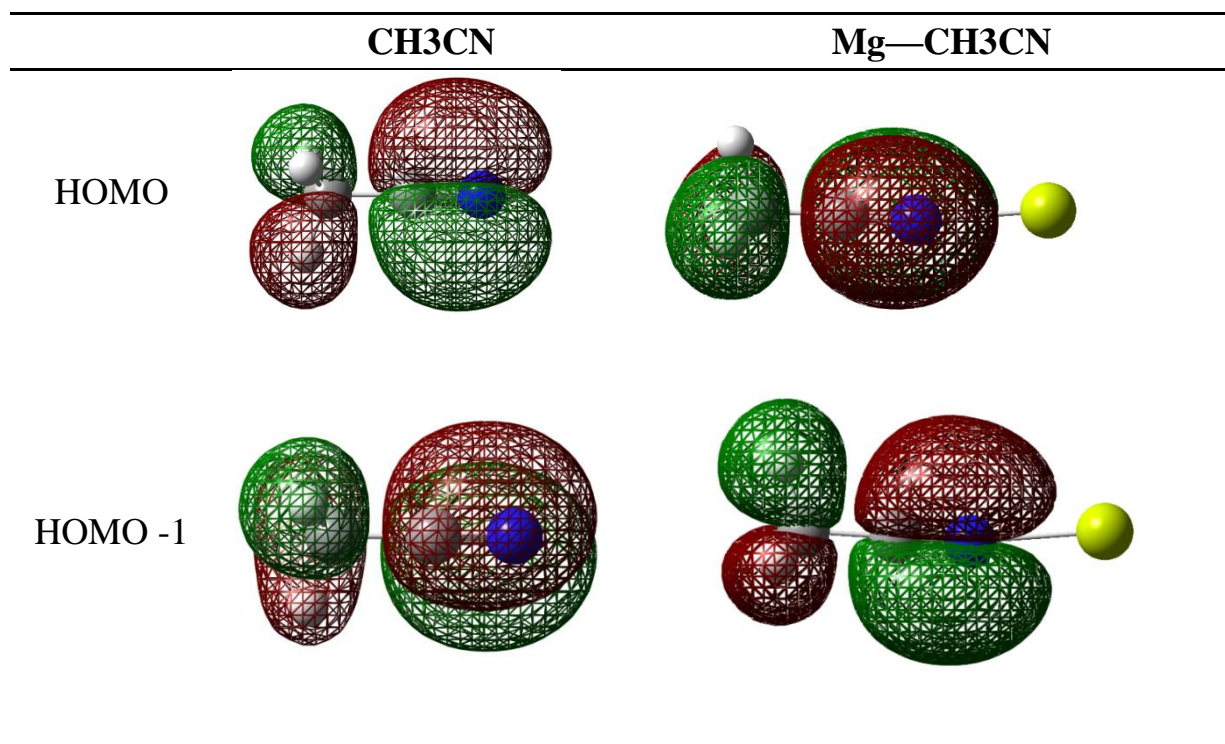


Mg--*n*-Pentane carbonitrile

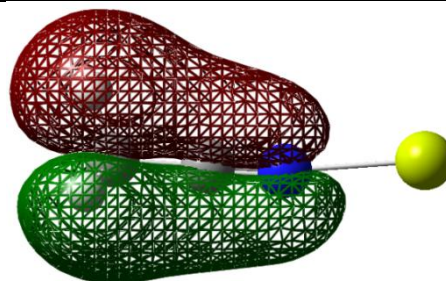
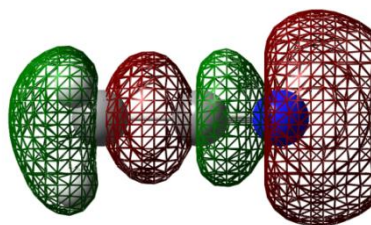


Mg(II)-2 CH₃CN

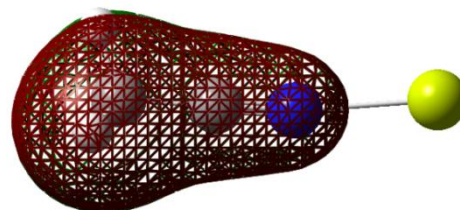
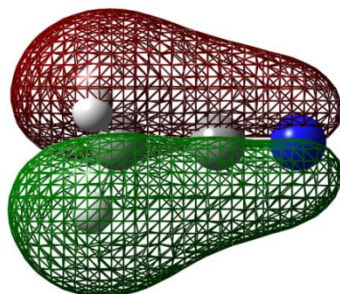
7. Molecular Orbitals



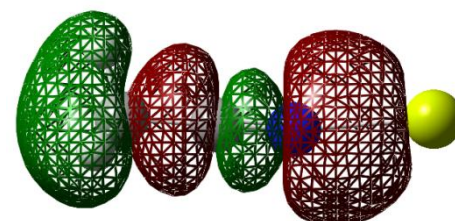
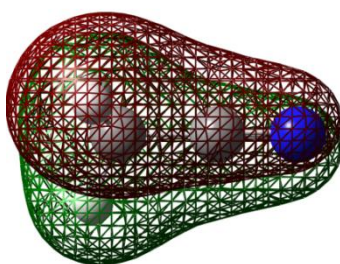
HOMO -2



HOMO -3



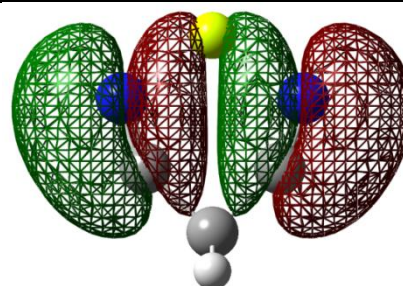
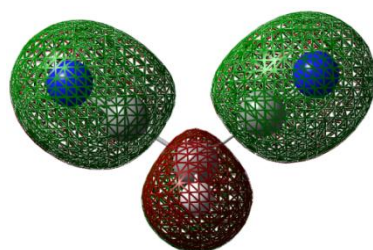
HOMO -4



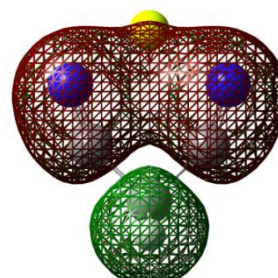
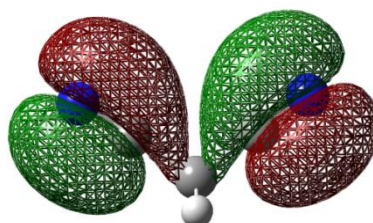
Malono Nitrile

Be--Malono Nitrile

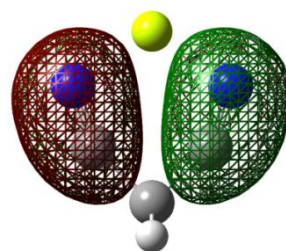
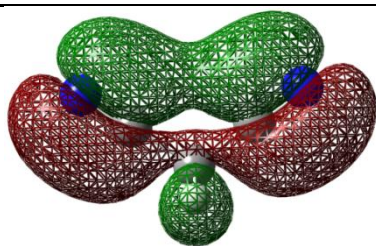
HOMO



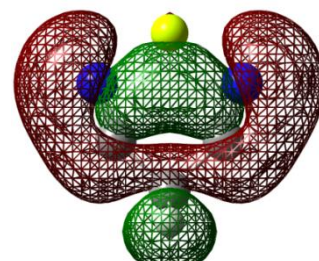
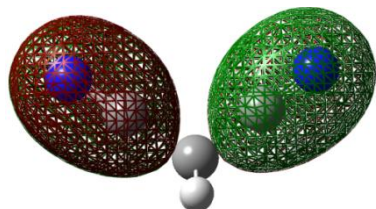
HOMO -1



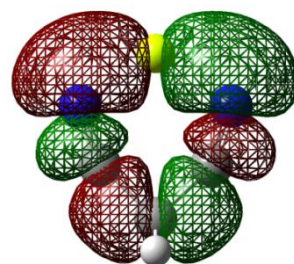
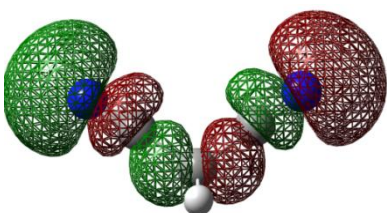
HOMO -2



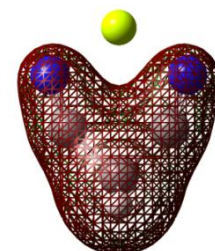
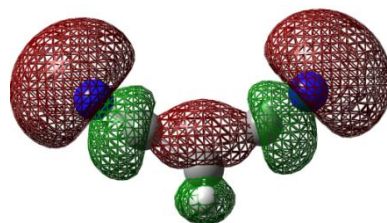
HOMO -3



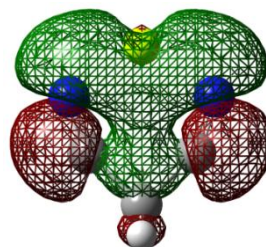
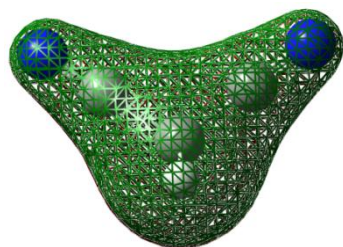
HOMO -4



HOMO -5



HOMO -6



Appendix B

Supplementary Information for Chapter 5

Contents:

1. Geometrical Structure

2. AOMix Plots

1. Geometrical Structure

2 CN Keto(1a)				
Tag	Symbol	X	Y	Z
1	C	1.083122	-0.37951	0.142858
2	C	-0.02615	0.680821	0.084762
3	C	-1.36683	0.106465	-0.01689
4	O	2.221612	-0.12659	-0.16884
5	N	-2.41608	-0.38388	-0.09678
6	H	0.784666	-1.38117	0.509941
7	H	0.040612	1.276661	1.005915
8	H	0.173546	1.357722	-0.75207

2 CN Enol(1b)				
Tag	Symbol	X	Y	Z
1	C	1.188583	0.452385	-0.00009
2	C	-0.07364	0.921087	0.000081
3	C	-1.2267	0.087146	-5.1E-05
4	N	-2.19294	-0.56366	0.000034
5	O	1.474009	-0.86746	-0.00012
6	H	2.030179	1.140946	-0.00011
7	H	-0.22921	1.993994	0.000154
8	H	2.428071	-1.01338	0.001013

2 CN Enolate(1c)				
Tag	Symbol	X	Y	Z
1	C	-1.28109	0.317569	0.000019
2	C	0.02456	0.847752	0.000011
3	C	1.207012	0.085359	-1.6E-05
4	N	2.222914	-0.5087	-3.9E-05
5	O	-1.6674	-0.87452	0.000013
6	H	-2.06066	1.123688	0.000052
7	H	0.136568	1.929278	0.000029

1,2 Dicyanoethylene (2)				
Tag	Symbol	X	Y	Z
1	C	-0.67474	1.041331	0.000024
2	C	0.674741	1.041331	0.000009
3	C	-1.48552	-0.13263	0.000015
4	N	-2.18493	-1.06297	0.000008
5	C	1.48552	-0.13263	-1.9E-05
6	N	2.184926	-1.06297	-4.2E-05
7	H	-1.20672	1.988594	0.000045
8	H	1.206721	1.988594	0.000018

2 CN Keto(1a)-Mg				
Tag	Symbol	X	Y	Z
1	C	1.218112	-0.94521	-5.4E-05
2	C	1.617767	0.535892	-8E-06
3	C	0.354301	1.265072	-6.8E-05
4	O	0.041618	-1.3281	0.000141
5	N	-0.79689	1.438067	0.000095
6	H	2.028154	-1.68931	-0.0003
7	H	2.239984	0.761105	0.883533
8	H	2.240135	0.761292	-0.88338
9	Mg	-1.70034	-0.36744	-7.3E-05

2 CN Enol(1b)-Mg				
Tag	Symbol	X	Y	Z
1	C	1.516117	0.529055	0.000149
2	C	1.454837	-0.81692	0.000398
3	C	0.127648	-1.3019	0.000146
4	N	-1.04375	-1.33717	-0.00087
5	O	0.335313	1.304305	-0.00081
6	Mg	-1.60921	0.546231	0.000612
7	H	2.4352	1.1093	0.000391
8	H	2.335699	-1.45353	0.000793
9	H	0.571759	2.253784	-0.00015

2 CN Enolate(1c)-Mg				
Tag	Symbol	X	Y	Z
1	C	1.398207	-0.58876	-6.5E-05
2	C	1.384439	0.801882	0.000312
3	C	0.08054	1.289176	0.000597
4	O	0.334773	-1.34836	-0.00016
5	Mg	-1.39693	-0.64606	0.000276
6	N	-1.10337	1.31672	-0.0008
7	H	2.271841	1.418777	-8.2E-05
8	H	2.357552	-1.11001	-0.00139

1,2 Dicyanoethylene (2)-Mg				
Tag	Symbol	X	Y	Z
1	C	-1.81614	-0.68315	0.00001
2	C	-1.81614	0.683151	0.000011
3	C	-0.51947	-1.29172	-3E-06
4	N	0.634804	-1.45358	-1.1E-05
5	C	-0.51947	1.291715	0.000006
6	N	0.634804	1.453576	0.000009
7	H	-2.72732	-1.27991	0.000016
8	H	-2.72732	1.279914	0.000022
9	Mg	2.04956	0	-1.4E-05

Ether Carbonyl-Mg				
Tag	Symbol	X	Y	Z
1	C	-2.34594	0.047872	1.807408
2	O	-0.9556	0.058906	1.780786
3	C	-3.11704	0.009154	0.705235
4	C	-2.64836	-0.02453	-0.6779
5	O	-1.41233	-0.02635	-0.93798
6	H	-2.76303	0.074148	2.809369
7	C	-3.64254	-0.05663	-1.78149
8	H	-4.29495	-0.93367	-1.66912

9	H	-4.30396	0.818094	-1.71255
10	H	-3.15121	-0.07838	-2.75387
11	H	-4.18869	0.00533	0.878165
12	H	-0.60942	0.100415	2.688798
13	Mg	0.21923	0.000568	0.049151
14	O	1.691378	1.321241	-0.01504
15	O	1.673412	-1.32121	-0.12886
16	C	2.923558	0.703859	-0.51119
17	C	2.991837	-0.70935	0.04136
18	C	1.665285	2.780663	-0.15604
19	H	0.694248	3.11976	0.205557
20	H	2.462152	3.206505	0.456504
21	H	1.794812	3.04787	-1.20746
22	C	1.684853	-2.78718	-0.13812
23	H	2.110293	-3.15293	0.79918
24	H	0.650053	-3.11415	-0.2417
25	H	2.270868	-3.12865	-0.99345
26	H	3.731778	-1.28934	-0.51743
27	H	3.244652	-0.72837	1.106673
28	H	2.895581	0.718162	-1.60595
29	H	3.781221	1.284461	-0.15939

Ether Carbonyl-Ca				
Tag	Symbol	X	Y	Z
1	C	2.938038	0.016815	1.734185
2	O	1.563091	0.014749	1.884075
3	C	3.585806	0.011935	0.552384
4	C	2.981667	0.002839	-0.77562
5	O	1.728604	0.001366	-0.90616
6	H	3.482198	0.022633	2.674225
7	C	3.869135	-0.00458	-1.97199
8	H	4.52844	0.873563	-1.95244
9	H	4.531714	-0.87983	-1.93955
10	H	3.287221	-0.01226	-2.89328
11	H	4.669511	0.014361	0.613032
12	H	1.360061	0.015583	2.834583
13	O	-2.02001	-1.37945	0.016976
14	O	-2.02646	1.365411	-0.13965
15	C	-3.22575	-0.71759	-0.46893
16	C	-3.293	0.684096	0.10414
17	C	-2.0879	-2.83441	-0.08571
18	H	-1.1279	-3.22874	0.252259
19	H	-2.8852	-3.20515	0.562714
20	H	-2.26801	-3.12642	-1.12382
21	C	-2.14984	2.81931	-0.19771
22	H	-2.57251	3.194137	0.73825
23	H	-1.14685	3.223505	-0.34514

24	H	-2.78287	3.094432	-1.04452
25	H	-4.09921	1.232173	-0.39368
26	H	-3.48267	0.677251	1.183532
27	H	-3.19993	-0.70951	-1.5646
28	H	-4.10378	-1.28128	-0.13697
29	Ca	-0.19305	0.010426	0.117449

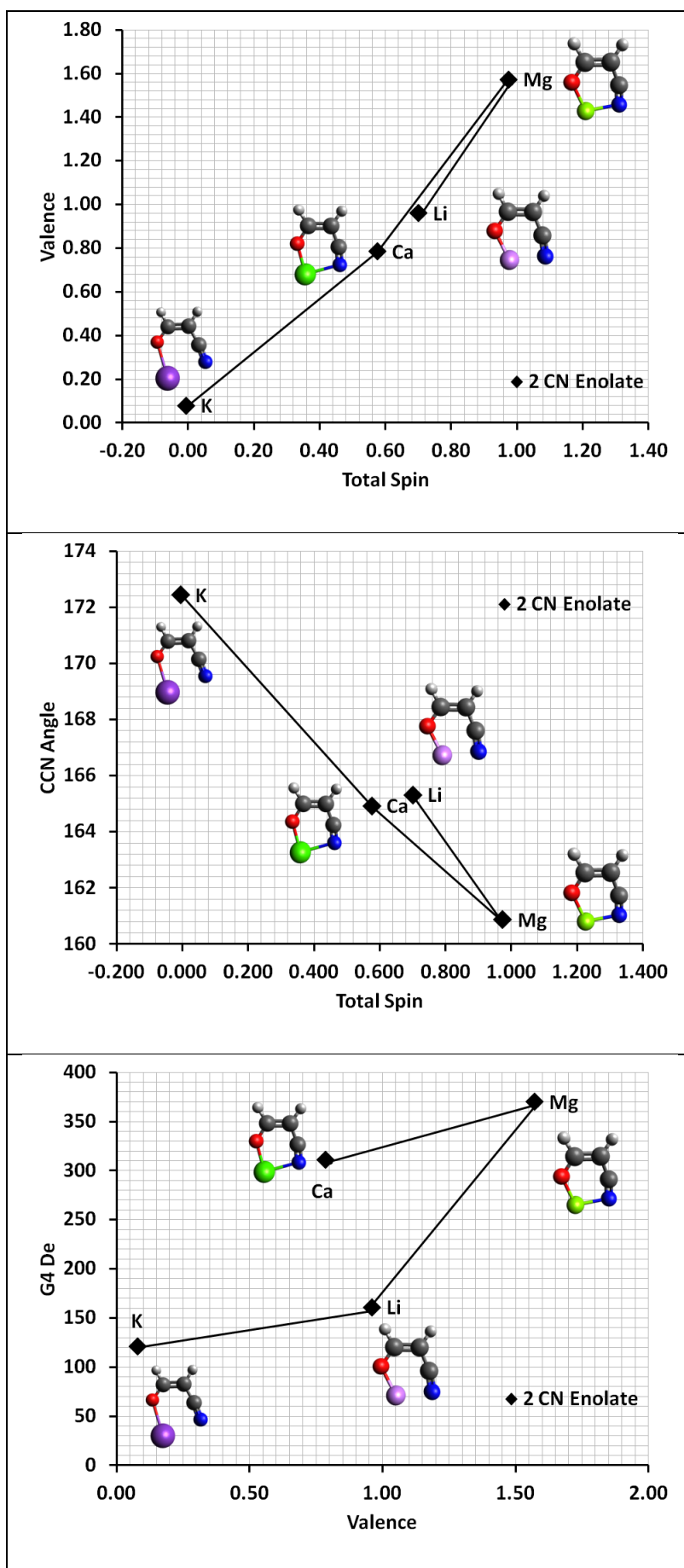
3 ligands 2 CN enol-Mg				
Tag	Symbol	X	Y	Z
1	C	0.851655	2.681507	-1.43842
2	O	0.258516	1.443678	-1.50936
3	H	0.669724	3.320464	-2.29778
4	C	1.601724	3.084618	-0.3948
5	H	2.025469	4.080985	-0.46156
6	C	1.844887	2.314688	0.821065
7	O	1.413366	1.141715	0.951369
8	Mg	0.440147	-0.2501	-0.05571
9	O	1.407893	-1.55409	-1.3286
10	O	0.891114	-1.78548	1.241786
11	C	1.173648	-3.02729	0.55889
12	C	2.025285	-2.68567	-0.64781
13	H	1.728399	-3.69883	1.222111
14	H	0.228908	-3.50537	0.273077
15	H	3.041812	-2.39833	-0.35748
16	H	2.067621	-3.5376	-1.3334
17	C	0.48283	-1.93445	2.626675
18	H	0.33166	-0.92995	3.021954
19	H	-0.44433	-2.51219	2.685536
20	H	1.279305	-2.43243	3.185023
21	C	1.942772	-1.35096	-2.66428
22	H	3.024569	-1.19766	-2.61249
23	H	1.710204	-2.22143	-3.28259
24	H	1.46193	-0.46535	-3.07785
25	C	-4.1644	-0.82168	0.007987
26	H	-4.49623	-1.85416	0.02301
27	C	2.615985	2.954665	1.927502
28	H	2.108125	3.870773	2.25597
29	H	2.729323	2.271521	2.768764
30	H	-0.36974	1.410996	-2.24835
31	H	3.603228	3.266726	1.563122
32	C	-5.08119	0.183052	0.059628
33	C	-2.78248	-0.5849	-0.05916
34	O	-4.72529	1.461779	0.039115
35	N	-1.62569	-0.43028	-0.11578
36	H	-6.14158	-0.0539	0.118735
37	H	-5.48938	2.056564	0.095124

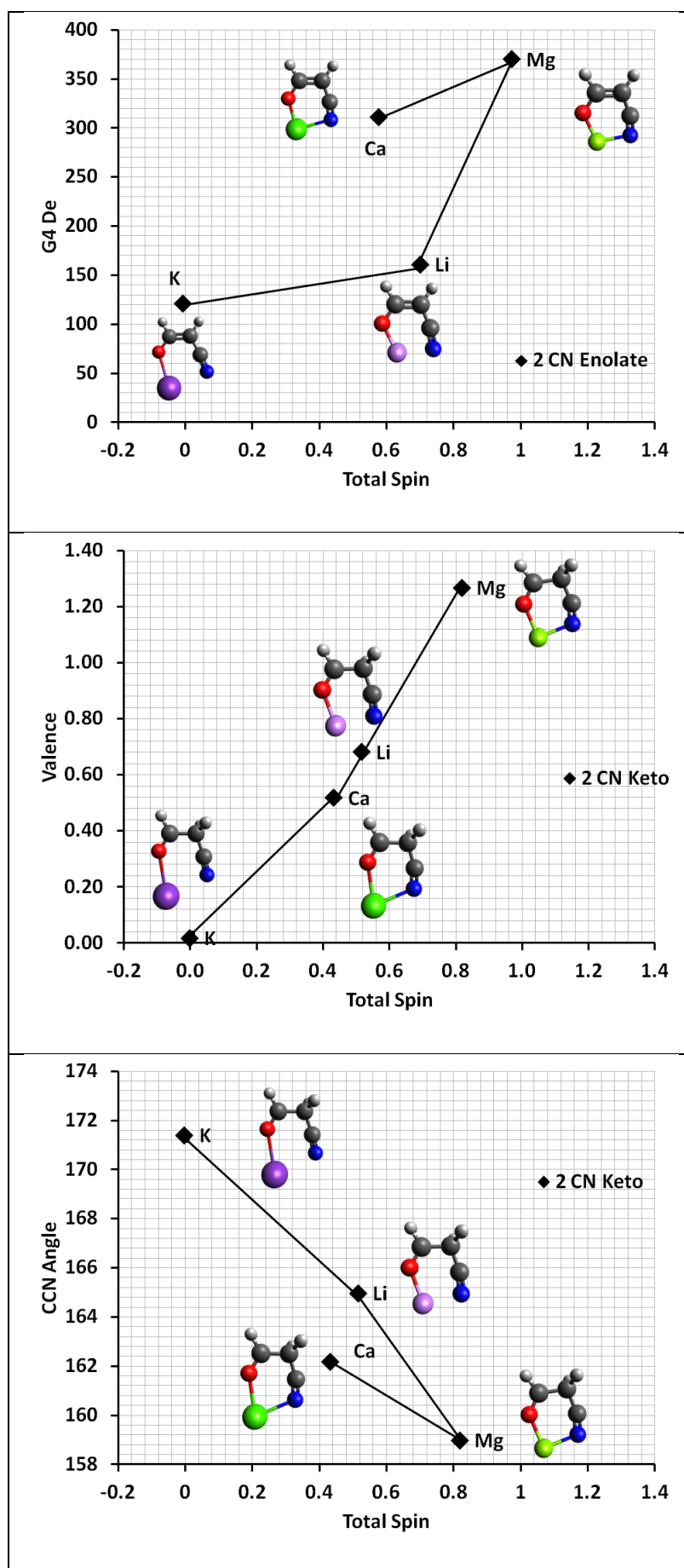
3 ligands 2 CN Enolate-Mg				
Tag	Symbol	X	Y	Z
1	C	-2.55299	-1.09882	-1.23726
2	O	-1.27179	-0.74353	-1.51593
3	H	-3.02643	-1.74896	-1.96757
4	C	-3.20442	-0.66058	-0.14005
5	H	-4.23369	-0.98051	-0.02234
6	C	-2.63235	0.211927	0.885329
7	O	-1.44155	0.580472	0.858666
8	Mg	0.260366	-0.05587	-0.0585
9	O	0.468573	1.858581	-0.99728
10	O	1.770976	0.859079	1.063347
11	C	2.401044	1.962588	0.387511
12	C	1.296287	2.772954	-0.25673
13	H	2.943508	2.581285	1.111132
14	H	3.104057	1.574538	-0.35973
15	H	0.683528	3.280751	0.499387
16	H	1.724362	3.518725	-0.93685
17	C	2.623291	0.192253	2.020606
18	H	2.032759	-0.6122	2.455277
19	H	3.508221	-0.21408	1.519631
20	H	2.921241	0.905164	2.795199
21	C	-0.50813	2.52294	-1.81694
22	H	-1.19116	3.111979	-1.19431
23	H	-0.00248	3.173085	-2.53777
24	H	-1.0619	1.750899	-2.34944
25	C	1.711096	-3.10694	-0.3819
26	H	2.248176	-4.02676	-0.56183
27	C	-3.53201	0.664574	1.998902
28	H	-3.84703	-0.2062	2.588046
29	H	-3.01022	1.369042	2.646755
30	H	-0.89597	-1.20147	-2.28631
31	H	-4.44407	1.121836	1.598844
32	C	0.924871	-2.86381	0.740887
33	C	1.714956	-2.01789	-1.25686
34	O	0.295476	-1.76444	0.964961
35	N	1.50941	-0.98079	-1.77686
36	H	0.833538	-3.65767	1.490843

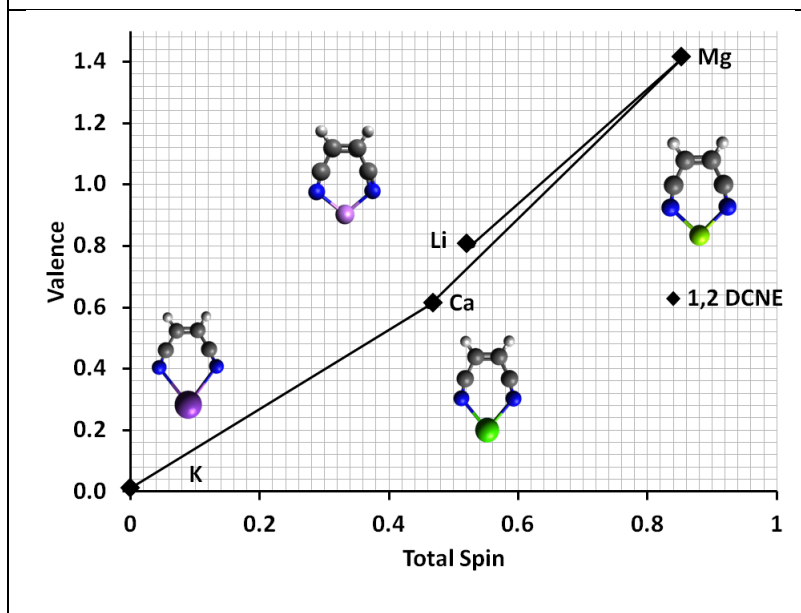
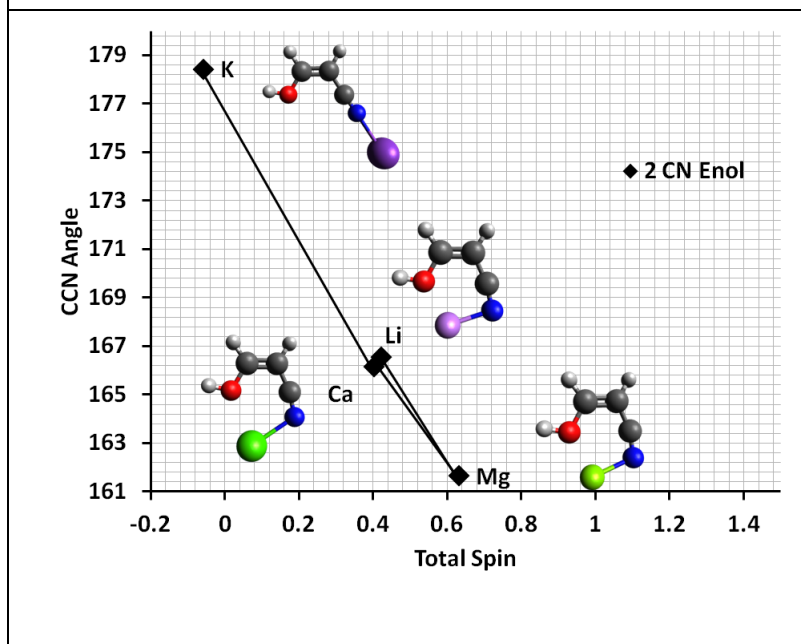
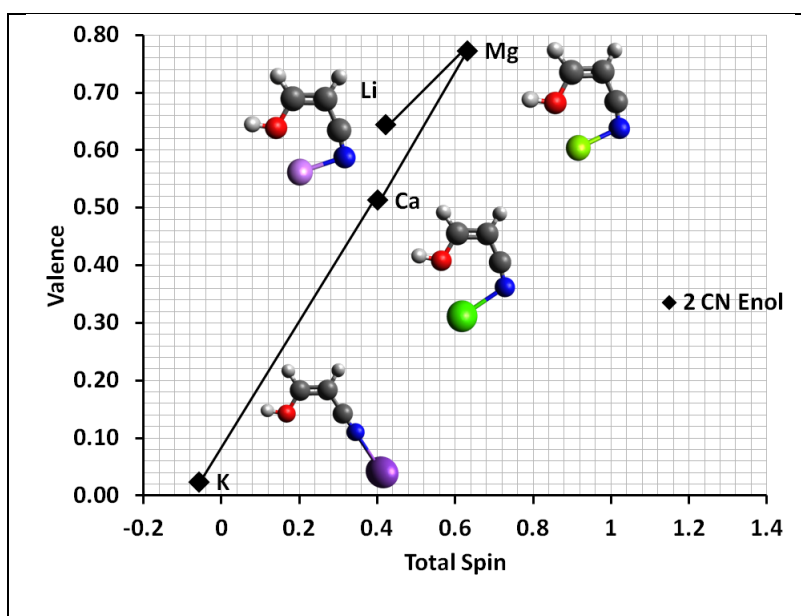
3 Ligands 1,2 Dicyanoethylene (2)-Mg				
Tag	Symbol	X	Y	Z
1	C	-2.01856	-1.8565	-1.40707
2	O	-0.9583	-1.17402	-1.5759
3	H	-2.29103	-2.54534	-2.2234
4	C	-2.8871	-1.81818	-0.3077
5	H	-3.74815	-2.47713	-0.33054
6	C	-2.71367	-0.96396	0.808177
7	O	-1.74311	-0.15357	0.942329
8	Mg	-0.01748	-0.15001	-0.10571
9	O	-0.69713	1.808054	-1.04543
10	O	0.822293	1.448913	1.156025
11	C	0.802466	2.737205	0.540852
12	C	-0.54135	2.89693	-0.13714
13	H	0.922966	3.517917	1.304218
14	H	1.623146	2.813455	-0.18549
15	H	-1.35128	2.874238	0.605287
16	H	-0.57536	3.851546	-0.68148
17	C	1.914142	1.267595	2.071154
18	H	1.802568	0.271779	2.495636
19	H	2.872292	1.337493	1.543295
20	H	1.859535	2.029126	2.858528
21	C	-1.92345	1.86254	-1.78103
22	H	-2.78286	1.818231	-1.10085
23	H	-1.96221	2.7867	-2.37152
24	H	-1.93236	0.995357	-2.43974
25	C	3.872053	-0.90608	-0.52373
26	H	4.889584	-0.52951	-0.59854
27	C	-3.73269	-0.98634	1.929036
28	H	-3.23978	-1.32218	2.848488
29	H	-4.09536	0.030805	2.112831
30	H	1.390597	-0.22607	-2.4977
31	H	-4.58063	-1.64225	1.718729
32	C	3.509685	-1.99338	0.373095
33	C	2.911497	-0.44859	-1.34968
34	N	1.732112	-0.03917	-1.54941
35	H	4.126373	-2.86687	0.544142
36	C	2.191249	-1.92264	0.761992
37	N	1.065879	-1.61281	0.975493

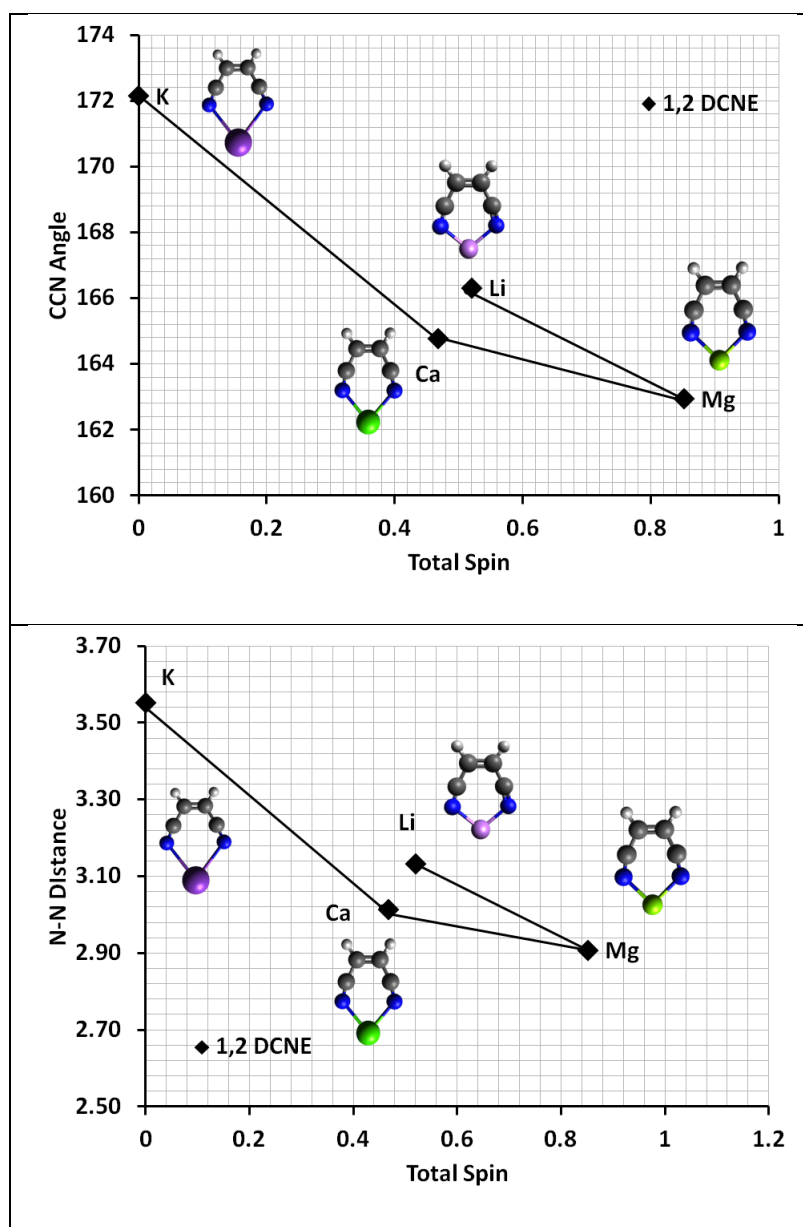
3 Ligands Carboxylate-Mg				
Tag	Symbol	X	Y	Z
1	C	2.801495	0.712756	-1.07185
2	O	1.486808	0.786582	-1.39495
3	H	3.481609	1.22129	-1.74986
4	C	3.241949	0.035912	0.010307
5	H	4.314182	0.005131	0.167621
6	C	2.383773	-0.6328	0.984681
7	O	1.137289	-0.60551	0.908507
8	Mg	-0.30456	0.401719	-0.08526
9	O	-0.99529	-1.27336	-1.18252
10	O	-1.96884	-0.20293	1.023436
11	C	-2.83868	-1.1066	0.320729
12	C	-1.95693	-2.06385	-0.45433
13	H	-3.45454	-1.66407	1.035891
14	H	-3.49139	-0.53246	-0.34895
15	H	-1.42183	-2.74831	0.215858
16	H	-2.56384	-2.64529	-1.15754
17	C	-2.6442	0.604883	2.015486
18	H	-1.89945	1.280458	2.432549
19	H	-3.44729	1.181636	1.544658
20	H	-3.05218	-0.04761	2.793095
21	C	-0.28055	-2.02643	-2.18004
22	H	0.276066	-2.84654	-1.71264
23	H	-0.98653	-2.42369	-2.91559
24	H	0.40846	-1.33996	-2.67068
25	O	-0.27054	2.296096	0.751536
26	O	-0.95782	1.958955	-1.32071
27	C	-0.74518	2.740818	-0.33723
28	H	-0.97344	3.81205	-0.43648
29	C	3.045558	-1.36275	2.116882
30	H	3.607302	-0.64946	2.733339
31	H	2.300641	-1.86604	2.733293
32	H	1.288189	1.440404	-2.08597
33	H	3.772436	-2.08853	1.734325

2. AOMix Plots









Appendix C

Supplementary Information for Chapter 6

Contents:

1. Benchmark Details
2. Geometrical Structure
3. Intrinsic Reaction Coordinate
- 4 Molecular orbitals

1. Benchmark Details

BeO			
Symbol	X	Y	Z
Be	0	0	-0.90418
O	0	0	0.45209

BeO + H2 → Be + H2O						
	BeO	H2	Be	H2O	ΔH_{rxn}	Error
NIST	32.6	0.00	77.438	-57.8	-13.0	0.0
G3	-89.8432	-1.16407	-14.657364	-76.378265	-17.8	4.8
CBS-QB3	-89.7677	-1.16278	-14.61818	-76.333703	-13.4	0.5

BeH			
Symbol	X	Y	Z
Be	0	0	0.269683
H	0	0	-1.07873

BeF			
Symbol	X	Y	Z
Be	0	0	-0.95364
F	0	0	0.423838

BeH + F₂ → BeF + HF						
	BeH	F2	BeF	HF	ΔH_{rxn}	Error
NIST	81.7	0	-40.6	-65.1	-187.4	0.0
G3	-15.2316	-199.423	-114.55231	-100.3978	-185.5	1.9
CBS-QB3	-15.1907	-199.343	-114.47119	-100.35663	-184.6	2.8

BeF₂			
Symbol	X	Y	Z
Be	0	0	0
F	0	0	1.386233
F	0	0	-1.38623

Be + F2 > BeF2					
	Be	F2	BeF2	ΔH_{rxn}	Error
NIST	77.438	0	-190.3	-267.74	0.0
G3	-14.6574	-199.423	-214.50438	-266.16	1.6
CBS-QB3	-14.6182	-199.343	-214.38241	-264.30	3.4

2. Geometrical Structures

2 CN BD mono				
Tag	Symbol	X	Y	Z
1	C	-0.7156	1.80043	0.00001
2	C	-0.16271	0.568784	0.000005
3	H	-1.78995	1.944055	-1.2E-05
4	H	-0.08673	2.685406	0.000036
5	C	1.290264	0.340215	0.000034
6	C	1.886888	-0.86023	0.00003
7	H	1.891243	1.247395	0.000061
8	H	2.968672	-0.94273	0.000053
9	H	1.3182	-1.78607	0.000003
10	C	-1.0261	-0.58717	-3.1E-05
11	N	-1.70541	-1.53146	-0.00006

Be—2 CN BD Cyclic				
Tag	Symbol	X	Y	Z
1	C	-0.11183	1.197422	-0.11268
2	C	-0.92106	-0.01318	0.03633
3	C	-0.00906	-1.1252	0.069207
4	H	-0.64065	2.075038	-0.49791
5	C	1.282408	1.263428	0.118046
6	H	1.538132	0.884631	1.144349
7	H	1.768242	2.2189	-0.0737
8	N	1.05465	-1.60851	-0.03867
9	C	-2.28791	-0.06961	0.014944
10	H	-2.8301	-1.00857	0.124259
11	H	-2.87517	0.842058	-0.09458
12	Be	1.985419	-0.31741	-0.27171

Mg—2 CN BD Cyclic				
Tag	Symbol	X	Y	Z
1	C	0.605038	-1.23603	-0.10179
2	C	1.269616	0.072864	0.018598
3	C	0.282821	1.097233	0.204499
4	H	1.182044	-2.00048	-0.62685
5	C	-0.65974	-1.55311	0.352089
6	H	-1.01097	-1.0367	1.264489
7	H	-1.01983	-2.57285	0.235401
8	N	-0.77337	1.599524	0.221962
9	C	2.602626	0.289879	-0.14253
10	H	3.041663	1.279369	-0.03588
11	H	3.274952	-0.53762	-0.36048
12	Mg	-2.05471	0.137218	-0.33464

Ca—2 CN BD Cyclic				
Tag	Symbol	X	Y	Z
1	C	-1.11554	1.238751	-0.17745
2	C	-1.65374	-0.13329	-0.01948
3	C	-0.58485	-1.04399	0.214416
4	H	-1.68555	1.892117	-0.83673
5	C	0.007096	1.705765	0.419865
6	H	0.416416	1.180953	1.29336
7	H	0.304063	2.743807	0.300976
8	N	0.471423	-1.53202	0.296047
9	C	-2.94111	-0.50432	-0.17219
10	H	-3.26377	-1.53192	-0.03847
11	H	-3.70202	0.229703	-0.42164
12	Ca	2.117988	-0.0684	-0.19804

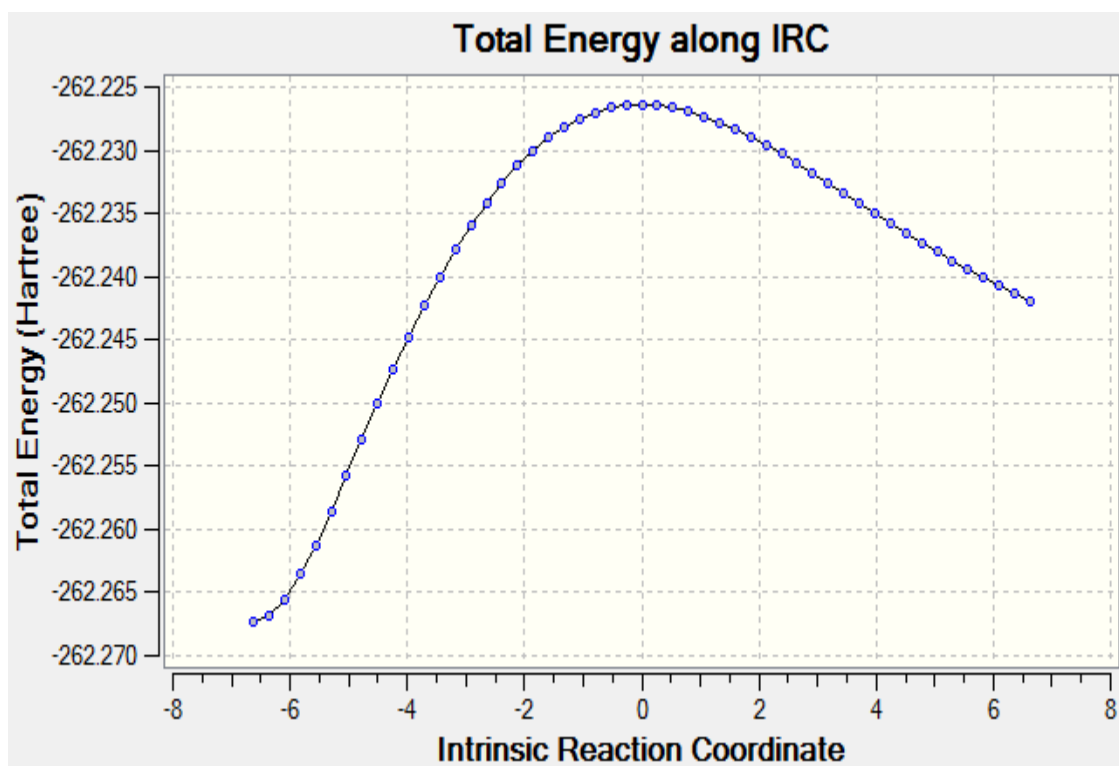
3 CN P				
Tag	Symbol	X	Y	Z
1	C	-1.19407	0.081776	-0.00012
2	C	-0.07058	1.023098	0.000195
3	C	1.297549	0.371522	-0.00016
4	C	1.545929	-0.93841	0.000188
5	H	-0.17369	1.677246	-0.87617
6	H	-0.17356	1.676392	0.877203
7	H	2.121389	1.083123	-0.00085
8	H	0.748854	-1.67698	0.000827
9	H	2.565799	-1.30962	-0.00027
10	N	-2.08026	-0.6683	-0.00019

Be—3 CN P				
Tag	Symbol	X	Y	Z
1	C	1.123092	0.449546	0.071093
2	C	-0.0136	1.370373	0.089631
3	C	-1.19591	0.42414	-0.1921
4	C	-1.26236	-0.91054	0.173458
5	H	-0.12871	1.891105	1.059694
6	H	0.086884	2.143274	-0.68733
7	H	-1.99864	0.861571	-0.79534
8	H	-0.79085	-1.1799	1.154443
9	H	-2.16802	-1.47549	-0.04953
10	N	1.652683	-0.58671	-0.06065
11	Be	0.380797	-1.53368	-0.27746

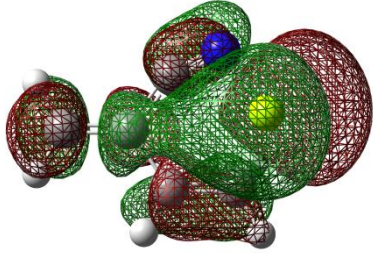
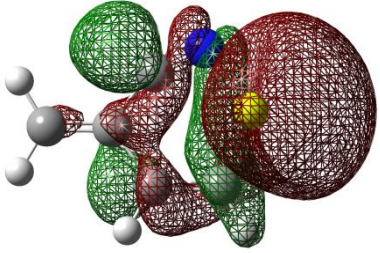
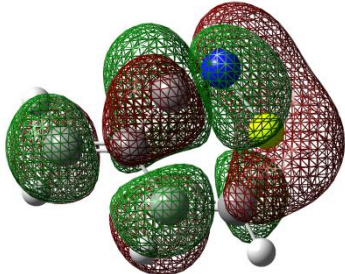
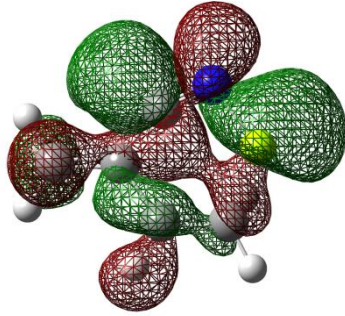
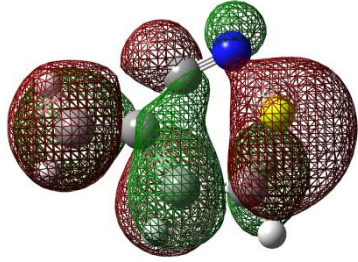
Mg-3 CN P				
Tag	Symbol	X	Y	Z
1	C	0.169221	-1.30781	0.118086
2	C	1.514141	-0.76288	-0.0389
3	C	1.305822	0.745702	-0.25522
4	C	0.370831	1.522351	0.366113
5	H	2.141241	-0.94786	0.850496
6	H	2.016924	-1.23302	-0.89393
7	H	1.99278	1.202977	-0.97036
8	H	-0.07109	1.176097	1.318222
9	H	0.373639	2.59968	0.205392
10	N	-0.99386	-1.38882	0.143642
11	Mg	-1.63805	0.478303	-0.22132

3. Intrinsic Reaction Coordinate

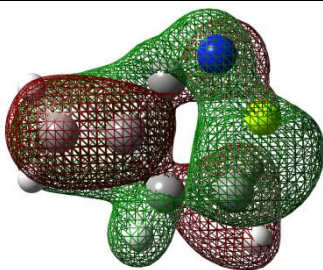
Be—2 CN BD TS				
Tag	Symbol	X	Y	Z
1	C	2.160834	-0.73795	0.008007
2	C	0.902758	-0.20222	-0.01927
3	C	0.543614	1.241502	0.114524
4	C	-0.65128	1.815823	-0.13084
5	C	-0.26458	-0.96805	-0.08624
6	N	-1.40649	-1.26271	-0.0546
7	H	2.337089	-1.80702	-0.08405
8	H	3.028411	-0.0894	0.114663
9	H	1.378269	1.865806	0.439112
10	H	-0.82693	2.866892	0.08001
11	H	-1.45408	1.319893	-0.69647
12	Be	-2.69136	-0.55295	0.302943



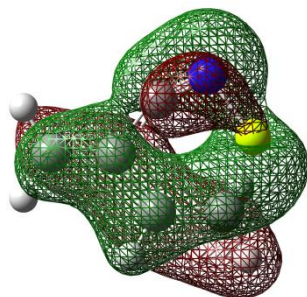
4. Molecular Orbitals

MO No		2 CN BD
27	LUMO+4	
26	LUMO+3	
25	LUMO+2	
24	LUMO+1	
23	LUMO	

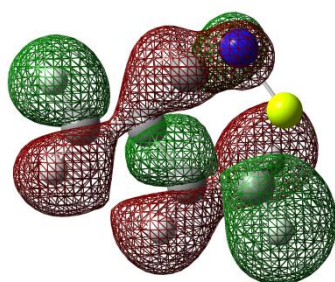
22 HOMO



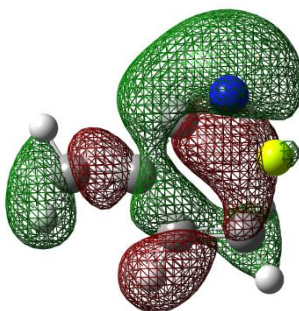
21 HOMO-1



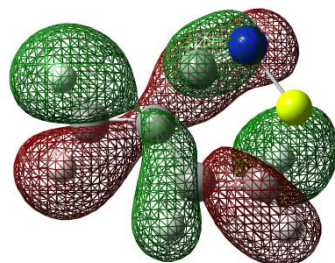
20 HOMO-2



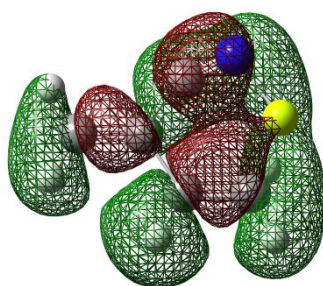
19 HOMO-3



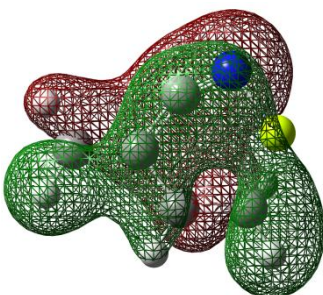
18 HOMO-4



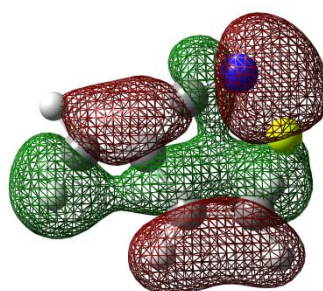
17 HOMO-5



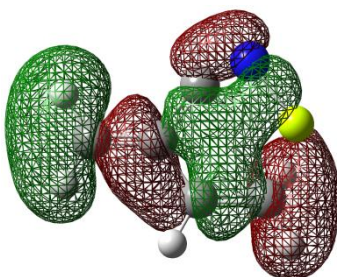
16 HOMO-6



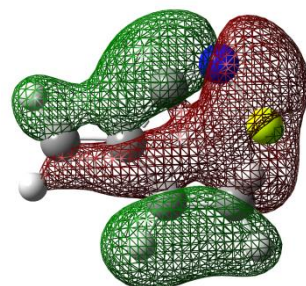
15 HOMO-7



14 HOMO-8



13 HOMO-9



12 HOMO-10

